

**DEVELOPMENT AND CHARACTERIZATION OF
Al-Si BASED FUNCTIONALLY GRADED MATERIAL
THROUGH DIRECTIONAL SOLIDIFICATION**

Thesis

Submitted in partial fulfillment of the requirements for the degree of

DOCTOR OF PHILOSOPHY

by

RAMESH BABU N

(135040ME13P03)



DEPARTMENT OF MECHANICAL ENGINEERING
NATIONAL INSTITUTE OF TECHNOLOGY KARNATAKA,
SURATHKAL MANGALORE - 575025

May - 2020

DECLARATION

I hereby *declare* that the Research Thesis entitled "**Development and characterization of Al-Si based functionally graded material through Directional Solidification**" which is being submitted to the **National Institute of Technology Karnataka, Surathkal** in partial fulfillment of the requirements for the award of the Degree of **Doctor of Philosophy in Department of Mechanical Engineering** is a *bonafide report of the research work carried out by me*. The material contained in this Research Thesis has not been submitted to any University or Institution for the award of any degree.

Register Number : 135040ME13P03

Name of the Research Scholar : Ramesh Babu N

Signature of the Research Scholar :

N. Ramesh Babu 21/05/20

Department of Mechanical Engineering

Place: NITK, Surathkal

Date: 21-May-2020

CERTIFICATE

This is to *certify* that the Research Thesis entitled "**Development and characterization of Al-Si based functionally graded material through Directional Solidification**" submitted by **Ramesh Babu N (Registration number: 135040MEP03)** as the record of the research work carried out by him, is *accepted as the Research Thesis submission* in partial fulfillment of the requirements for the award of the degree of **Doctor of Philosophy**

Dr. M R Ramesh

(Research guide)

Date

Chairman – DRPC

Date:



Dedicated to...

My beloved Parents, Wife, Daughter....

&

*All of my Teachers and Colleagues who
taught and encouraged with positive
thoughts...*



ACKNOWLEDGMENTS

It has been indeed a great honor and privilege for me to work under the guidance of my advisor **Dr. M R Ramesh**, Department of Mechanical Engineering, NITK Surathkal. With deep sense of gratitude and humility, I express my sincere thanks to him for his valuable guidance, untiring perseverance and unending patience which made the research not merely educational but also enjoyable. I also take this opportunity to thank the Director, NITK Surathkal and Head of Mechanical Engineering Department, NITK Surathkal for allowing me to carry out my doctoral studies.

I sincerely thank the Research Progress Assessment Committee consisting of **Dr. H Shivananda Nayaka** (Mechanical Engineering Department), **Dr. Suresha S N** (Civil Engineering Department) for their valuable comments and constructive criticism which have helped the enrichment of this doctoral work. My heartfelt thanks to **Dr. Narendranath.S**, Professor and former Head, Department of Mechanical Engineering, NITK, Surathkal **Dr. D. Chakradhar**, (Department of Mechanical Engineering, IIT, Palakkad), **Dr. Kiran Aithal S**, Professor , Department of Mechanical Engineering, NMIT, Bangalore, **Dr. P B Shetty**, Professor , Department of Mechanical Engineering, NMIT, Bangalore and **Dr. P G Mukunda**, Professor , Department of Mechanical Engineering, NMIT, Bangalore for their valuable suggestions and constant support during my research work. I am indeed extremely indebted to all of them

My sincere thanks to **Professor NR Shetty**, Director, NMIT, Bangalore, **Dr HC Nagaraj**, Principal, NMIT, Bangalore, **Dr. Sudheer Reddy**, HOD, Department of Mechanical Engineering , **Dr. Madhusudhan**, Professor, NMIT, Bangalore for rendering their support and advice. I am immensely indebted to the unending help and support I received from my co-research colleagues **Mr. Manjunath HN**, **Mr. Sachin B** during the course of my research work. I also thankful to Dr. Gajanan Anne, Department of Mechanical Engineering, SODE, Udupi, Dr. Shivaprasad C G, Senior Faculty, HAL

Management Academy who provided me continuous support during my research work. My sincere thanks to **Mr. Kotgi Kotresh, Mr. Ananda MN, Mr. Veeresh Kumar S** for extending their help while conducting the experiments.

I would like to thank **TEQIP-II** for partially funding my research work. I would also like to acknowledge BMSCE, Bangalore for providing the testing facility.

I am indebted to my parents **Late. E. Narayanappa** and **Mrs Yashodamma** for inculcating in me the right values and virtues. I am indebted to my wife **Mrs. Kanchan Priya J C** and my daughter **Ms. Neeharikaa R** for their constant inspiration, encouragement and motivation during my research work. I am extremely grateful to my brother **Mr. Sridhar N** for providing continuous encouragement and support. I wish to express my special thanks to all my family members and friends who were a constant source of motivation and encouragement during the entire course of my doctoral work

I would also thank the Teaching and Non-Teaching staff members of NITK Surathkal and NMIT, Bangalore for their kind help and support during the Ph.D programme.

Finally, I want to express my thanks to all those who helped me directly or indirectly at various stages of this research work. I THANK YOU ALL.....!

N. Ramesh Babu 21/05/20

Ramesh Babu N

ABSTRACT

Many structural components encounter service conditions and hence required material performance vary with location within the component. It is well known that abrupt transitions in materials composition and properties within a component often result in sharp local concentrations of stress, whether the stress is internal or applied externally. It is also known that these stress concentrations are greatly reduced if the transition from one material to the other is made gradual.

By definition, functionally graded materials (FGM's) are used to produce components featuring engineered gradual transitions in microstructure and/or composition, the presence of which is motivated by functional performance requirements that vary with location within a part. With functionally graded materials, these requirements are met in a manner that optimizes the overall performance of the component. The research on FGM's is encouraged by the need for properties that are unavailable in any single material and the need for graded properties to offset adverse effects of discontinuities for layered materials. Directional solidification is the common method for fabricating FGM's which is mainly a composite material which has high differences of density and low solubility on different phases or different materials of the same alloy. The main thrust in the present work is to fabricate FGM's for solid valve lifter applications.

The first phase of study was to fabricate Al-Si based and Al-Si reinforced with 2wt% graphite FGM's, to accomplish this a novel directional solidification technique combined with lateral vibrations was developed.

In the second phase of study, optimization of process parameters i.e. chill material, chill volume and pouring temperature were carried out using taguchi technique through the experiments performed according to the L_{27} orthogonal array. The optimization was carried out by investigating the influence of process parameters(chill material, chill volume and pouring temperature) on hardness values across the top and bottom portion of the cast specimen. The castings obtained by both with vibrations and without vibrations

were tested. From the obtained results it was revealed that optimized samples obtained with lateral vibrations exhibited better variation in properties compared to the ones obtained without vibrations

In the third phase of study, evaluation of mechanical and tribological characteristics was carried out on the optimized sample of Al-Si based FGM and Al-Si reinforced with 2wt% graphite FGMs to understand the significance of lateral vibrations. The FGM's have been analyzed for microstructure by the scanning electron microscope (SEM) morphologies which revealed that concentration of Si was more at the top portion. The spatial transition of Si can be attributed to the presence of the chill at the bottom and to the influence of lateral vibrations which has led to variation of properties within the structure, these observations were also supported by the hardness values. Ultimate tensile strength (UTS) results also showed shift in the properties from bottom to top portion of the cast. Wear analysis carried out at the top and the bottom portion of the FGM showed that there is a decrease in wear loss, coefficient of friction and specific wear rate at the top portion compared to the bottom portion. Worn-out surface analysis revealed that graphite addition had imparted the self-lubricating property at the top portion which could serve as anti-friction and anti-wear applications in the automotive sector.

Keywords: Functionally graded material. Directional solidification, Chill, Lateral vibrations, Taguchi technique, Hardness, Strength, Wear resistance.

CONTENTS

<i>Declaration</i>	
<i>Certificate</i>	
<i>Dedication</i>	
<i>Acknowledgments</i>	
<i>Abstract</i>	
<i>Contents</i>	i
<i>List of Figures</i>	v
<i>List of Tables</i>	ix
<i>Nomenclature</i>	xi
1 INTRODUCTION	1
1.1 FUNCTIONALLY GRADED MATERIAL	1
1.2 DESIGN OF EXPERIMENTS	5
1.3 APPLICATIONS OF FGC	7
1.4 OVERVIEW OF THE DISSERTATION	9
2 LITERATURE REVIEW	11
2.1 ALUMINUM ALLOYS	11
2.1.1 Properties of Aluminum	12
2.1.2 Aluminum-Silicon alloys	12
2.2 HISTORY OF FGM	14
2.3 PROCESSING TECHNIQUES OF FGM.	15
2.3.1 Powder Metallurgy	16
2.3.2 Deposition techniques	19
2.3.3 Electro-magnetic separation Technique	21
2.3.4 Centrifugal casting	22
2.3.5 Centrifuge casting	24

2.3.6	Directional solidification	25
2.3.6.1	Purpose of chill	26
2.3.6.2	Heat diffusivity and volumetric heat capacity	27
2.3.6.3	Chill material and size of the chill	28
2.4	EFFECT OF EXCITATION SOURCE ON SOLIDIFYING ALUMINUM ALLOYS	29
2.4.1	Ultrasonic vibration	29
2.4.2	Electro-magnetic vibrations	31
2.4.3	Mechanical vibrations	32
2.5	INFLUENCE OF GRAPHITE REINFORCEMENTS IN ALUMINUM ALLOYS	34
2.6	MECHANICAL AND TRIBOLOGICAL CHARACTERIZATION	36
2.6.1	Hardness	37
2.6.2	Strength	38
2.6.3	Wear	40
2.7	SUMMARY AND MOTIVATION FROM LITERATURE SURVEY	43
2.8	OBJECTIVES OF THE RESEARCH WORK	44
3	MATERIALS AND METHODOLOGY	45
3.1	Al-Si ALLOY	45
3.2	DEVELOPMENT OF EXPERIMENTAL SET UP	46
3.2.1	Mold	47
3.2.2	Chill	48
3.2.3	Lateral vibration set up	49
3.2.4	Positioning of thermocouple	50
3.2.5	Processing of FGM through DS coupled with vibrations	52
3.2.6	Optimization of process parameters	53
3.3	HARDNESS EVALUATION	57
3.4	MICROSTRUCTURAL CHARACTERIZATION	58
3.5	MECHANICAL PROPERTIES	60
3.5.1	Tensile test	60

3.5.2	Diametrical compression test	60
3.6	WEAR	63
3.6.1	Wear quantification	64
3.6.2	Pin on disc wear testing machine	65
4	Al-18wt%Si FGM SYNTHESIZED WITHOUT LATERAL VIBRATIONS	69
4.1	INTRODUCTION	69
4.2	CASTING OF FGM	69
4.3	EVALUATION OF PROPERTIES OF FGM FABRICATED WITH OPTIMAL PARAMETERS	71
4.3.1	Hardness	74
4.3.2	Effect of chill on solidification	75
4.3.3	Microstructure	76
4.3.4	Strength	80
4.3.5	Wear analysis	81
4.3.6	Worn out surface analysis	82
4.4	SUMMARY	86
5	Al-18wt%Si FGM SYNTHESIZED WITH LATERAL VIBRATIONS	87
5.1	INTRODUCTION	87
5.2	CASTING OF FGM	87
5.3	EVALUATION OF PROPERTIES OF FGM FABRICATED WITH OPTIMAL PARAMETERS	87
5.3.1	Hardness	92
5.3.2	Effect of chill on solidification	93
5.3.3	Microstructure	95
5.3.4	Strength	95
5.3.5	Wear analysis	98
5.3.6	Worn out surface analysis	100
5.4	SUMMARY	103
6	Al-18wt%Si REINFORCED WITH 2wt% GRAPHITE FGC SYNTHESIZED WITH LATERAL VIBRATIONS	105

6.1	INTRODUCTION	105
6.2	CASTING OF FGM	105
6.3	EVALUATION OF PROPERTIES OF FGM FABRICATED WITH OPTIMAL PARAMETERS	106
6.3.1	Hardness	110
6.3.2	Effect of chill on solidification	112
6.3.3	Microstructure	113
6.3.4	Strength	117
6.3.5	Diametrical compression	118
6.3.6	Wear analysis	118
6.3.7	Worn out surface analysis	121
6.4	SUMMARY	124
7	CONCLUSIONS	127
8	SCOPE FOR FUTURE WORK	129
	REFERENCES	129
	LIST OF PUBLICATIONS	
	BIODATA	

LIST OF FIGURES

Figure 1.1	Types of FG structure (a) Continuous (b) Step-wise gradation	3
Figure 1.2	Typical applications of FGC	8
Figure 2.1	Al-Si binary phase diagram	13
Figure 2.2	Processing techniques of FGM and their classification	16
Figure 2.3	Types of chills (a) Internal chill (b) External chill (c) Location of chill	26
Figure 2.4	Silicon morphology: Ultrasonic vibration	29
Figure 2.5	Direction of vibrating force F formed by the action of the stationary magnetic field B and alternating electric field J	31
Figure 2.6	Cooling curve of Al12wt%Si	33
Figure 2.7	Silicon Morphology: Mechanical Vibrations	33
Figure 2.8	Influence of graphite content on mechanical properties of MMC's	35
Figure 2.9	Effect of hardness on wear rate of graphite composite at a sliding velocity of 0.37 m/s	36
Figure 2.10	Load application in DC Test	39
Figure 3.1	Methodology of the research work	46
Figure 3.2	Insulation mold	48
Figure 3.3	Chill: (a) Copper (b) Mild steel (c) Cast iron	49
Figure 3.4	Lateral vibration set up	51
Figure 3.5	Experimental set up	51
Figure 3.6	Thermocouple positioning (a) Location (b) Data acquisition system	52
Figure 3.7	Directional solidification coupled with vibration	53
Figure 3.8	Cast sample: (a) Solid Cylinder (b) Top and bottom portion of FGC	54
Figure 3.9	Taguchi analysis procedure	54
Figure 3.10	Selection of Process parameters and levels	55

Figure 3.11	Representation of Indentation	57
Figure 3.12	Points of measurements in Hardness test	58
Figure 3.13	Metallographic specimen	59
Figure 3.14	Scanning electron microscope	59
Figure 3.15	Round tension test specimen (ASTM E8 standards)	60
Figure 3.16	Pictorial image of Tensile specimen	61
Figure 3.17	Electronic tensometer	61
Figure 3.18	Tensometer specimen holder	62
Figure 3.19	Schematic representation of different loading conditions (a) Hertz point (b) Hondros, and (c) Uni-axial diametrical compression	62
Figure 3.20	Photograph of tribometer	66
Figure 3.21	Pin on disc	66
Figure 3.22	Wear specimen	67
Figure 4.1	Main effects plot for hardness based on S/N ratio for top portion	73
Figure 4.2	Main effects plot for hardness based on S/N ratio for bottom portion	73
Figure 4.3	Volumetric heat capacity on hardness: Top portion	76
Figure 4.4	Volumetric heat capacity on hardness: Bottom portion	77
Figure 4.5	Hardness across the section	77
Figure 4.6	Cooling Curves of FGM	78
Figure 4.7	Temperature Difference between top and bottom portion vs time	78
Figure 4.8	Microstructural analysis of FGM (a) Representative SEM image of top portion (b) Representative SEM image of bottom portion (c) EDS for top portion (d) EDS for bottom portion (e) Histogram for frequency of particle size distribution	79
Figure 4.9	Porosity check of Al-18wt% Si FGM fabricated without lateral vibrations	80
Figure 4.10	Strength of FGM (Without vibrations) and as-cast	81
Figure 4.11	Fractography of tensile specimens (Without vibrations): (a) Top portion (b) Bottom portion	81
Figure 4.12	Wear loss of FGM (Without vibrations) and as-cast	82

Figure 4.13	Coefficient of friction of FGM (Without vibrations) and as-cast	83
Figure 4.14	Specific wear rate of FGM (Without vibrations) and as-cast	83
Figure 4.15	SEM images of wear surfaces for the optimized samples (Without vibrations): (a) Top portion (b) Bottom portion	84
Figure 4.16	Wear debris analysis of FGM (Without vibrations): (a) Top portion (b) Bottom portion (c) EDS for top portion (d) EDS for bottom portion	85
Figure 5.1	Main effects plot for hardness based on S/N ratio for top portion	90
Figure 5.2	Main effects plot for hardness based on S/N ratio for bottom portion	90
Figure 5.3	Volumetric heat capacity on hardness: Top portion	91
Figure 5.4	Volumetric heat capacity on hardness: Bottom portion	92
Figure 5.5	Hardness across the section	93
Figure 5.6	Cooling Curves of FGM	94
Figure 5.7	Temperature Difference between top and bottom portion vs time	94
Figure 5.8	Microstructural analysis of FGM (a) Representative SEM image of top portion (b) Representative SEM image of bottom portion (c) EDS for top portion (d) EDS for bottom portion (e) Histogram for frequency of particle size distribution	96
Figure 5.9	Porosity check of Al-18wt% Si FGM fabricated with lateral vibrations	97
Figure 5.10	Strength of FGM (With vibrations) and as-cast	97
Figure 5.11	Fractography of tensile specimens (with vibrations): (a) Top portion (b) Bottom portion	98
Figure 5.12	Wear loss of FGM (With vibrations) and as-cast	99
Figure 5.13	Coefficient of friction of FGM (With vibrations) and as-cast	99
Figure 5.14	Specific wear rate of FGM (With vibrations) and as-cast	100
Figure 5.15	SEM images of wear surfaces for the optimized samples (With vibrations): (a) Top portion (b) Bottom portion	101
Figure 5.16	Wear debris analysis of FGM (With vibrations): (a) Top portion (b) Bottom portion (c) EDS for top portion (d) EDS for bottom portion	102
Figure 6.1	Main effects plot for hardness based on S/N ratio for top portion	109
Figure 6.2	Main effects plot for hardness based on S/N ratio for bottom portion	109

Figure 6.3	Volumetric heat capacity on hardness: Top portion	111
Figure 6.4	Volumetric heat capacity on hardness: Bottom portion	112
Figure 6.5	Hardness across the section	113
Figure 6.6	Cooling Curves of FGM	114
Figure 6.7	Temperature Difference between top and bottom portion vs time	114
Figure 6.8	Microstructural analysis of FGM (a) Representative SEM image of top portion (b) Representative SEM image of bottom portion (c) EDS for top portion (d) EDS for bottom portion (e) Histogram for frequency of particle size distribution	115
Figure 6.9	Porosity check of Al-18wt% Si reinforced with 2wt% graphite FGC fabricated with lateral vibrations	116
Figure 6.10	Strength of FGC (With vibrations) and as-cast	117
Figure 6.11	Fractography of tensile specimens: (a) Top portion (b) Bottom portion	118
Figure 6.12	Diametrical compression (a) Top portion (b) Bottom portion	119
Figure 6.13	Ultimate strength of sample subjected to DC test	119
Figure 6.14	Variation of wear loss with load	120
Figure 6.15	Coefficient of friction of FGC and as-cast	120
Figure 6.16	Specific wear rate of FGC and as-cast	121
Figure 6.17	SEM images of wear surfaces for the optimized samples: (a) Top portion (b) Bottom portion	122
Figure 6.18	Wear debris analysis of FGC : (a) Top portion (b) Bottom portion (c) EDS for top portion (d) EDS for bottom portion	123

LIST OF TABLES

Table 2.1	Overview of processing techniques in FGM	17
Table 2.2	Effect of vibration on solidifying Al and its alloys	30
Table 3.1	Chemical composition of Al-Si alloy	45
Table 3.2	Volume of the chills used in the present work	48
Table 3.3	Volumetric heat capacity of chill materials	50
Table 3.4	Parts of lateral vibration set up	52
Table 3.5	Specifications of a thermocouple	52
Table 3.6	Factors and levels designated for the experimental work	55
Table 3.7	L ₂₇ full factorial orthogonal array	56
Table 4.1	Control factors and level	69
Table 4.2	Response table for hardness (Without Vibrations)	70
Table 4.4	Analysis of means based on S/N ratio for top portion (Without vibration)	71
Table 4.5	Analysis of means based on S/N ratio for bottom portion (Without vibration)	72
Table 4.6	ANOVA for hardness based on S/N ratio for top portion	74
Table 4.7	ANOVA for hardness based on S/N ratio for bottom portion	74
Table 4.8	Optimal control factor setting and optimal values for hardness at top and bottom portion	75
Table 5.1	Response table for hardness (With Vibrations)	88
Table 5.3	Analysis of means based on S/N ratio for top portion (With vibration)	89
Table 5.4	Analysis of means based on S/N ratio for bottom portion (With vibration)	89
Table 5.5	ANOVA for hardness based on S/N ratio for top portion	91
Table 5.6	ANOVA for hardness based on S/N ratio for bottom portion	91

Table 5.7	Optimal control factor setting and optimal values for hardness at top and bottom portion	92
Table 6.1	Response table for hardness (With Vibrations)	107
Table 6.3	Analysis of means based on S/N ratio for top portion (With vibration)	108
Table 6.4	Analysis of means based on S/N ratio for bottom portion (With vibration)	108
Table 6.5	ANOVA for hardness based on S/N ratio for top portion	110
Table 6.6	ANOVA for hardness based on S/N ratio for bottom portion	110
Table 6.7	Optimal control factor setting and optimal values for hardness at top and bottom portion	111

NOMENCLATURE

\bar{y}	: Average observed data
ρ	: Density of the chill material
σ_x and σ_y	: Principal stresses
$^{\circ}C$: Celsius
C_p	: Specific heat of the chill
K	: Kelvin
Pa	: Pascal
SS	: Sum of squares
S_y^2	: Variation of y
Al	: Aluminum
Al-18wt%Si	: Alumium alloy used in the present work
ANOVA	: Analysis of variance
BHN	: Brinell Hardness Nmber
COF	: Co-efficient of friction
DF	: Degrees of freedom
DOE	: Design of Experiments
DS	: Directional solidification
FGC	: Functionally graded composite
FGM	: Functionally graded material

n	: Number of observations
S/N	: Signal to Noise ratio
SEM	: Scanning Electron Microscope
Si	: Silicon
SPWR	: Specific wear rate
V	: Volume of the chill
VHC	: Volumetric heat capacity of a chill
y	: Observed data

CHAPTER 1

INTRODUCTION

In the recent years, with the introduction to alloys and functionally graded materials (FGM's) the usage of pure metals has faded drastically as the pure metals do not fulfil all the requirements. Hence, the concept of processing newer materials has taken place. FGC are different from conventional materials in which properties like density, young's modulus, poisson's ratio of the material vary in chosen directions. For example, one side of the cast may have high mechanical strength and the other side may have high thermal resistant property, thus it will be characterized by different aspects in a single material. This multi-functional behavior of FGC enables a wide scope in the aerospace, automobile, electronics, biomedical applications. The components such as pistons, cylinder liners, engine heads, connecting rods, turbine parts, medical implant, rocket nozzle, tool inserts etc, which necessitate to meet the functional performance requirements that vary with location within the component, FGC's provides the best solutions under such situations (Birman and Byrd 2007).

1.1 FUNCTIONALLY GRADED MATERIAL

FGM's are those materials in which the composition or microstructure or both are locally varied so that a specific form of the local material properties are attained. This varying property gives rise to different functions within the material. The concept of FGM was first proposed in Japan in the year 1984 during a space plane project and has attracted the interests of numerous researchers (Koizumi and Niino 1995). In conventional composites, the reinforcement or constituent phases are evenly distributed thereby the properties on an average will be uniform. However in FGMs, the composition and microstructure vary smoothly in space and the properties and performance, therefore, vary from one end of the specimen to the other. The functional gradient can be tailored to the specified service conditions, thus ensuring the best response of the system. One of the advantages

of continuously varying volume fraction of the constituent phases is the elimination of stress discontinuity that is often encountered in laminated composites. Accordingly delamination problems are avoided and further the gradual transition also allows the creation of superior and multiple properties without any mechanically weak interface. Moreover, the gradual change of properties can be tailored to suit different applications and service environments.

The concept of FGM includes two important features. The first feature is the ability to tailor the microstructure and chemical composition as per the desired function, while the second feature is the availability of the fabricating process which has good and controlled reproducibility of the desired properties. FGM's are the materials which can be purposefully processed to obtain higher hardness, higher wear resistance, desired friction, increased toughness, reduced internal stress, thermal properties and crack retardation. FGM's possess various advantages compared to the conventional materials. For example, multi-functionality of the material, dynamic response, ability to control deformation, wear, corrosion etc. In general FGM is classified into two types i.e. continuously graded and discontinuously graded material. In its simplest form FGM's are the material in which gradation takes place from end to the other as illustrated in Figure 1.1 (a). In the second type, material gradation changes in a discontinuous way such as step-wise gradation which is illustrated in Figure 1.1 (b) The use of FGC's as structural materials is determined by their physical and their mechanical properties. The mechanical properties of a composite can be attributed to the individual properties of its main phase components and to the volume fraction and morphology of these components. In the last two decades, more attention is given to the research on processing techniques of FGC's that include deposition techniques, directional solidification, powder metallurgy, centrifugal casting, electromagnetic separation etc.(Kieback et al. 2003). But each technology has specific aspects that intervene with the generation of a desired microstructure and accordingly affects the mechanical properties adversely.

To fabricate a wear resistant material with considerable strength, a material with heterogeneous microstructure can be designed in which a high volume fraction of hard particles is dispersed at the surface, where better wear properties are needed, and a

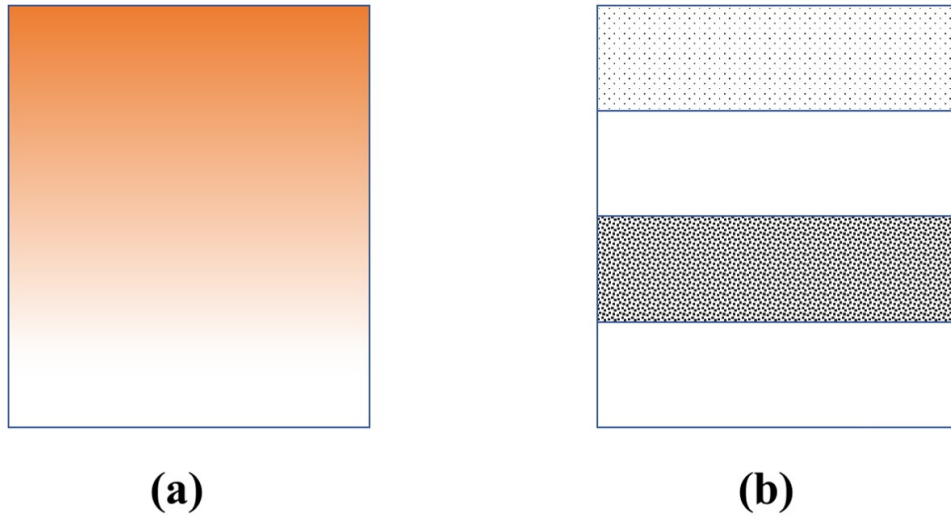


Figure 1.1 Types of FG structure (a) Continuous (b) Step-wise gradation

gradually decreasing lower volume fraction of hard particles below the surface where better strength and ductility are desired. Casting techniques with external force allows producing a material of desired tribological surface at one end and with good strength on the other end (Qudong et al. 2005).

Aluminum matrix composites are tailored to feature the toughness of the alloy matrix and the hardness, strength and stiffness of hard reinforcements. As a result composite materials exhibit a good combination of strength and toughness. The use of Al-Si alloys as structural materials is ascertained from the physical and their mechanical properties which are influenced by both chemical composition and the microstructure. In Al-Si based composites the tensile properties and fracture behavior depends upon the volume percentage of reinforcement particulates(Si) shape and size.

Controlling the microstructure and mechanical properties along the length of the cast are one of the major challenges faced in today's foundry industry. With the researcher's attention to increasing in developing series of techniques in the preparation of FGC's which include centrifugal casting, stir casting, centrifuge casting, magnetic separation, powder metallurgy, directional solidification (Khor and Gu 2000; Peng et al. 2007; Seifried et al. 2001; Song et al. 2007a; Watanabe et al. 2001). A group of researchers found that an economical way of fabricating FGC's was through Directional solidification

(DS) technique (Mazare et al. 2010) in which by providing external chills local controlled properties and soundness of the casting can be achieved. It is seen that in DS technique, solidification starts with lower temperature at the melt/chill interface compared to other locations of the casting (Hemanth 2014). Like the monolithic materials, the properties of FGC's are largely dependent on solidification behavior, which is dictated by the thermophysical properties of the chill/melt interface. The resistance towards heat flow near the chill/melt interface usually varies with time, due to the time-dependence of plasticity of the freezing melt and growth of oxides on the surface (Rajan et al. 2007). The efficiency of the chill is further dependent on volumetric heat capacity (VHC) of the chill which takes in to account the chill volume, density and specific heat of the chill material (Hemanth 2000) and is given by

$$VHC = \rho * C_p * V \quad (1.1)$$

where ρ is the density of the chill material, C_p is the specific heat of the chill, V is the volume of the chill.

Among the various commonly used chills, copper was found to have better heat extraction rate, thereby steep temperature gradient can be established promoting DS (Hemanth 2006; Hiremath et al. 2018). However, DS is associated with problem like precipitation of reinforcements from the chill/metal interface. As a result, to increase the precipitation of the reinforcements and improve the soundness of the casting an external force is required. It has been found that inducing mechanical vibrations during solidification will have a positive effect on precipitation and distribution of reinforcements (Abu-Dheir et al. 2005; Chaturvedi et al. 2017; Chirita et al. 2009a; Fisher 1973; Hernandez and Sokolowski 2006; Ivanov and Krushenka 1993; Jian et al. 2006b; Kocatepe 2007; Rasgado and Davey 2002). Therefore influence of vibrations during solidification will promote significant changes in the microstructure (Abu-Dheir et al. 2005), thereby exhibiting changes in mechanical and tribological properties of the casting.

Researchers who have worked on directional solidification technique have developed the process based on the chill material and chill length but not much of the work has been

carried out considering the excitation source. This clearly conveys the message for the need for development of an appropriate manufacturing technique for fabrication of FG composite to meet the requirement for lightweight materials, with suitable mechanical and tribological properties for a range of engineering applications. Very little literature is available on the solid blocks processed by DS process coupled with excitation source. It is clear that many factors play an important role in defining the mechanical properties and tribological properties of FG composites. In order to meet the growing demand for high performance Al-Si based FG composites, it is thus essential that investigations be carried out to develop FG composites and to study the effect of process parameters on mechanical properties. Therefore, Design of experiments (DOE) can be used for planning the experiments so that the desired objectives can be obtained from the optimization of process parameters.

1.2 DESIGN OF EXPERIMENTS

DOE is an economical, analytical and very effective technique which is used to conduct industrial trials in an organized way. Instead of trial and error method, Multiple process variables and product design parameters can be studied at the same time with efficient DOE techniques providing a very satisfactory results (Douglas 2012). Due to statistical balance in the design, large number of potential combination of experiments with numerous factors (at varying levels) can be evaluated for overall optimum operating combinations, by conducting a small number of experiments. DOE is an effective technique for planning of experiments so that the obtained data can be analyzed to validate the objective conclusions.

In a trial, deliberate changes are made to one or more process factors to investigate the interactive effect of those changes that have on one or more response factors. The analysis is carried out using the commercial available software specifically used for DOE applications known as MINITAB 15. Therefore, after determining the process variables which affects the response, the next step is to optimize the level of factors which results in best possible response. Taguchi technique was invented by a Japanese statistician Dr.Genichi Taguchi to enhance the quality of manufacturing products and production processes. He initiated the fractional factorial experimental designs through

which results and optimization of process variables can be determined by carrying out minimum number of trials. Therefore, Taguchi techniques have been extensively utilized in engineering design successfully (Phadke 1989; Ross 1996). Conventional DOE process is difficult and tedious to use. Moreover, a large number of trials have to be carried out to get the results, and it becomes complex when a large number of process variables are involved. To resolve this problem, Taguchi technique follows a unique design of orthogonal arrays by carrying out the minimum number of trials to study the effects of process variables (Taguchi 1986).

Taguchi technique uses parametric design, which is an engineering technique for process or product design that emphasizes on determining the control factor settings. Thereby, producing the best levels of a quality performance measure with a least noise variation. Taguchi method offers an efficient and powerful technique for design processes that operates optimally and consistently under a wide variety of conditions. The core concept of Taguchi's technique in quality enhancement is Taguchi's loss function. Therefore, loss function signifies that society's loss because of the badly accomplished products which is proportional to the square of the deviation of the performance characteristic from its target value.

Orthogonal array is finalized by considering the number of control factors and levels, interactions between them and the range of control factors. Taguchi has employed Signal–Noise (S/N) ratio as the quality characteristic of choice. Therefore, S/N ratio is used as measurable value instead of standard deviation because as the value of mean decreases, Hence, standard deviation cannot be minimized first and the mean value is brought to the target. In general, the value of target mean may vary the process development. S/N ratio characteristics is divided into three categories which are given by the equations depending upon the quality characteristic.

$$\text{Nominal is the best characteristic } \frac{S}{N} = 10 \log \frac{\bar{y}}{\bar{S}_y^2} \quad (1.2)$$

$$\text{Smaller is the best characteristic } \frac{S}{N} = -10 \log \frac{1}{n} (\sum y^2) \quad (1.3)$$

$$\text{Larger the best characteristic } \frac{S}{N} = -10 \log \frac{1}{n} \left(\sum \frac{1}{y^2} \right) \quad (1.4)$$

Where \bar{y} = average observed data, S_y^2 = variation of y, y= observed data, n=number of observations.

Experimental design methods which were developed earlier were not practical and were widely used by statisticians rather than practitioners (Phadke 1989). Moreover, Taguchi's approach to DOE is practical which can also be executed even with minimum knowledge of statistics and are very easy to use. Because of these significant features, it has been successfully accepted and acknowledged method in the engineering field and scientific community. A large number of researchers have successfully implemented taguchi technique in material processing for optimization of process parameters(Bouacha et al. 2014; Khanna and Davim 2015; Koyee et al. 2014).

1.3 APPLICATIONS OF FGC

In the current scenario researches on FGC have been carried out extensively. FGC's offers great promise in the applications where the operating conditions are severe. The potential applications of those include engineering and structural uses that necessitates combination of incompatible functions such as hardness with toughness or refractoriness. On the other hand, it is used in fabrication of engine components, cutting tools, machine parts, which require heat, wear, corrosion resistance and mechanical shock. FGC's also find their application in defense, energy, medicine, sports and aerospace sectors. Examples of available FGC products are shown in Figure 1.2. The applications of FGC's are further elaborated upon below.

1. Defense: One of the most significant characteristics of FGC is the ability to restrict the crack propagation. This property makes it very useful in defense application, as it is used as a penetration resistant materials in bulletproof vests and armour plates.
2. Energy: FGC are used to provide thermal barrier and are also used as a protective coating for turbine blades in gas turbine engines.
3. Medicine: Living tissues such as teeth and bones are characterized as FG materials



Figure 1.2 Typical applications of FGC

from nature. Therefore as a replacement to these tissues, a compatible material is required which will serve the purpose of the original bio-tissue. The potential candidate for this application is the FG material. FGM has found a broad scope in dental and orthopedic applications for teeth and bone replacement.

4. As the FGC's offer graded combinations of elasticity, flexibility, rigidity. They are used in the making sports equipment such as tennis rackets, golf clubs and skis.
5. Aerospace: FG materials can resist very high thermal gradient, which makes it suitable for use in rocket engine component, space plane body etc. If processing technique are improved, FG materials can be used in wider areas of aerospace.

In the present study, the main thrust is to fabricate FGM's for solid valve lifter application. Novel directional solidification technique coupled with lateral vibration was developed to fabricate FGM's. Two alloys used in the present work to synthesize FGM are Al-18wt%Si and Al-18wt%Si reinforced with 2wt% graphite to achieve graded properties. The optimization of process parameters was carried out by applying taguchi technique. Mechanical and tribological properties were evaluated for the samples obtained with optimal process parameters to check the gradation.

1.4 OVERVIEW OF THE DISSERTATION

The organization of the thesis is as follows.

CHAPTER 1

In this chapter introduction to FGM, importance of FGM over conventional materials have been described. This chapter also deals with design of experiments, applications of FGM.

CHAPTER 2

This chapter presents detailed literature review which is closely related to FGM, processing techniques, directional solidification, Al-Si alloys, Effect of excitation source on the microstructure, Hardness, strength and Wear studies. Finally objectives and scope of the present study have been presented.

CHAPTER 3

This chapter presents the methodology and experimental procedure employed to fabricate FGC. A detailed explanation of the procedures adopted to study the hardness, microstructure, strength, wear have presented.

CHAPTER 4

This chapter discusses parametric optimization of process parameters for the FGM fabricated without lateral vibrations. The alloy used in this study was Al-18wt%Si. For the FGM fabricated with optimized process parameter conditions, evaluation of mechanical and tribological properties was carried out to study the gradation.

CHAPTER 5

This chapter deals with parametric optimization of process parameters for the FGM fabricated with lateral vibrations. The alloy used in this study was Al-18wt%Si. For the FGM fabricated with optimized process parameter conditions, evaluation of mechanical and tribological properties was carried out to study the gradation.

CHAPTER 6

This chapter deliberates parametric optimization of process parameters for the FGC fabricated with lateral vibrations. The alloy used in this study was Al-18wt%Si reinforced with 2wt% graphite. For the FGC fabricated with optimized process parameter conditions, evaluation of mechanical and tribological properties was carried out to study

the gradation.

CHAPTER 7

In this chapter conclusions have been derived from the FGM's fabricated with optimal process parameters. Based on the results and observations, directions and recommendations of future work are discussed briefly in this dissertation. References and list of publications based on the present research work have been listed at the end.

CHAPTER 2

LITERATURE REVIEW

Over the last few decades significant work has been carried out in the field of FGM's. A large volume of information is available on FGM's exploring the mechanical properties, tribological properties and processing techniques but still many problems exist that needs to be addressed. The structured literature survey done so far on FGM's will help in planning the research work. The literature is collected methodically for the present work and is presented under the following headings.

1. Aluminum Silicon alloys
2. History of FGM
3. Processing techniques of FGM
4. Directional Solidification
5. Effect of excitation source on the mechanical properties
6. Hardness, strength and Wear studies

2.1 ALUMINUM ALLOYS

Aluminum (Al) alloys have been the predominant material of choice for aircraft structural components since 1930. Even though the polymer matrix composites (PMC's) being used largely in high-performance military aircraft applications and are specified for the reduced structural weight, Al alloys have been used continuously in various commercial military applications. Due to their known fabrication costs, performance characteristics, design experience, well-accomplished manufacturing techniques and their usage in hybrid structures. Therefore, due to these reasons Al alloys have gained continued confidence which will ascertain their significant usage in large quantities for many years (Starke and Staley 2011). Al alloys are widely used in automotive, aerospace

industries because of its excellent strength to weight ratio and thereby reducing the fuel consumption. The main alloying elements used are silicon, copper, manganese, magnesium, zinc. Due to the formation of oxide shielding layer, Al alloys boasts a brilliant lustre. Al alloys containing additives of Si, Mg are used in the industry to replace steel (Gaber et al. 2007).

2.1.1 Properties of Aluminum

Aluminum possesses a wide range of physical and mechanical properties such as.

- (i) The density of Aluminum is about 2.7g/cm^3 which is one-third of the steel 2.7g/cm^3 and copper 8.93g/cm^3 .
- (ii) Unlike steel, aluminum prevents progressive oxidation on its surface when exposed to air.
- (iii) Al surfaces can be reflective, hence electromagnetic waves, visible light and radiant heat can be reflected efficiently.
- (iv) Al alloys possess superior electrical and thermal conductivities. The thermal conductivity of Aluminum is twice that of Copper.

2.1.2 Aluminum-Silicon alloys

Binary Al-Si alloys is associated to the eutectic phase with eutectic temperature of 577°C (Gruzleski et al. 1990). The eutectic point composition has been reported to be varying from 11.7-14.5% Si with a most presumed value at 11.7% Si (Okamoto et al. 2016). The eutectic composition in binary Al-Si system shifts depending on the casting techniques and alloying elements. In addition to the above attributes the Al-Si alloy system also has the advantage of high thermal conductivity and improved mechanical properties over a wide temperature range. The low density 2340 Kg/m^3 of Si in particular provides the following advantages in a Al-Si system.

1. Overall weight of the component is reduced.
2. Si has a diamond crystal structure that provides good hardness.
3. It also has very low solubility in Al which improves wear characteristics.

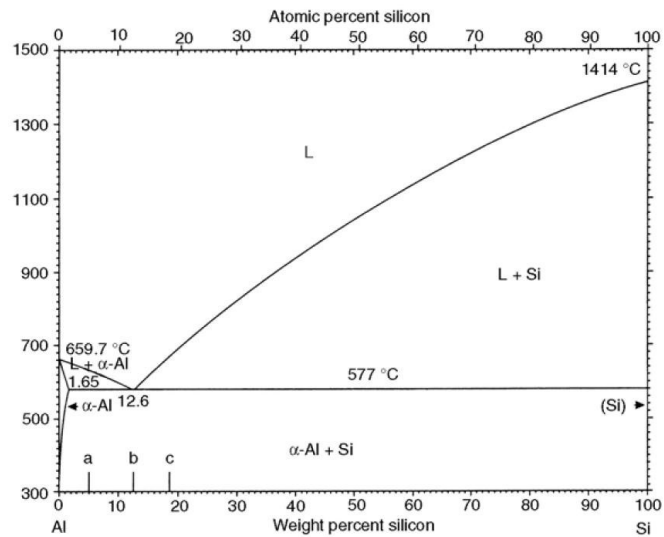


Figure 2.1 Al-Si binary phase diagram (Murray and McAlister 1984)

4. Si content imparts low shrinkage and fluidity, resulting in sound casting and welding. characteristics.

The alloys are classified into 3 groups based on the Si content.

- (a) Hypoeutectic (<11.7%Si).
- (b) Eutectic (=11.7%Si).
- (c) Hypereutectic (>11.7%Si).

Good castability and corrosion resistance characterize the binary hypoeutectic and eutectic alloys while hypereutectic alloys are known for low thermal expansion and excellent wear resistance (Prasad et al. 1998). The use of Al-Si system as a structural materials is ascertained by its physical properties which is mainly influenced by chemical composition. Also the mechanical properties are influenced by their microstructure and chemical composition. Hence, the specific tensile strength of Al alloys is greatly influenced by their poly-phase microstructure. The silicon content in a standardized commercially cast Al-Si alloys is in the range of 5 to 23 wt%. The structure of these alloys can be in the form of hypoeutectic, eutectic or hypereutectic as shown in equilibrium phase diagram in Figure 2.1. Hypoeutectic alloys are used in many applications such as marine, electrical, automotive and aircraft industries specifically to produce cylinder

heads, cylinder blocks and engine body castings. It is reported that Si varying from 6% to 8.5% has been used extensively in making cylinder heads. Researchers have added grain modifiers to increase the tensile strength and ductility. Some of the modifiers such as Cu have increased the thermal stability, lowered the thermal expansion of the hypo Al-Si alloys promoting their application in internal Combustion Engines (Basavakumar et al. 2008). Eutectic Al-Si alloy has been used in engine parts and marine castings. These alloys offer high resistance during machining, which causes tool wear. Hypereutectic alloys are used extensively these days in automotive industries because of their excellent wear resistance and low thermal expansion.

Different techniques are used to control the microstructural features. These include casting technology, use of grain refiners and modifiers etc. The fast cooling gives rise to a fine eutectic structure, reduced grain size and small α -Al dendrite arm spacing. Slower cooling rates result in randomly oriented coarse eutectic Si needles and coarse columnar α -Al dendrites. A few researchers have reported the use of modifiers like Selenium or Sodium to obtain finely dispersed eutectic (Basavakumar et al. 2009) and use of grain refiners AlB_2 , etc. to reduce the primary α -Al grain size. The use of modifiers and refiners has led to obtaining of fine equiaxed structure during solidification which resulted in good surface finish during machining. In hypereutectic alloys primary silicon appears in different forms like polyhedral, star and dendrite. The Si morphology is dependent highly on the solidification parameters such as temperature gradient, freezing rate and liquid composition.

2.2 HISTORY OF FGM

The original thought of structural gradient and composition in material microstructure was first suggested for polymeric and composites materials. (Bever and Duwez 1972) investigated the overall material properties of various graded composites to review potential applications. (Shen and Bever 1972) reported that the variation in the chemical nature of the monomers have resulted in gradation of polymeric material. Until 1985, the practice of continuous texture control was followed to enhance the adhesion strength and to minimize the thermal stresses developed in the joints and ceramic coatings for a reusable rocket engines (Koizumi and Niino 1995). By continuous control of

the microstructure, more general concepts were applied to discover new functions and properties of materials. Hence, the design of such newer materials was initially introduced.

Therefore in 1986, the term FGM was coined for these graded composites. Due to their unique graded material properties, more researchers were attracted to this new area which is applicable widely in numerous fields. Apart from thermal barrier coatings, FGM's are nowadays used for many applications such as gradient structural alloy materials to obtain wear resistance.

Metal matrix composites with considerable strength and high volume fraction of hard particles at one end of the surface for superior wear properties and a gradually lowered volume fraction of hard particles at the other end of the surface where better strength and ductility of the material can be achieved. Also FGM's have considerable potential to be extended from structural to optical, nuclear, electrical, chemical and biomedical areas (Kato et al. 2006; Mishina et al. 2008; Müller et al. 2003; Pompe et al. 2003; Zhou et al. 2009).

2.3 PROCESSING TECHNIQUES OF FGM.

The overall properties of FGM are different and unique from any of the conventional material. Hence, FGM boasts wide range of applications which is expected to increase as the material cost are reduced by improving the processing techniques. Microstructure or atomic orders, chemical composition which is position-dependent are among the key factors that influences the gradation of properties in the materials. By controlling all these factors, the gradation of properties could be tailored to meet any particular need for best utilization of the composite (Lannutti 1994; Mahamood et al. 2012). A suitable processing technique is needed which makes it possible to synthesize the required compositional gradient and microstructure thereby assuring high reproducibility.

The manufacturing technique of FGM is categorized according to methodology of attaining spatially inhomogeneous structure which is known as 'Gradation' and the transformation of this structure into a bulk material is known as 'Consolidation'. The gradation process can be categorized into constitutive, homogenizing and segregation

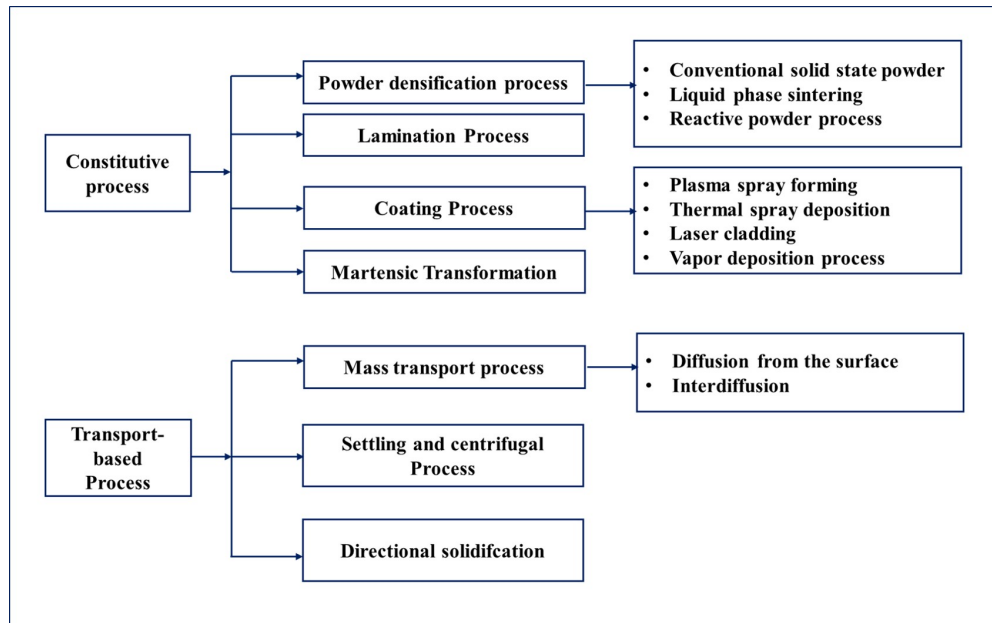


Figure 2.2 Processing techniques of FGM and their classification (Suresh and Mortensen 1998)

processes. Constitutive process is based upon a step-wise building of gradation in structure from the precursor materials or powders. In homogenizing process, sharp interface between the two materials is transformed into a gradient by material transport. Whereas the segregation process starts with macroscopically homogeneous material which is converted in to graded structure by an external field (viz. gravity, vibrations, electric field) (Figure 2.2). Homogenizing process and segregation process produces continuous gradients, but have limitations concerning the type of gradation which can be produced (Kieback et al. 2003). The prevailing techniques used in practice to fabricate FGM include powder metallurgy technique, deposition techniques, power ultrasonic technique, electromagnetic separation, power ultrasonic, gradient slurry disintegration technique, directional chill casting, centrifugal casting, centrifuge etc. An overview of the processing techniques is tabulated in Table 2.1. and explained in detail in the following subsections.

2.3.1 Powder Metallurgy

Kawasaki and Watanabe (1997) have extensively worked on FGM from the late 1990s. Powder metallurgy (PM) technique demands the material combination selection of metals and ceramics, optimum distribution of composition, continuous or stepwise stacking

Table 2.1 Overview of processing techniques in FGM (Kieback et al. 2003)

Processing Technique	Variability in transition function	Versatility in phase component	Layer thickness	Type of FGM
Powder stacking	V	V	Me, L	Bulk
Wet powder spraying	V	V	VT, T ^b	Bulk
Sedimentation / Centrifuging	G	V	C	Bulk
Diffusion	M	V	C	Coating, Joint
Directed solidification	M	V	C	Bulk
Electrochemical gradation	M	G	C	Bulk
Foaming of polymers	M	G	C	Bulk
Thermal spraying	V	V	T	Bulk, Coating
PVD, CVD	V	V	C	Coating
Sheet lamination	V	V	T ^b	Bulk
Slurry dipping	V	V	VT, T ^b	Coating
Jet solidification	V	V	Me, L	Bulk
Filtration / Slip casting	V	V	C	Bulk
Laser cladding	V	V	Me, L	Coating, Bulk

V: Very good; G: Good; M: Moderate; L: Large(>1mm); Me: Medium(100-1000 μ m); T: Thin(10-100 μ m); VT: Very thin(<10 μ m); C: Continuous,
^bDepending on the available powder size

followed by die compaction, isostatic pressing and sintering. Among of all the steps involved, sintering is the most significant process. Further, any imbalance in sintering will result in various faults such as warping, splitting and cracking, frustum formation. Later the authors have shown that this imbalance can be avoided by pressure sintering. However there are also drawbacks in this production route. Therefore prior to the forming operation, practical considerations towards an effective process design proposes the use of powdered mixture with changing average size of the particles or composition of the material during deposition. The method exercised for powder deposition technique

determines whether stepwise variation or a smooth change is obtained in the green compact. As a consolidation of the green parts during sintering or pressing requires high temperature, due to which there may be adverse changes on the microstructure related with the sintering.

Lin et al. (1999) proposed a mechanical working process through which the need for sintering can be eliminated. An additional step from which mechanical vibration was introduced in the mechanical working route. Therefore, in order to enhance the continuity of the compositional gradient, this working process was employed successfully for the fabrication of SiC/Al 2124 FGMs. It was revealed that the vibration stage has modified the distribution of SiC from the layered structure to a smoothly changing content with position along the sample. The influence of vibration also further improved the local homogeneity by breaking up of coarse SiC agglomerates in the regions where SiC content is high.

Zhu et al. (2001) produced ZrO₂-Ni FGM by hot pressing and pressure less sintering. To optimize the FGM fabrication process Powder metallurgy technique was developed to further improve its performance. The FGM produced had continuity of both components and eliminated the macroscopic interface. The PM technology route for fabrication of materials and engineering parts comprises of production of powder, powder processing, forming operations and pressure or sintering assisted hot consolidation. Powders of many alloys, compounds, metals and ceramic materials with sizes of the particles ranging from nanometers to hundred micrometers are easily available from the industrial sources or may be processed by the methods formulated over decades in PM or ceramics field (Kieback et al. 2003).

Liu et al. (2008) have extensively worked on W-Cu FGM's. They have shown that it is difficult to process W-Cu graded materials by liquid phase sintering following mechanical alloying process with nearly full density. Therefore, by increasing the sintering temperature and holding time, the quality of sintering in W-Cu composites can be improved. It was revealed that the structural homogeneity and changes in the initial composition design was developed. To overcome this particle size adjustment method

was used wherein to promote sintering density, two kinds of powders with different particle sizes are added to powder mixtures. This caused production of W-Cu graded heat sink materials to be synthesized nearly with full density at a sintering temperature of 1060⁰C, pressure of 85 MPa and with holding time of 3hrs.

Nemat-Alla et al. (2011) investigated that to overcome the limitations of transition joints of aluminum/steel FGM's. Investigations and manufacturing of aluminum/steel FGM's by PM technique were carried out. Various samples with different layers of aluminum/steel FGM were compacted by using steel die and punch at the same compacted pressure and sintered temperature. It was revealed that by increasing the number of layers in steel/aluminum FGM can reduce the occurrence of sharp interfaces between layers and hence produced FGM instead of FG layers material.

2.3.2 Deposition techniques

The process of applying a thin film of material on a substrate layer or on a deposited layers is known as deposition techniques. It can be classified in to two types.

1. Chemical Deposition
2. Physical Deposition

Tronche and Fauchais (1987) studied the wear resistance of hard coatings of Cr₂O₃ and WC-Co, plasma sprayed on aluminum substrates. The authors studied the composition, microstructure, porosity, mechanical and thermal properties of the coating. The study concluded that the coatings greatly alter the surface properties of Al alloys and when the thickness is 0.3 mm or greater. (Tronche and Fauchais 1988) also studied the frictional behaviour against steel of the coated specimens and concluded that a minimum thickness of 0.3 mm and an adhesion coating of at least 20 MPa had enabled the substrates to sustain loads of up to 600 N and also the wear rates were low.

Fu et al. (1997) studied the wear behaviour of laser treated plasma-sprayed ZrO₂, ceramic coatings on Al alloys. The results revealed that the roughness and porosity of the coatings were significantly reduced after the laser treatment. It was also shown that the bonding strength was increased apparently by the remelting process. However, there were wide

network cracks, as well as a few large bubbles in the laser-treated coatings. The Non-lubricated pin-on-disc wear results revealed that the wear resistance was significantly improved after laser treatment when compared with the sprayed ceramic coatings.

Beal et al. (2006) showed that selective laser sintering technique works with the fine layers of powder deposited over a platform. In this process each layer is sintered selectively from the energy delivered by the laser beam. Therefore, the laser beam sinters a new layer adding it to the previous one and the process is repeated until the part is built. Direct metal laser sintering technique is based on the similar process of selective method but it employs the power of the laser to fully synthesize the powder, without the necessity of special post processing in an oven to enhance the density of the part. Laser cladding technique works by spraying the powder with a gas shield over a high power-density laser spot. Selective laser fusion works with the finely powdered layers which is spread over a platform and are melted fully layer by layer by the laser scanning.

Gibbons and Hansell (2007) investigated a range of coatings using atmospheric plasma spraying and HVOF techniques for the purpose of protection and upgradation of aluminum injection mould tooling. A wide spectrum of thermal spray coatings were evaluated covering pure ceramics (alumina, zirconia, chromium oxide), monolithic materials and the particulate composites, pseudo alloys and metal ceramic composites. They concluded that HVOF process provided better bond strengths for this application.

Sahu et al. (2010) worked on the synthesizing, characterization and the response of erosion wear for a new class of metal ceramic composite coatings deposited by plasma spraying on Al substrates. Fly ash coatings premixed with Al powder in different proportions of weight at a varied plasma torch power levels ranging from 9 to 18 kW DC were formulated. The coatings were characterized in terms of interface adhesion strength, thickness and deposition efficiency. Therefore with 15wt% of aluminum content in the fly ash aluminum mix, the maximum adhesion strength of 34.5 MPa was recorded. The study also revealed that the impact velocity was the most significant factor which has influenced the erosion wear rate of the coatings.

2.3.3 Electro-magnetic separation Technique

Song et al. (2005) developed a new process for in situ multilayer FGMs called electro-magnetic separation method. The principle behind this method is that when the molten metal is subjected to an electro-magnetic field, it results in electro-magnetic force in the liquid metal. Due to lower electrical conductivity, smaller force will be induced in the primary Si particles in Al-Si alloy. Hence when the melt comprising of primary Si particles is exposed to the electromagnetic field, due to the differences in the electrical conductivity between the primary Si particles and the parent melt, electro-magnetic archimedes force will be induced on the primary Si particles. During solidification, when the temperature of the melt is below the liquidus temperature, primary Si particles from the parent melt will precipitate and then progress with a particular speed in a direction of the resultant force to the one side of the sample. Hence with further decreasing temperature, primary Si particles precipitate on one side of the sample. Therefore, by controlling the electromagnetic force and solidification rate of the melt, the desired distribution of the primary Si particles can be achieved and the in situ FGM's are produced. Based on this in-situ multi-layer process, FGM's are produced using alloy Al-22wt%Si-3.9wt%Ti-0.78wt%B . Results revealed that there are three layers which has been classified as,

- (i) The layer of the primary ternary intermetallic compound.
- (ii) Al-Si-Ti particles with rich Si.
- (iii) The layer of Al-Si eutectic structure and layer of the primary Si particles.

In the ternary Si rich intermetallic compound, Al-Si-Ti particles are formed above 700⁰C, the precipitation of Si particles takes place in the range of eutectic temperature from 720⁰C to about 577⁰C and therefore eutectic reaction occurs at the eutectic temperature. Therefore in the in-situ multilayer FGM, the interfaces between the layers revealed the gradient transition in the microstructure from one layer to another. By using the above technique (Song et al. 2007a; 2006) produced Al/Mg₂Si alloy FGM's. In this work the authors have analyzed the process parameters such as preheating temperature of the mold, electromagnetic force, and melt temperature. It was shown that when the

electro-magnetic force increases in the melt, the maximum volume fraction of primary Mg_2Si particles increases in the lower part of the sample and therefore, the length of the particle free region increases. As a result the gradation in the FGM increases with the increase of electromagnetic force. Moreover, size of the particle decreases with the increase in electro-magnetic force. When the mold temperature is increased, the volume fraction of the particle packed regions increases resulting in the shorter length of the particle packed regions. The change in the pouring temperature from $750^{\circ}C$ to $850^{\circ}C$ showed no effect on the volume fraction distribution of primary Mg_2Si particles. Al-Si FG alloy with microstructure showing a gradation from hypereutectic to hypoeutectic structure through intermediate eutectic region from one side of the sample to the other has been successfully produced (Song et al. 2007a).

The sample yielded gradation in volume fraction of Si particles and the hardness. In continuation of work on electro-magnetic separation technique to fabricate Al/ Al_3Ni FG alloy, Song et al. (2007b) investigated the distribution of primary particle and the alloy composition effects on microstructural and hardness gradient. Three compositions were investigated; Al-12wt%Ni, Al-17wt%Ni, and Al-23wt%Ni. The result shows that the size of primary Al-3wt%Ni particles and volume fraction in the sample are of gradient distributions from one side to the other. It was revealed that the particle volume fraction in Al-17wt%Ni sample is highest among all compositions. It is reported that major axis of the primary Al_3Ni particles at the lower part tends to be perpendicular to the direction of electro-magnetic archimedes force. However, orientation structure of primary particles is in random manner due to the small effect of the electromagnetic force in the upper part.

2.3.4 Centrifugal casting

The centrifugal casting process differs from that of the conventional casting processes in which, the gravitational force is enhanced by spinning the mold. In general, the segregation is caused by the density-difference between the particles and melt. However, due to the difference in material density, material with compositional gradient can be achieved (Watanabe et al. 1998). Centrifugal casting is primarily used for obtaining the cylindrical parts. The two basic types of casting machines which are used for the

synthesizing the centrifugal castings are:

- (i) Horizontal axis
- (ii) Vertical axis machines.

Horizontal axis machines are generally used to make tubes, pipes, bushing, cylinder liners and cylindrical or tubular castings which are of simple shapes. The scope of applications of a vertical axis machines is substantially wider: pulley sheaves, gear blanks, wheels, electric motor rotors, impellers, plugs, valve bodies, brackets, etc. In vertical axis machines, castings which is not of cylindrical shape, or even symmetrical, can be made. Centrifugally cast components have a superior degree of metallurgical cleanliness and homogeneous microstructures, and also they do not possess the anisotropic properties which is evident in welded/rolled or forged parts (Royr and Vasseur 1988).

Centrifugal casting is usually associated for obtaining FG materials through the metallic materials or composites which have high density difference and low solubility of different phases in the same alloy (Suresh and Mortensen 1998). The compositional gradient developed by the centrifugal technique is influenced by the density difference between the particulates and a melt, size of the particle, applied G number, mean volume fraction of particulates, viscosity of the melt, thickness of the fabricated ring and solidification time of the melt (Watanabe et al. 1998). It is clear that both viscosity and density are the material constants and therefore the volume fraction and thickness of the cast are the constants of synthesized products. Moreover, solidification time and the applied G number indicate a mutual relation and the other easily changing parameter for controlling the graded composition is the size of the particle. Intermetallic compound particles could also be pertinent for the centrifugal technique as dispersed particles. Developing of intermetallic compound particles dispersed FGM's by centrifugal casting technique can be categorized into two types based on the relation between the processing and liquidus temperature of the master alloy (Watanabe et al. 2005).

Sequeira et al. (2007) investigated that as the volume fraction of the Al_3Ti platelets precipitates in the outer region of the ring. In case of larger applied G specimen, steeper distribution profile of the Al_3Ti platelets is formed. It is therefore, noticed that Al_3Ti

particulates along with their platelet planes are oriented close to perpendicular in the radial direction of a ring. As the mean volume fraction and platelet size increases, the orientation of graded distribution becomes steeper. The effect of centrifugal radius and mold rotation speed on microstructure showed that the size of the grain decreased gradually with increase in the centrifugal radius and also at the same radius for higher rpm. The grain size was finer for higher rpm compared to that of low rpm. It was concluded that the reason for the above phenomenon is the combined effect of the centrifugal force, convective flow and mechanical vibration (Sui et al. 2010).

Chirita et al. (2008) revealed that the influence of centrifugal force has yielded significant increase in rupture strength and in rupture strain when compared to gravity casting. Even though the vibration is not directly related with the centrifugal castings, it is associated forever with the centrifugal process due of the inherent vibration of the equipment. Hence, it is important to consider that, this feature may also have an significant influence on mechanical and tribological properties.

2.3.5 Centrifuge casting

The influence of L/D (Length to Diameter) ratio of the Al-Si based FGM is investigated for microstructure and hardness along the length of the cast. Three L/D ratios: 0.5, 1.0, 1.5 were cast with the centrifuge casting technique. Microstructures revealed that primary Si enrichment was largest in 1.5 ratio compared to other two. Hardness value of the FG cast were examined at the outer and inner region and it was found that gradation of hardness value was more in 1.5 case. High volume fraction of primary Si was 26% in the outer region and an hypoeutectic structure in the inner region (Kiran et al. 2011).

Centrifuge casting process has been used to synthesize Al-Si based FGM's. Various process parameters determine the distribution of phases and the microstructure in the casting. These parameters include the initial concentration of alloying element and size of the particle, the centrifugal force, cooling rate, solidification rate. it was found that for a particular mold temperatures and melt by increasing the rotation speed of the mold, segregation of the primary Si particles at one end of the cast will be enhanced (Aithal 2013).

2.3.6 Directional solidification

Directional solidification (DS) is a processing technique in which a molten metal cools in a mold and solidifies. The volumetric shrinkage of the melt is categorized in three stages:

- (i) liquid contraction
- (ii) Solidification contraction
- (iii) Solid contraction

Liquid contraction takes place when the melt cools from the temperature at which it is poured to the temperature at which solidification begins. Solidification contraction occurs during the time at which melt is transformed from liquid to the solid state. Solid contraction occurs when the solidified metal is cooled from the solidification temperature to the room temperature (Jain 2003).

Seah et al. (1996) investigated that Aluminum composites freezes over a wide temperature range and are very difficult to feed during the solidification. Due to the long freezing range of alloy castings, the porosity caused due to the pasty type of solidification can be reduced effectively by the use of chills. Chills are the metallic inserts used to extract heat at a faster rate and therefore inducing directional solidification. Therefore chills are used widely by the foundry men for the production of quality castings.

The important requirement of the chill is that it should not melt. Therefore, the melting temperature of the chill must be sufficiently higher than the casting metal. The chills have been classified in to two types depending on their location.

- (i) External chill
- (ii) Internal chill

External chills are those which are placed at the surface of the castings which is presented in Figure 2.3(b). It is further classified in to touching and non-touching chills. Internal chills are those which are placed inside the casting and it becomes a part of the casting which is presented in Figure 2.3(a).

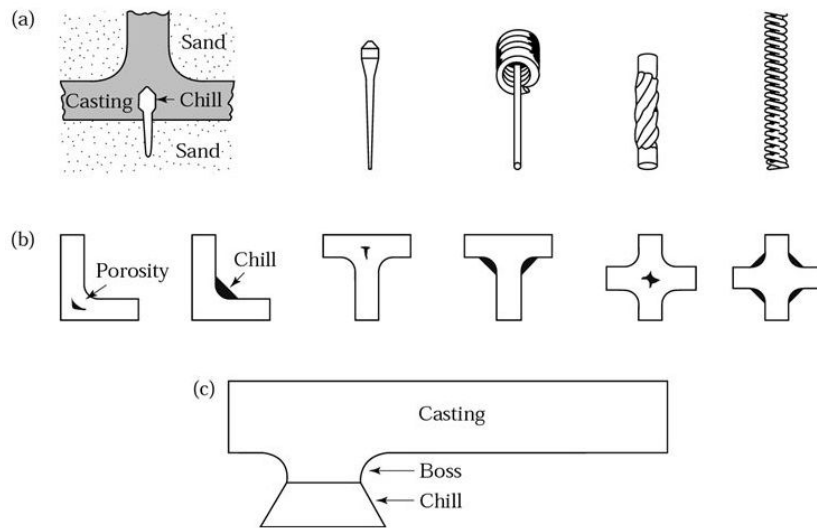


Figure 2.3 Types of chills (a) Internal chill (b) External chill (c) Location of chill (Kalpakjian and Schmid 2003)

2.3.6.1 Purpose of chill

The chills are best used in

1. Removing excess heat locally, resulting in a lower sectional modulus.
2. Promoting directional solidification.
3. Obtaining a particularly structure locally with
 - Finer grain size
 - Increasing hardness and wear resistance.
 - Less porosity
 - Increasing pressure tightness
4. Avoiding hot cracks

Kurz and Fisher (1986) showed that chills are used to extract heat from a casting to produce a fine microstructure, to improve metal flow in a complex pattern or to enhance localized or DS. Growth rate takes place in a direction which is parallel to and opposite to that of the direction of heat flux which impacts the grain size, secondary dendrite arm spacing and mechanical properties of the alloys. Leela and Rao (2012) reported that

chill material has a great influence on microstructure of the castings. It was found that by using copper chills finer structure and better mechanical properties can be obtained. Contrarily, using stainless steel and cast iron chills gave rise to a coarse structure with reduced mechanical properties.

2.3.6.2 Heat diffusivity and volumetric heat capacity

The ability of the material to extract the heat from the melt has been described as heat diffusivity (Campbell 2011).

$$\rho * c * k \quad (2.1)$$

where ρ is the density of the material, c is the specific heat and k is the thermal conductivity of the material. This is not to be confused with thermal diffusivity

$$\rho^{-1} * c^{-1} * k \quad (2.2)$$

Instead, it is a parameter which is obtained when one solves the case of unidirectional solidification of a metal. The heat diffusivity describes the material when the mold is infinitely thick. When cast iron or graphite chill is used, the full chilling potential is not utilized. The cooling rate of limited chill thickness is reduced since it becomes saturated with heat. The amount of heat capable of being absorbed is described as volumetric heat capacity (VHC). The efficiency of the chill is further dependent on VHC of the chill which takes in to account the chill volume, density and specific heat of the chill material (Hemanth 2000) and is given by

$$VHC = \rho * C_p * V \quad (2.3)$$

where ρ is the density of the chill material, C_p is the specific heat of the chill, V is the volume of the chill. Among the various commonly used chills, copper was found to have better heat extraction rate, thereby steep temperature gradient can be established promoting DS (Hemanth 2006; Hiremath et al. 2018; Ramesh Babu et al. 2018).

Like the monolithic materials, the properties of FGC's are largely dependent on solidification behavior, which is dictated by the thermophysical properties of the chill/melt

interface. The resistance towards heat flow near the chill/melt interface usually varies with time, due to the time-dependence of plasticity of the freezing melt and growth of oxides on the surface (Rajan et al. 2007).

2.3.6.3 Chill material and size of the chill

Huang et al. (1990) presented the effectiveness of copper, cast iron and mild steel chills during the solidification of pure Al. It was revealed that chill size does not have a strong effect at the beginning of solidification, but have a significant effect after a period of time. Regardless of chill material cast-iron was found to be more effective than copper and mild steel for smaller chills. However cast-iron became less effective than copper chills as the size of the chill increased.

DS has become one of the major casting processes to develop FGM's. In this process the placement of chill at the bottom defines the degree and extent of solidification which results in high rate of solidification near the chill and gradually decreases the rate as the distance increases from the chill. Controlling the microstructure and properties along the length of the cast is one of the challenges faced in today's foundry industry. Various processing techniques have enabled to produce FGM's. With the researchers attention increasing in developing series of processing techniques in the preparation of FGM's which includes vapor deposition, powder metallurgy, centrifugal casting, magnetic separation (Khor and Gu 2000; Peng et al. 2007; Seifried et al. 2001; Song et al. 2007a; Watanabe et al. 2001).

Mazare et al. (2010) found that an economical way of fabricating FGC's was through DS technique. Thereby, local controlled properties and soundness of the casting can be achieved by providing external chills. It is seen that in DS technique, solidification starts with lower temperature at the melt/chill interface compared to other locations of the casting (Hemanth 2014). However, DS is associated with few problems like precipitation of reinforcements from the chill/metal interface. As a result, to increase the precipitation of the reinforcements and improve the soundness of the casting an external force is required. It has been found that inducing mechanical vibrations during solidification will have a positive effect on precipitation and distribution of reinforcements (Abu-

Dheir et al. 2005; Chaturvedi et al. 2017; Chirita et al. 2009a; Fisher 1973; Hernandez and Sokolowski 2006; Ivanov and Krushenka 1993; Jian et al. 2006b; Kocatepe 2007; Rasgado and Davey 2002; 2004). Therefore influence of vibrations during solidification will promote significant changes in the microstructure , thereby exhibiting changes in mechanical and tribological properties of the casting (Abu-Dheir et al. 2005).

2.4 EFFECT OF EXCITATION SOURCE ON SOLIDIFYING ALUMINUM ALLOYS

In general, mechanical vibrations is described as the motion of particles in a elastic body or medium in alternatively opposite directions from the position of equilibrium. Pillai et al. (2004) have published an extensive survey on the effects of various sources of vibration on the resulting casting quality of a solidifying Al and its alloys. Table 2.2 presents the summary of this survey.

2.4.1 Ultrasonic vibration

A number of researchers have exploited the use of ultrasonic vibrations in melt treatment. Eskin (1998) discussed the use of ultrasonic melt treatment for spatial solidification, direct-chill casting, melt degassing, cavitation, non-dendritic solidification, fine filtration of melt, improved semi-solid deformation and for the production of Al alloys.

Jian et al. (2006a) investigated that ultrasonic vibrations could be employed to refine eutectic Si in hypoeutectic Al-Si alloys which is shown in Figure 2.4. However ultrasonic

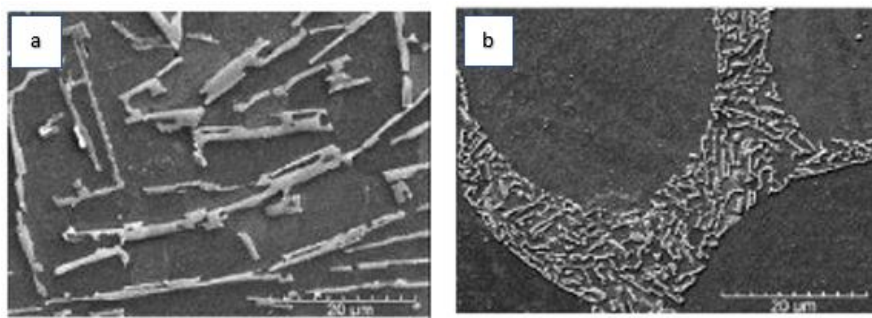


Figure 2.4 Silicon morphology: Ultrasonic vibration (Jian et al. 2006b)

vibrations have exhibited beneficial effects on the solidification characteristics of Al alloys, its commercial applications have been restricted mainly because of the difficulties encountered in the use of ultrasonic instruments on the foundry floor(Jian et al. 2005).

Table 2.2 Effect of vibration on solidifying Al and its alloys (Pillai et al. 2004)

Sl no	Alloy	Source of vibration	Effects
1	Al	Ultrasonic vibration	<ul style="list-style-type: none"> • Degassing
2	Pure Al	Magnetostriction	<ul style="list-style-type: none"> • Grain refinement • Reduced gravity segregation of FeAl₃
		Lateral vibrations (2Hz)	<ul style="list-style-type: none"> • Reduced pipe formation • Reduction in solidification time
3	Al-12wt% Si	Lateral vibrations (2Hz)	<ul style="list-style-type: none"> • Reduction in solidification time with rise in eutectic temperature by 4K. • Reduction in eutectic cell size
4	Al-20wt% Si	Low frequency melt agitation	<ul style="list-style-type: none"> • Significant reduction in gas content.
5	Light alloy (500 kg of Al)	Ultrasonic vibration	<ul style="list-style-type: none"> • Reduction in porosity . • Reduced gravity segregation of FeAl₃. • Improved degasification
6	Al- 8.5wt%Si- 1.75wt%Cu	Ultrasonic vibration at 990K	<ul style="list-style-type: none"> • Increased hardness .
7	Al-6/11/15 Cu	Mechanical vibration	<ul style="list-style-type: none"> • Improvement in tensile strength.
8	Al alloy	Combined effect of magnetic field and passing of AC through the molten metal	<ul style="list-style-type: none"> • Distribution of inclusions. • Grain refinement.
9	Al - 4.5wt% Cu	Lateral vibrations (2Hz)	<ul style="list-style-type: none"> • Reduction in solidification time. • Shrinkage elimination. • grain refinement.

Yao et al. (2011) studied the influence of ultrasonic vibration on solidification structure and properties of Mg-8Li- 3Al alloy. The results showed that the morphology of α -phase was modified from coarse rosette-like structure to fine globular one. Corrosion resistance of the alloy was improved compared with the alloy without ultrasonic vibration with ultrasonic vibration for 90 seconds. Tensile strength and elongation of the alloy was enhanced by 9.5% and 45.7% respectively with ultrasonic vibration.

2.4.2 Electro-magnetic vibrations

As the name indicates, the electro-magnetic vibrations comprises of two different force fields, an alternating electric field and a stationary magnetic field. When a stationary magnetic field with current density J , magnetic flux density B and an alternating electrical field with a frequency F and is applied to a melt, a vibrating electromagnetic body force with a density

$$F = J * B \quad (2.4)$$

is induced inside the melt. This force sets the melt into vibration with a frequency equal to the frequency of the alternating electrical field, vibrating normal to the plane of B and J (Radjai and Miwa 2000). Due to the induced force and the applied magnetic force, another electro-magnetic force is established inside the melt, This force is partly rotational and stirs the melt (Radjai and Miwa 2000). GUO et al. (2014) imposed

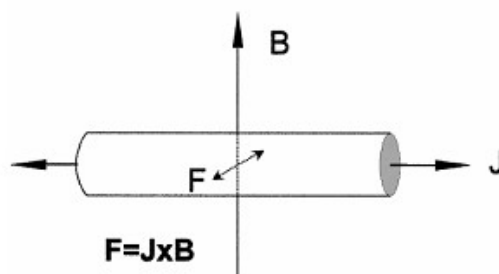


Figure 2.5 Direction of vibrating force F formed by the action of the stationary magnetic field B and alternating electric field J (Radjai and Miwa 2000)

electro-magnetic vibrations on an Al-7wt%Si alloy and reported that with increasing the intensity of the vibrations, the primary α -Al dendrites approached a globular shape of about $25 \mu\text{m}$ in size. Shi-jie et al. (2006) revealed that microstructure of the conventional direct chill cast ingots exhibited relatively fine dendritic grains at the surface area, coarse

dendritic grains at half the radius and large equiaxed dendritic grains at the center. However under the influence of electromagnetic vibration, the microstructure of the castings were refined significantly, especially those at the surface and at the center.

2.4.3 Mechanical vibrations

In this technique, the entire mold is set into vibration by means of a vibration source. Even though, the use of mechanical vibrations allows limited degrees of freedom to the user, it is one of the most favorable technique of inducing vibrations to solidifying melts due to its ruggedness and the simplicity of the equipment. Campbell (2011) reported that mechanical vibrations during the solidification of the melt alloy enhances the mechanical and corrosion properties. Dommaschk (2003) reported that the dependence of the castings wall thickness on casting characteristics could be minimized with the use of mechanical vibrations.

Bast et al. (2004) reported that the Al12wt%Si alloy showed large differences during solidification of vibrated and non-vibrated samples. As shown in Figure 2.6, a non vibrated samples shows a clear undercooling. Whereas, the vibrated sample solidified at a faster rate without undercooling. Also, the influence of vibration has caused refinement in grain texture compared to the test without vibrations has central globular grain and columnar dendrites. Kocatepe and Burdett (2000) reported that applying vibrations with a frequency of 15 to 41.7 Hz and an amplitude of 0.125 to 0.5 mm to Al-12.3wt%Si alloy. It was found that at 41.7 Hz the solidification time of the casting was reduced by 24%, grain size was reduced by 52% and pipe volume was reduced by 55% as compared to the non-vibrated casting. Kocatepe and Burdett (2000) also investigated that the due to the influence of vibrations there is an increase in diffusivity of silicon in the liquid resulting in coarsening of the eutectic silicon. It was also observed that grain refinement can be attributed mainly to the fragmentation of dendrites and the growing crystallites during the early stages of solidification.

Abu-Dheir et al. (2005) used an electromagnetic shaker to induce mechanical vibrations in a permanent mold. The mold was vibrated with a frequency ranging from 100 Hz to 2 kHz and amplitudes ranging from 3.73 μm to 199 μm for AA356 alloy. It was revealed

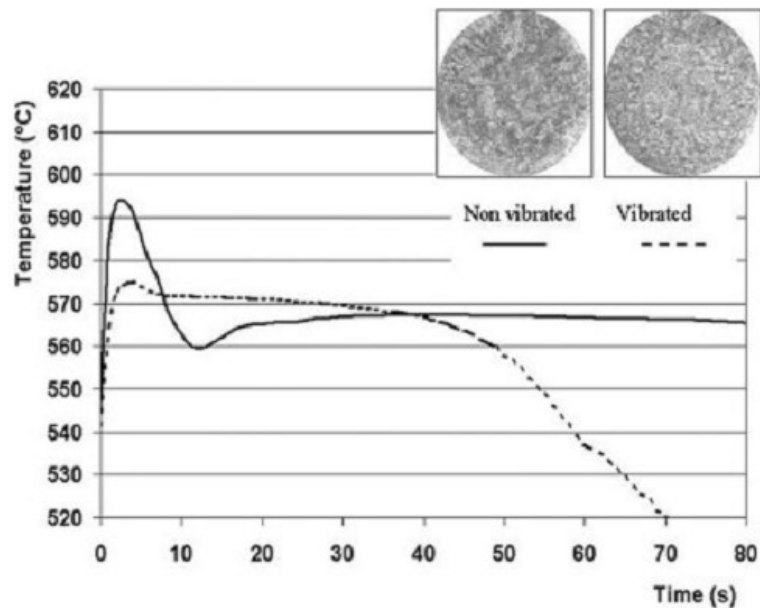


Figure 2.6 Cooling curve of Al12wt%Si (Bast et al. 2004)

that vibration homogenizes the temperature distribution in the mold and promotes a faster cooling rate. Therefore, this has manifested itself in a more uniform dendrite structure and less porosity in the castings from which the degree of fragmentation increased with the amplitude of vibration. It was also reported that the eutectic structure was transformed from flaky structure to a more fibrous structure as shown in Figure 2.7 with increasing amplitude up to $149\mu\text{m}$. Beyond $149\mu\text{m}$, the fibrous eutectic silicon agglomerated to form a structure of coarse flakes. Fisher (1973) showed that reduced solidification time

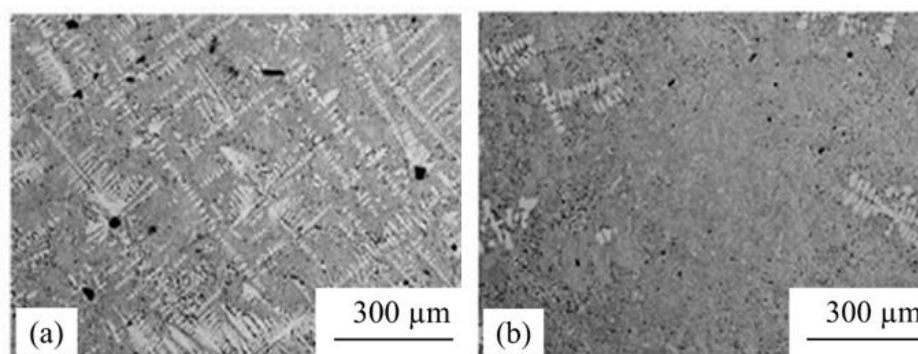


Figure 2.7 Silicon Morphology: Mechanical Vibrations (Abu-Dheir et al. 2005)

and fragmented primary dendrites with thicker dendrite arm thickness were obtained for Al-8wt%Si alloy by transforming rotary motion to rectilinear vibrations at 100

Cycles/min ($\approx 2 \text{ Hz}$). Also when the same level of vibration was applied to Al–12% Si alloy, it was revealed that there is a tendency of coarsening of eutectic Si and a reduction of eutectic cell size from 5 to 1.6 *mm*.

Omura et al. (2009) studied the significance of mechanical vibration on macrostructure and mechanical properties of AC4C Al alloy castings. In this study the ingots were allowed to solidify at different frequencies of vibration. In comparison with the grains formed in the as-cast state, it was revealed that the grains in the inner area of specimen became finer with columnar structure in its outer region under all frequencies of vibration. Casting defects were observed to have reduced and became smaller under the influence of vibration. Chirita et al. (2009b) studied the influence of vibrations on mechanical properties and solidification behavior of Al-18wt%Si. It was reported that heat-transfer mechanism which is acceleration dependent was found to be responsible for the shift in mechanical properties.

2.5 INFLUENCE OF GRAPHITE REINFORCEMENTS IN ALUMINUM ALLOYS

Al alloys with graphite as a reinforcement have been used as a self-lubricating materials due to the superior lubricating property of the graphite during sliding. Self-lubrication is the ability of the material to offer lubrication by transmitting the embedded solid lubricants (Dorri Moghadam et al. 2015; Omrani et al. 2015) such as graphite (Clauss 1972; Shanmughasundaram and Subramanian 2013) to reduce COF, wear rate in the absence of external lubricant. Graphite in Al alloys act as a solid lubricant at contact interface, thereby enhancing the tribological properties of the composite compared to the un-reinforced Al matrix (Srivastava et al. 2012).

The biggest challenge in promoting Aluminum/graphite composites in industrial applications is the unfavorable effects of graphite on mechanical properties. It was reported that by increasing the amount of graphite in the matrix, the mechanical properties of the graphite reinforced Al composite decreases (Baradeswaran and Perumal 2014). The influence of graphite content on the mechanical properties of a self-lubricating Al composite is presented in Figure 2.8. Low hardness and high brittleness of graphite particulates

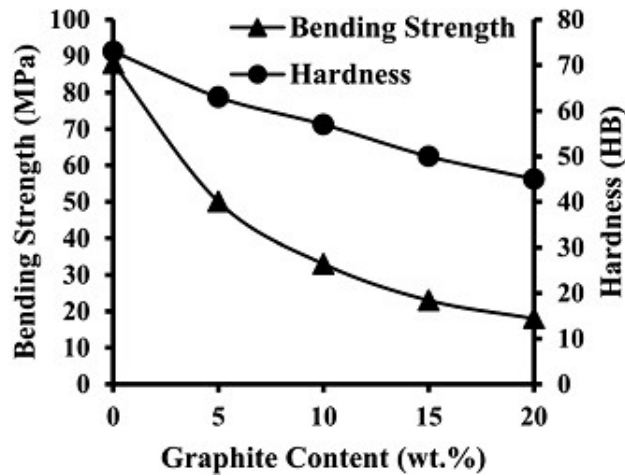


Figure 2.8 Influence of graphite content on mechanical properties of MMC's (Jinfeng et al. 2009)

with reference to Al and its alloys could reduce the mechanical properties and also plastic deformation of a composite (Baradeswaran and Perumal 2014; Shanmughasundaram and Subramanian 2013). To accomplish enhanced wear and mechanical properties of the composite and to examine the potential use of Al/Graphite composite for tribological applications, graphite particulate distribution and the interface that exists between matrix and graphite particulates should be enhanced. Also, by employing new synthesizing techniques, it is possible to enhance the properties. Hardness is one of the significant factors that influence tribological properties of self-lubricating Al composites according to Archard equation.

$$Q = K \frac{W}{H} \quad (2.5)$$

Where Q =Wear rate mm^3/km ; K =wear coefficient; W =Volume of the worn out material per distance; H =Hardness of the specimen.

Figure 2.9 shows the effects of load, hardness and graphite content on wear rate at a sliding velocity of 0.37 m/s. It is reported that the wear rate has an inverse relation with hardness, thereby the wear rate decreases with increasing hardness. It is also found that the wear rate is proportional to the applied load, and therefore wear rate increases with increasing load as shown in Figure 2.9. Earlier studies show that properties such as low thermal expansion (Rohatgi et al. 1976), excellent antiseizure effect(Vedula et al. 1988), low friction and wear (Kurita et al. 2015), high damping capacity (Rohatgi

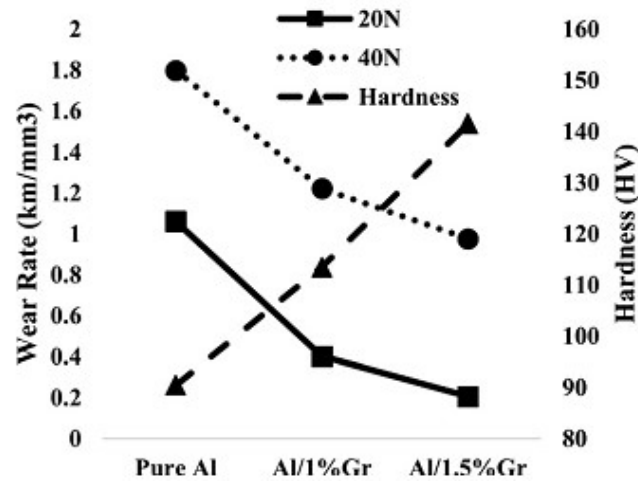


Figure 2.9 Effect of hardness on wear rate of graphite composite at a sliding velocity of 0.37 m/s (Deaquino-Lara et al. 2015)

et al. 1992) and reduced temperature rise at the worn surface are the main factors that constitute a self-lubricating Al/Graphite composite an alternative to Al alloys in a dominant tribological applications (Baradeswaran and Elaya Perumal 2013). As the Al/Graphite composites have predominant tribological behavior, which is the most desirable factor in automotive industries for the manufacturing of components such as pistons, bearings, and bushings(Rohatgi et al. 2013).

2.6 MECHANICAL AND TRIBOLOGICAL CHARACTERIZATION

Many factors have to be considered when evaluating the mechanical properties of Al-Si alloys which depend upon the processing techniques, eutectic modification and grain refinement. Based upon processing techniques, casting parameters and micro-alloying additions that promote rapid undercooling due to high heat transfer rates, and the addition of reinforcements enhances the mechanical properties. The use of Al-Si alloys as structural materials is ascertained by their physical properties which are mainly influenced by its chemical composition and the mechanical properties are influenced by its chemical composition and microstructure. The high specific tensile strength of Al-alloys are strongly dependent on its poly-phase microstructure.

Shabestari and Moemeni (2004) have explored several techniques can be used to control these microstructural features, for example by introducing special reinforcements to

refine the grain. Royr and Vasseur (1988) revealed that common solution to enhance mechanical properties of Al-Si alloys is through casting techniques . Each technique has unique aspects that interferes on microstructure and therefore influencing mechanical properties. The important mechanical property which is used routinely in design calculations is the tensile strength which are being governed by the microstructure, as well as the intermetallics and the formation of porosity.

Radhakrishna and S. Seshan (1981) investigated that the relation between any of the mechanical properties and porosity is non-linear. The shape of the non-linear graphs gives an indication of the pronounced influence of porosity on all the properties. Among the various mechanical properties measured, ultimate tensile strength is found to be the one which is most influenced by porosity, followed by the yield strength and percentage of elongation. An increase in the size of intermetallics and volume fraction also lead to a decrease in tensile properties(Chirita et al. 2009b).

2.6.1 Hardness

The term hardness is be termed as the ability of a material to resist localized plastic deformation when in contact with an indentation load. In general, hardness test comprises of pressing an indenter of known geometry and mechanical properties on the test material. Therefore, the hardness of material is evaluated through one of a variety of scales that directly or indirectly indicate the contact pressure involved in deforming the test surface. During testing, as the indenter is pressed on the material. Therefore, the hardness of the material is also observed as the ability of a material to resist compressive loads.

Brinell hardness is the most commonly used method to evaluate the bulk hardness of materials. In brinell hardness test a hard spherical indenter is pressed on the smooth surface of the test material with a fixed normal indentation load. After attaining equilibrium, the load and the spherical indenter are withdrawn from the surface. Therefore from the indented surface, the diameter of the indentation is measured using a microscope with a built-in millimeter scale. The brinell hardness is also described as the ratio of the indentation load W to the area of the contact surface of the spherical indentation which is assumed to support the load and is given as brinell hardness number (BHN) (Kuhn

et al. 2000).

The Al based FGMs fabricated through different processing techniques have reported that there is a variation in hardness from one end of the cast specimen to the other. Zhang et al. (2009) through Power ultrasonic field technique showed that for Al-18wt% Si alloy, gradation of 80HV to 55HV was obtained from outer to inner region of the cast sample with a primary Si volume fraction of 30% at the outer region. Song et al. (2007b) reported that there is a variation in hardness from 70HV to 122HV for Al-28wt%Si alloy fabricated by magnetic separation method. Rajan et al. (2007) reported that for Al-20wt% Ni alloy, the cast samples exhibited maximum hardness gradation from 55 BHN at outer periphery to 46BHN at the inner periphery followed by Al-10wt% Ni with (45-39 BHN). This gradation aspect was also clearly revealed from their respective microstructures.

Hiremath and Hemanth (2017) reported that hardness increases with increase in reinforcements. The researchers also have revealed the effect of different chill materials on hardness. Therefore, hardness results also revealed that copper chill has a significant influence on the hardness of the FG composites as compared with other chills. It is evident that the specimens prepared with the incorporation of metallic chills possess higher hardness value as compared to the specimens fabricated with nonmetallic end chills.

2.6.2 Strength

Tensile test is the most commonly used test to determine the tensile strength of materials, more so, in case of ductile materials. However, for materials that are brittle in nature, this test is extremely inaccurate due to eccentricity of loading, gripping difficulties, greater sensitivity to misalignment and position of defects (Shaw et al. 1975). With increased use of ceramic particles in composite materials, they tend to be brittle in nature. Due to this, researchers have used different techniques to determine the tensile strength.

Diametral Compression (DC) test also known as Brazilian test is more preferred than the other tests methods which includes compact hardness test, indirect tensile test and compact crushing test (Procopio et al. 2003). DC test was first proposed in 1953 to

determine the tensile strength of concrete (Wright 1955) and then gained popularity because of simplified test specimen preparation, quickness of conducting the test and simple specimen geometry (Amorós et al. 2008). This test has also been used to measure tensile strength of rock, coal, polymers, ceramics, cemented carbides, MMCs, tablets etc. (Bonollo et al. 2014; Chen et al. 1999).

The DC test is based on the fact that when a circular disc is subjected to compressive load on a diametrically opposite faces as shown in Figure 2.10, stresses are developed perpendicular to the loading direction and are proportional to applied compressive load (Fahad 1996). Timoshenko (1951) suggested that for a theoretical stress analysis of a

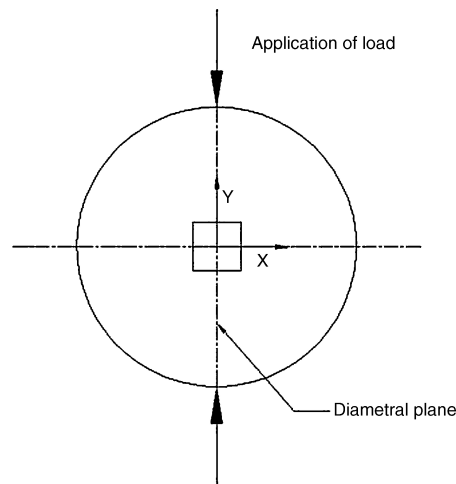


Figure 2.10 Load application in DC Test (Reddy et al. 2017)

circular disc loaded with to two opposite concentrated diametral forces, with the normal stress (σ_x) tensile and constant, while a compressive stress σ_y which is parallel to the loaded diameter and increases from $3\sigma_x$ at the center of a disc to infinity beneath the loaded points. The shear stress along the diameter plane is zero and therefore σ_x and σ_y are the principal stresses on the plane assuming a point load on the disc.

Hooper (1971) investigated that as the failure along the diametral plane is caused due to the applied load, it is assumed commonly that failure of the disc is due to tensile stress. However some researchers believed that due to high compressive stresses, failure is initiated under the load points rather than at the center as there is some disagreement about the exact mechanism of failure. In practice the load needs to be distributed over a finite area to avoid shear and/or compression failure at the loaded points. Hondros

(1959) developed an exact theoretical stress analysis for the case of pressure applied over two diametrically opposite arcs which has resulted in the finite maximum compressive stress at the point of applied load.

2.6.3 Wear

Wear according to ASTM is defined as the "Damage to a solid surface (generally involving progressive loss of material), caused by the relative motion between that surface and a contacting substance or substances". Under normal operating conditions, the changes in the property due to wear takes place in three stages:

- Primary or early stage, where rate of change can be high.
- Secondary process is a steady rate of aging process. Most of the working life of the component is comprised in this stage.
- Tertiary stage is a high rate of aging leading to rapid failure.

According to British stainless steel association (BSSA 2011) the important factors influencing wear and galling are:

- Design
- Lubrication
- Contact area
- Applied load
- Environment
- Material properties like hardness, surface finish, microstructure etc.

Literature available on the dry sliding wear behavior of homogenous Al-Si system showed that researchers have tried to optimize the Si content. It was also revealed that the transition in wear rate is a function of variations in sliding wear parameters, like applied load and sliding distance. In a study of dry sliding wear behavior of two Al-Si alloys (10.9 and 22.1%Si) against a steel counter face, two wear regimes were observed (Sarkar 1975). Clarke and Sarkar (1979) showed that the first wear regime

were represented as a mixed mode of elastic-plastic contact which also obeyed Archard's law. The second regime observed at a critical applied load, was described by gross plastic flow from which it was found that the wear rate was not directly proportional to the load. It was also noted that the hyper-eutectic alloy experienced a higher wear rate compared to the hypo-eutectic alloy. Shivanath et al. (1977) observed from the dry sliding behaviour of Al-Si alloys that wear mechanisms have been classified as oxidative wear and metallic wear.

Reddy et al. (1994) from wear studies on Al-Si alloy samples through pin on disc machine reported that three different wear regimes were identified as a function of load.

- Mild wear: The worn surface at low loads, were characterized by the formation of an iron-rich compacted debris layer.
- Severe wear: Due to the increase in load, delamination type wear mechanism was significant in which sub-surface deformation and cracking has resulted in the fragmentation of Si particles and removal of the iron-rich layer.
- Seizure wear: In this wear regime, the temperatures near the surface were high enough due to which shear strength in the sub-surface layer was lowered, thereby promoting extensive material transfer from the wearing alloy to the steel counter face.

With regard to the topographical features of worn surface of the Al-Si alloys in dry sliding, the mutual transfer of material between the steel counter face and wearing Al-Si alloy attributing to all wear regimes and gradually becomes more significant as load increases. The transition of wear regimes from mild to severe wear is related to the existence of a delamination wear process (Sarkar 1975). Reddy et al. (1994) showed that addition of (4-24%Si) improved wear resistance of Al. Clarke and Sarkar (1979) observed that wear rate increased linearly with applied pressure. It was also found that wear rate is independent of sliding velocity and coefficient of friction was found to be insensitive to applied pressure, Si content and sliding velocity.

The shear resistance and frictional force of Al-Si alloys, were the two significant con-

trolling factors exhibiting the initiation of seizure. For a given alloy subjected to sliding at different temperatures, it was observed that seizure was initiated at a sub-surface depth where the shear stress found equal the resistance to shear. The presence of Si was observed to contribute strengthening of this sub-surface region and to help inhibit bulk shear. It was also observed that seizure was associated with features like transfer of pin material to the counter face, rapid increase in wear rate, increased noise and vibration (Somi Reddy et al. 1995).

A few efforts have been made to determine the influence of Si in Al based FGM. Al-18wt%Si FGM produced by power ultrasonic method showed that wear resistance of the FGM sample decreased gradually from outer to inner and also revealed that it is in good accordance with the microstructure distribution (Zhang et al. 2009). Melgarejo et al. (2006) showed that for Al-Mg-B, wear resistance in the outer region increased with increase in hardness. The SEM analysis revealed oxidative and abrasive wear modes, the extent of which was dependent upon the content of boron. Al-(Al₃Ti+Al₃Ni) FGMs fabricated through centrifugal technique revealed that the size of the primary particles depends upon the applied G number and their location in the ring thickness. It was also observed that these materials exhibited superior wear resistance properties compared to the pure Al (Watanabe et al. 2001). Gomes et al. (2005) studied to determine the influence of lubrication using aqueous solution on Al based FGM which revealed that in the absence of lubrication while sliding, the COF were not significantly affected by SiC content. Results exhibited a lower friction and wear values as the reinforcing particles increased. It was also found that the wear rate of the FGM is not significantly affected by the presence of the aqueous solution.

It is clear from the documented literature that Al-Si alloy is the most sought of alloy for many engineering applications because of their good casting characteristics, low thermal expansion coefficient, high thermal conductivity, good corrosion resistance, and improved mechanical properties at wide temperature range. The performance of the alloys depends on the content of the Si and also on their microstructural characteristics. Not much of work has been done in achieving an Al based FGM with relatively high segregation of Si on one side using a very effective processing technique at low processing

cost. Wear of Al-Si alloy has been studied extensively in the past by varying the Si content. These studies only aimed at optimizing the content for maximum wear resistance. From the above discussion it was found that experimental findings are contradictory with regards to the role of Si content on wear resistance. Some of them reported that for wear resistance the optimum Si content is near Eutectic while some contradicted saying it is in the hypereutectic region.

It can be concluded that many mechanisms can play a significant role in the sliding wear behavior of alloys and that it is not a simple function of composition. The wear is a complex phenomenon which depends on different parameters viz., type of the matrix material, type of the reinforcement, processing technique, sliding speed, pressure, surface roughness, temperature, environment, type of friction etc (Bialo et al. 2000). As a matter of fact, the inconsistencies from the obtained results are not surprising. It was found that wear resistance is not a material property. It is always uniquely correlated with hardness or strength. It depends upon the combination of all intrinsic and extrinsic factors involved in the wear process.

2.7 SUMMARY AND MOTIVATION FROM LITERATURE SURVEY

FGM is a unique concept to accomplish a graded structure and properties within the same component which is not possible to achieve in a conventional homogenous material. Therefore, It is important to understand the influence of process parameters and different processes involved in achieving the gradation. The literature survey presented in the earlier sections of this chapter clearly reveals that considerable amount of research has been carried out on different non-ferrous alloy systems and their composites. While fabricating an FGM, one of the major requirements in terms of properties is obtaining higher hardness in one extreme of the cast sample compared to the other extreme. This feature should also assist improvement in wear characteristics of the material. Also, the maximum amount of work has been carried out in evaluating the FGMs for their mechanical and tribological properties, but it is indeed required to develop a suitable processing technique to produce FGMs with reproducible properties.

Researchers who have worked on directional solidification technique have developed the

process based on the chill material and chill length but not much of the work has been carried out considering the excitation source. This conveys the message for the need for development of a suitable processing technique for the FGM to meet the demand for lightweight materials, with suitable mechanical and tribological properties for a range of engineering applications. Very few literature is available in processing solid blocks through directional solidification technique combined with an excitation source which is very useful in automotive and aerospace sectors.

It is clear that many factors play an important role in defining the mechanical properties and tribological properties of FGMs. In order to meet the growing demand for high performance Al-Si based FGMs, it is thus essential that investigations be carried out to develop FGM's and to study the effect of process parameters on mechanical properties. The present study is focused on the optimization of process parameters during directional solidification of Al-Si alloy and Al-Si alloy reinforced with 2wt% graphite by the taguchi technique based on the obtained hardness value.

2.8 OBJECTIVES OF THE RESEARCH WORK

Looking at the continuous development in manufacturing of solid valve lifters with improved productivity the specific objectives have been derived from the literature survey.

1. To develop novel fabrication technique to synthesize FGM's
2. Optimization of process parameters to synthesize Al-18wt%Si (Without and with lateral vibrations) and Al-18wt%Si reinforced with 2wt% graphite(With lateral vibrations) based FGM through the hardness responses across the length of the cast.
3. To Study the effect of chill on solidification rate for the optimized sample.
4. To study the microstructural characterization for the optimized sample.
5. To study the mechanical and tribological characteristics of the optimized samples.

CHAPTER 3

MATERIALS AND METHODOLOGY

This chapter deals with methodology adapted and materials selected to fabricate FGM and also describes the processing technique used to synthesize FGM through directional solidification. The cast samples are obtained using unique processing technique developed to induce the lateral vibration. This chapter also deals with the experimental methods chosen to investigate the link between microstructural features, mechanical and tribological properties which is discussed in detail in the following subsections.

3.1 Al-Si ALLOY

Al-18wt%Si alloy finds extensive use in the automotive industry in the manufacturing of engine components like solid valve lifter, pistons, cylinder liners, engine heads, connecting rods. This is because Al-18wt%Si boasts excellent mechanical properties like good wettability and high strength to weight ratio making it a potential material for large scale production (Hiremath and Hemanth 2017). Therefore, in the present work to fabricate FGC for solid valve lifter application commercially available Al-18wt% Si was chosen. The methodology followed to fabricate FGC is presented in Figure 3.1. The matrix used in the present investigation were procured from Fenfe Metallurgicals, Bangalore, in as-cast condition. The chemical composition of the alloy matrix is presented in Table 3.1.

Table 3.1 Chemical composition of Al-Si alloy

Element	Si	Fe	Mg	Al
Composition (wt%)	18.0	0.1	1.0	Balance

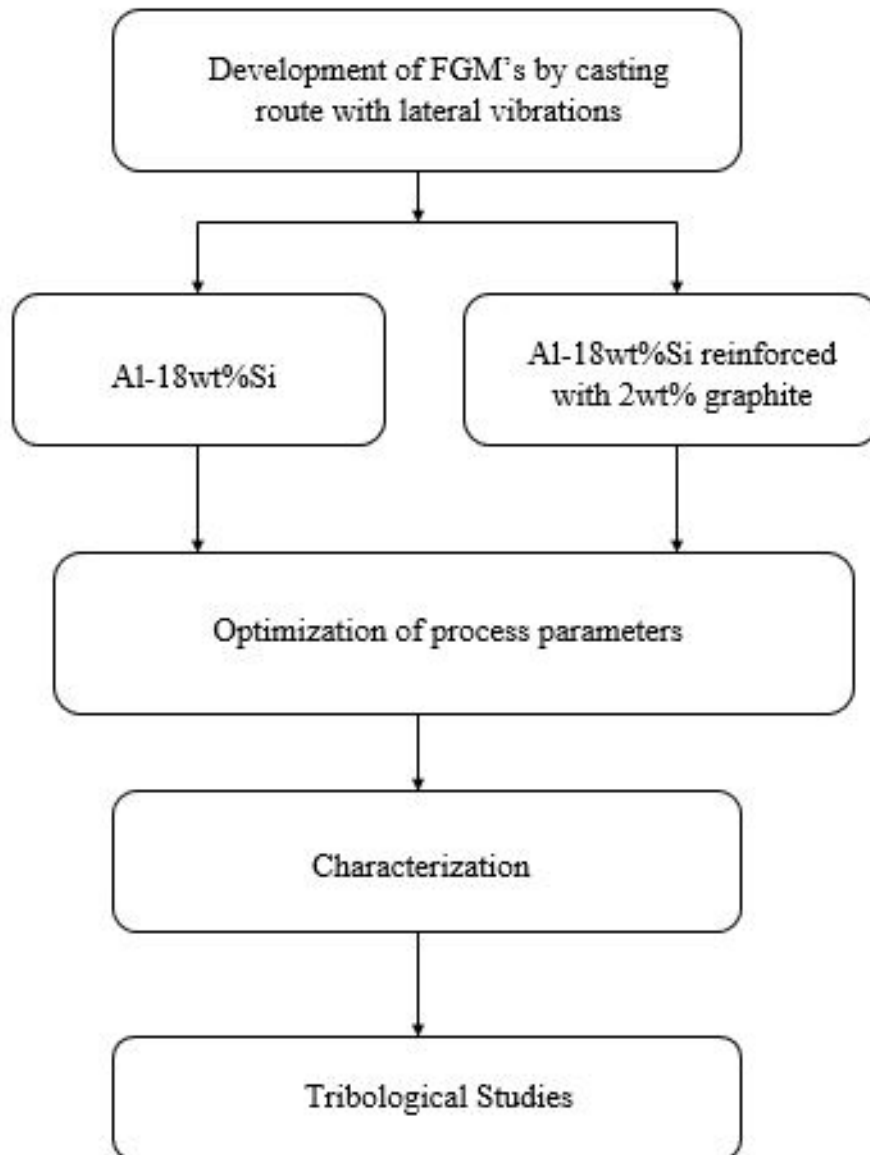


Figure 3.1 Methodology of the research work

3.2 DEVELOPMENT OF EXPERIMENTAL SET UP

FGM's are the most important innovations in the field of advanced materials. Among the various metal matrix available aluminum and its alloys are most commonly used alloys in fabrications of MMC's (Barekar et al. 2009), this is because of its excellent castability, high strength to weight ratio, thermal conductivity (Hua et al. 2017; Murty et al. 2003). It was found that addition of reinforcements to the aluminum alloy helps to achieve

high-level FGM's (Banthia et al. 2019; Radhika and Raghu 2016). Commonly used reinforcements in aluminum alloys are silicon carbide (SiC), aluminum oxide (Al₂O₃), graphite (Gupta et al. 1993; Prasad et al. 1993). Graphite in the form of particulates or fibers has been recognized as low-density, high strength material.

MMC's produced with aluminum graphite reinforced particulate represent a class of affordable materials for a variety of engineering applications in the automotive field due to improved wear and seizure resistance (Krishnan et al. 1980; Prasad and Asthana 2004; Yang et al. 2004). Some researchers (Akhlghi and Zare-Bidaki 2009; Hassan et al. 2007) have found that less dense graphite tend to float in the melt resulting in non-uniform distribution in the composites. This non-uniform distribution increases with increase in reinforcement percentage, thereby leading to reduced interaction and bonding between the matrix and reinforcement. Due to various advantages like good castability, good thermal conductivity, wear resistance, Al-Si Alloys are considered as one of the most commonly used alloys in foundry. Controlling the microstructure which results from casting to process FGM are the main challenges faced in the foundry industry which can be attained by an effective processing technique. Thereby, there is a need for the development of processing techniques. As the DS is associated with problems like precipitation, It was found through the literature that better gradation can be obtained by inducing external force. Therefore, emphasis in the present work is to develop a novel processing technique to fabricate the affordable Al-Si based FGM and to compare the properties with Al-Si reinforced with 2wt% graphite particulate FG composite because of the likely possibilities in forming a distinctly desirable composite (Ibrahim et al. 1991; Ray 1993; Rohatgi 2001). In the following subsections development of experimental set up is discussed.

3.2.1 Mold

The mold used is an insulation brick of volume $7.5 \times 7.5 \times 12 \text{ cm}^3$. A hole of diameter 2.5 cm is drilled at the center of the brick and is then cut into 2 equal halves along its length. This is done to make the removal of the cast from the mold easier. The mold is placed on the external end chill as shown in Figure 3.2 so that directional solidification is initiated when the molten metal is poured.



Figure 3.2 Insulation mold

3.2.2 Chill

Chills act as a heat sink from which heat transfer takes place between the chill/melt interface, thereby establishing a steep temperature gradient. The employment of external chill at the end of the mold is to promote directional solidification so that superior quality castings can be obtained. This is accomplished by the ability of the chill to extract heat at chill/melt interface at a faster rate, thus promoting DS (Hiremath et al. 2018). The use of end chills not only promotes DS but also has a significant influence on mechanical properties (Wankhede et al. 2019). In the present work to study the influence of chill during solidification three different chill materials as shown in Figure 3.3 with varying volumes which is presented in Table 3.2 were selected. However, volumetric

Table 3.2 Volume of the chills used in the present work

Sl no	Particular	Volume in cm^3
1	Chill-1	8.5*8.5*3
2	Chill-2	8.5*8.5*5
3	Chill-3	8.5*8.5*8

heat capacity which defines the rate of solidification has a significant influence on the properties of the casting (Hemanth 2002). The volumetric heat capacity of the chills used in the present study is presented in the Table 3.3

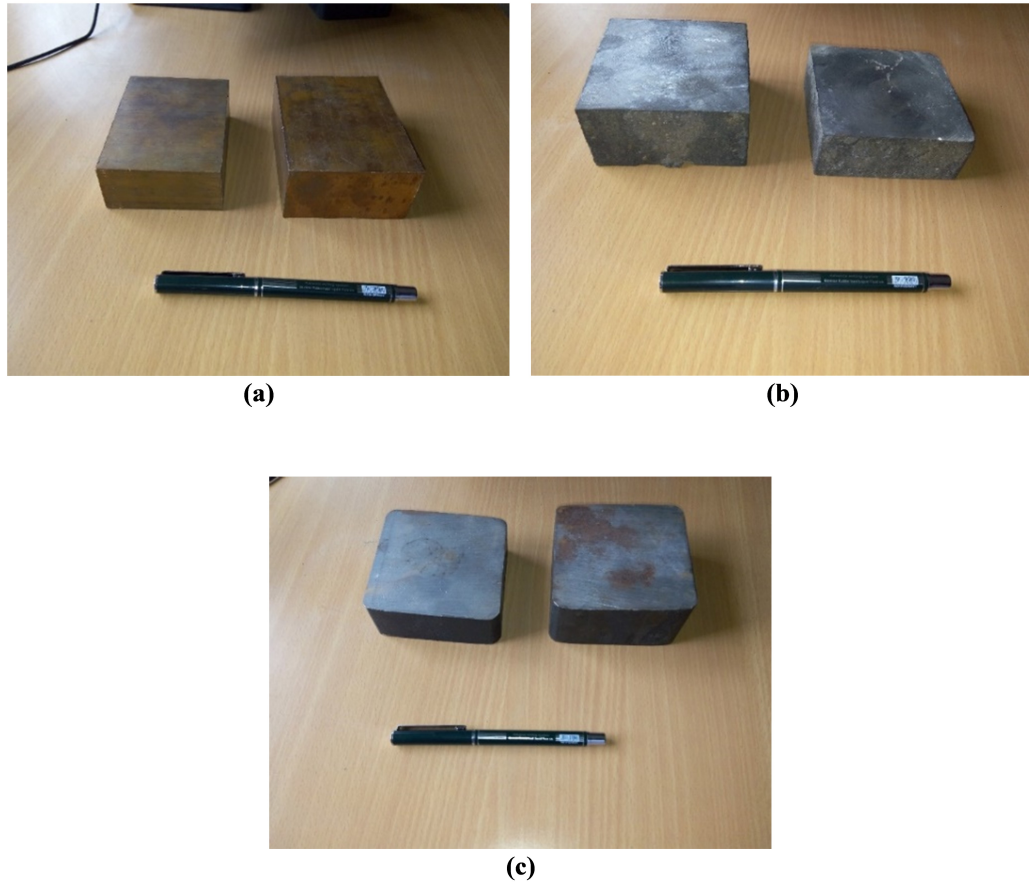


Figure 3.3 Chill: (a) Copper (b) Mild steel (c) Cast iron

3.2.3 Lateral vibration set up

Use of vibrations to directional solidification will have the advantage of promoting grain refinement. A group of researchers found fragmented particulates in the microstructure and reduced solidification time under the influence of lateral vibration at low frequencies (Fisher 1973). In another study, it was found that size and amount of pores increased with increasing frequencies (Kocatepe 2007). A study on the effect of low frequency vibrations concluded that mechanical vibrations improve the UTS, hardness and it was also found that there was significant reduction in gas content with low frequency melt agitation (Chirita et al. 2009b). Thus it is clear that vibration promotes changes in microstructure and consequently improve mechanical properties either by decreasing or increasing it.

Table 3.3 Volumetric heat capacity of chill materials

Chill Material	Density(ρ) kg/cm ³	Specific Heat(C_p) J/kg-k	Volume (cm ³)	VHC (J/k)
Copper	8.9	0.393	216.75	758.12
		0.393	361.25	1263.54
		0.393	578	2021.67
Mild Steel	7.85	0.42	216.75	714.62
		0.42	361.25	1,191.04
		0.42	578	1,905.66
Cast iron	7.61	0.4	216.75	659.78
		0.4	361.25	1,099.64
		0.4	578	1,759.43

Therefore, based on the literature survey and preliminary investigations, it was decided to maintain the constant frequency of 10Hz. From literature studies, it is observed that not much work has been done to fabricate FG composites through directional solidification coupled with lateral vibrations. Therefore, in the present work an attempt has been made to develop a novel processing technique to synthesize FGM and to study the influence of vibrations on microstructure, mechanical and tribological properties. The lateral excitation experimental set up consist of mold, chill, compression springs, eccentric motor, nuts and bolts, side plates which is shown in the Figure 3.4. The mold-chill set up as shown in Figure 3.2 is placed in the tray which is packed around with insulator. The carrier tray is fitted with rollers so that linear motion across the guide ways is produced. One end of the tray is fastened to the connecting rod which is coupled with motor. On the other side of the tray, compression springs are placed so that a restoring action is produced. The fabricated experimental se up is shown in Figure 3.5

3.2.4 Positioning of thermocouple

Thermocouple is used to measure the temperature at the different locations of the casting during the process of solidification. In the present work K-Type thermocouple is used because of its ability to measure high temperature up to 1350 °c. In the present work

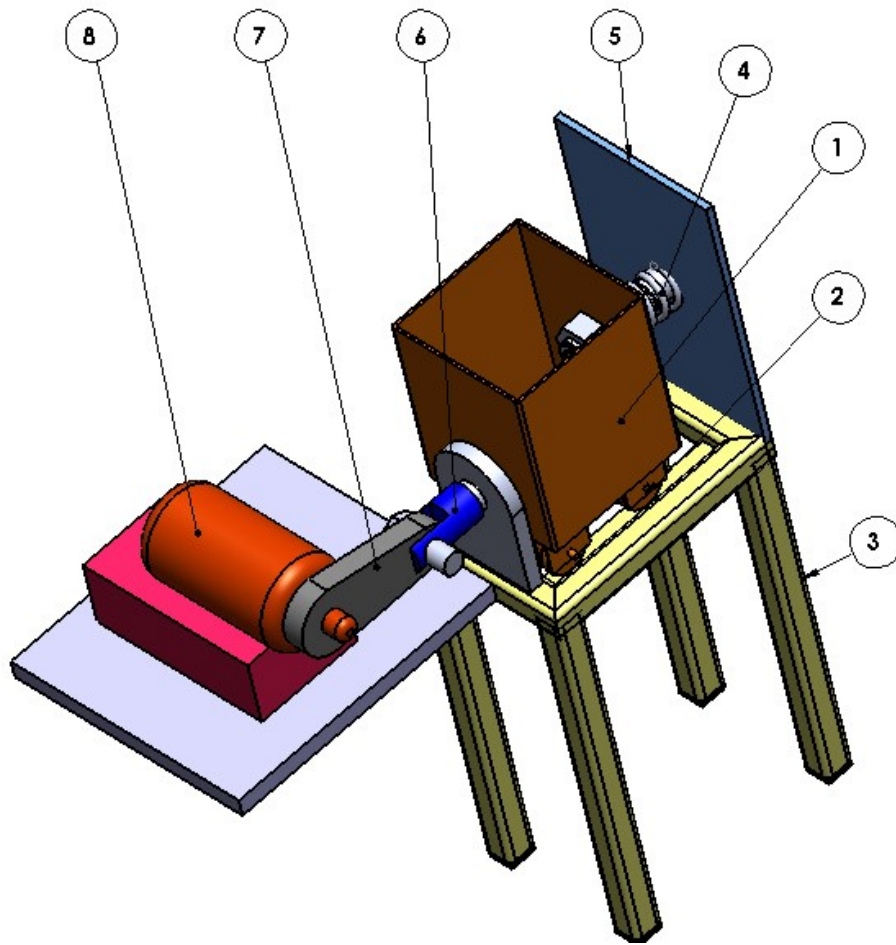


Figure 3.4 Lateral vibration set up



Figure 3.5 Experimental set up

Table 3.4 Parts of lateral vibration set up

Item number	Part name
1	Carrier tray
2	Tray wheel
3	Base frame
4	Spring
5	Side plate
6	Connecting rod and Tray Connector
7	Connecting rod
8	Motor

the thermocouples are positioned at top and bottom portion of the mold as shown in Figure 3.6. The specifications of thermocouple is shown in Table 3.5.

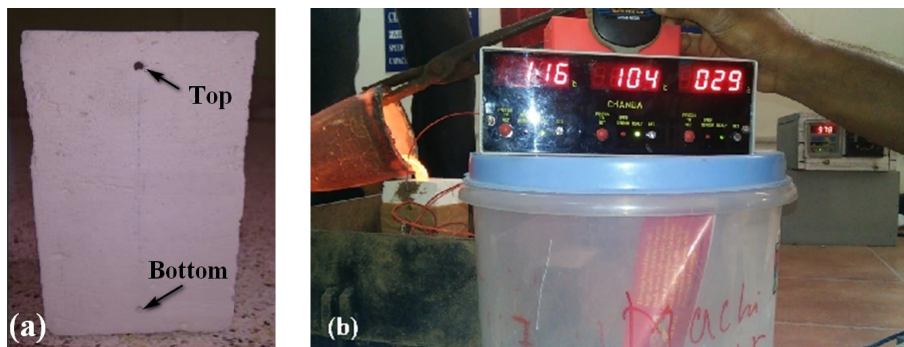


Figure 3.6 Thermocouple positioning (a) Location (b) Data acquisition system

Table 3.5 Specifications of a thermocouple

Type	Material	Temperature range in $^{\circ}\text{C}$	Percentage error
K	Chromel (+) Alumel (-)	-200°C to $+1350^{\circ}\text{C}$	± 1.1

3.2.5 Processing of FGM through DS coupled with vibrations

Figure 3.7 shows the schematic diagram of DS set up subjected to lateral vibrations, it comprises of mold made of insulation brick with a volume of $8.5\text{cm} * 8.5\text{cm} * 12\text{cm}$. The mold is cut in to two equal halves for easy removal of the material, A through

hole of 2.5cm diameter is made longitudinally. The mold is placed on a chill, to study the solidification behavior of the melt, two thermocouples of K-type were located at the bottom and top portion of the mold. Thereby, effect of chill on solidification is studied by connecting the thermocouples to the data acquisition system by calibrating the thermocouples at 1°C . The DS unit comprising of mold and chill is placed in a lateral vibration unit consisting of a vibrator and spring. The vibrator is attached to one end of the spring, whereas the other end of the vibrator is coupled to the motor through the connecting rod resulting in one directional lateral vibration as the vibrator is constrained to move in one direction. The lateral vibration set up is set in to vibrations with a frequency of 10Hz .

The melt comprising of Al-Si alloy matrix and graphite particles is poured in to the mold placed in vibration set up. The castings obtained are of solid cylinders with 25mm in diameter and 120mm in length as shown in Figure 3.8a. In order to validate the gradation in the structure, samples were cut cross-sectionally at top and bottom portion of the cast as shown in Figure 3.8b. The above procedure is repeated for different chill materials and different volumes to fabricate FGM's with Al-18wt%Si alloy and Al-Si reinforced with 2wt% graphite.

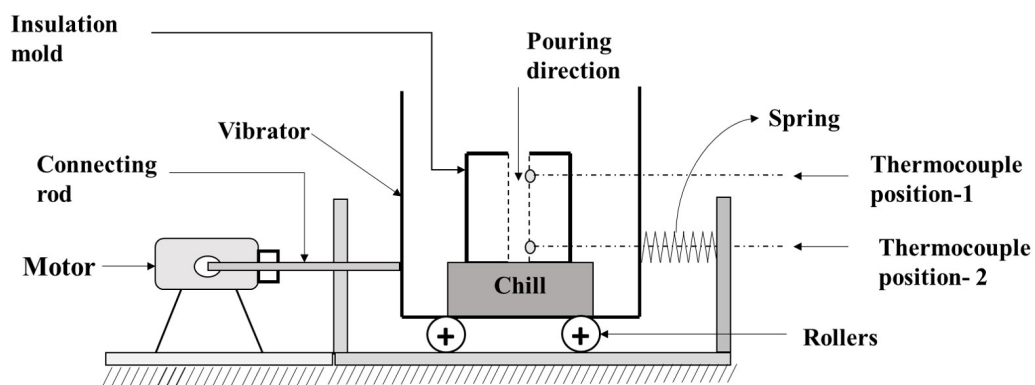


Figure 3.7 Directional solidification coupled with vibration

3.2.6 Optimization of process parameters

The experiments were designed using Taguchi method to optimize the process parameters, the procedure for Taguchi analysis is shown in Figure 3.9. The control factors and their levels were set to 3. The maximum possible test conditions for the set levels and factors

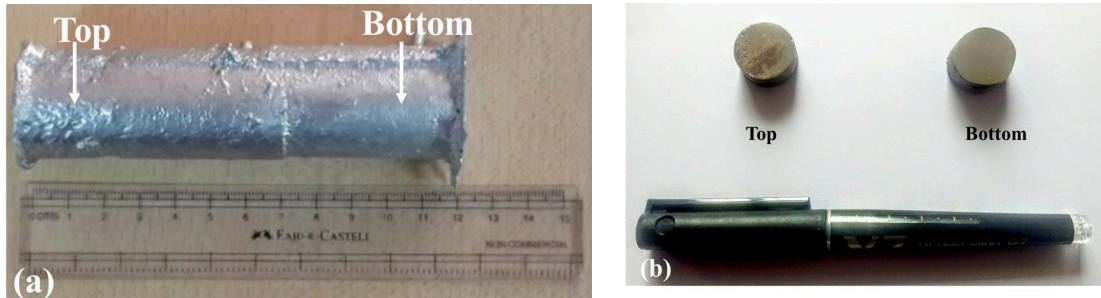


Figure 3.8 Cast sample: (a) Solid Cylinder (b) Top and bottom portion of FGC

are 27. Experiments were carried out using L_{27} orthogonal array to determine the performance characteristics at the top and bottom portion of the cast. From the data analysis through S/N ratio and mean of means optimization of process parameters were carried out for the castings synthesized with and without lateral vibrations.

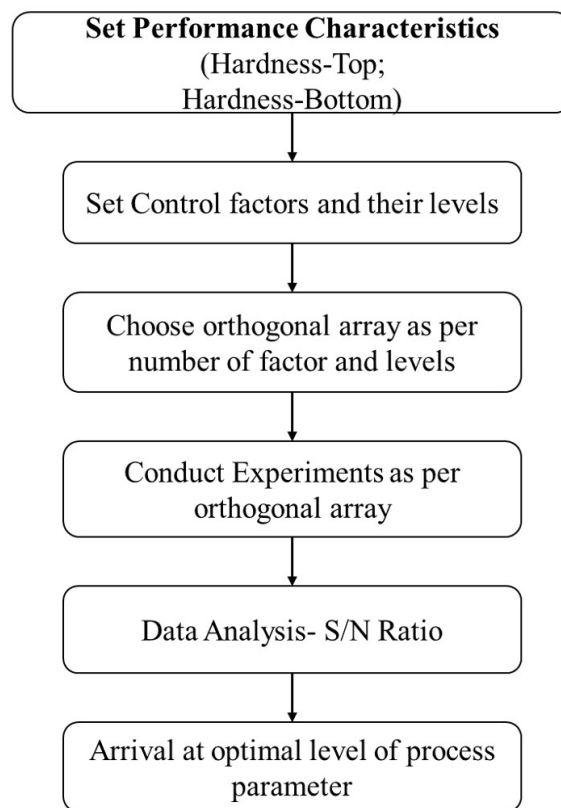


Figure 3.9 Taguchi analysis procedure

The design of experiments is used for analyzing the influence of control factors on the output (Douglas 2012). In the present work Taguchi approach is followed to design

the experiments as it reveals the complex cause and effect relationship between the process parameter and responses (Krishnaiah, K., Shahabudeen 2013). The process parameters and their levels selected is shown in Figure 3.10. L_{27} orthogonal array is

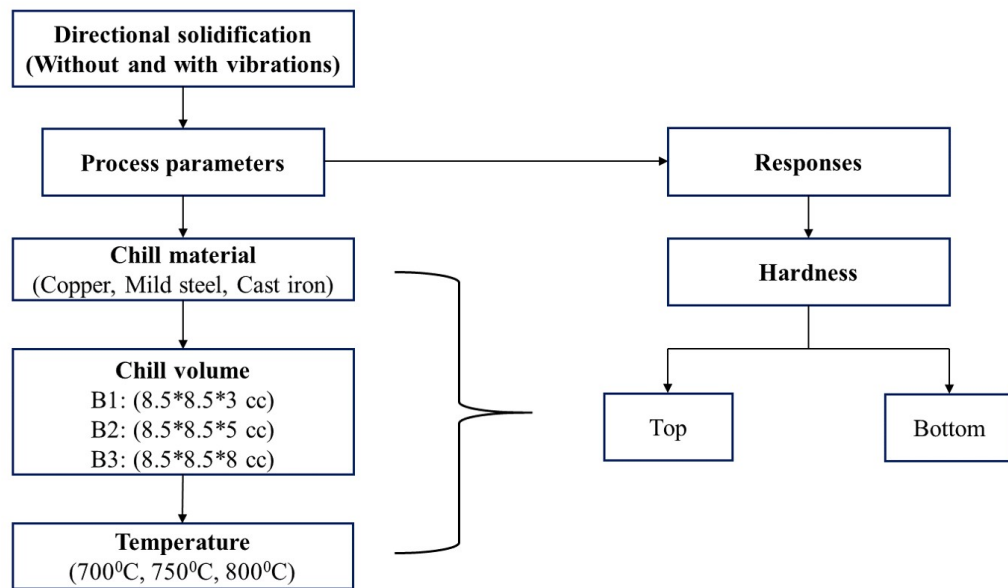


Figure 3.10 Selection of Process parameters and levels

used to synthesize the FGM from base alloy Al-18wt%Si with two different processing conditions (Without and with lateral excitation). Whereas for Al-18wt%Si reinforced with 2wt% graphite, FGM's are processed with only lateral excitation. Codes assigned for the process parameters and their levels are shown in Table 3.6. Table 3.7 shows the orthogonal array followed in the present work for optimization of process parameters for without and with lateral vibration processing conditions.

Table 3.6 Factors and levels designated for the experimental work

Factors	Code	Levels		
Chill Material	A	Copper-(A1)	Mild steel-(A2)	Cast iron-(A3)
Chill Volume (cm ³)	B	8.5*8.5*3-(B1)	8.5*8.5*5-(B2)	8.5*8.5*8-(B3)
Pouring Temperature (°C)	C	700 -(C1)	750-(C2)	800-(C3)

Table 3.7 L₂₇ full factorial orthogonal array

Experimental run	Chill Material (A)	Chill Volume (B)	Temperature (C)
1	A1	B1	C1
2	A1	B1	C2
3	A1	B1	C3
4	A1	B2	C1
5	A1	B2	C2
6	A1	B2	C3
7	A1	B3	C1
8	A1	B3	C2
9	A1	B3	C3
10	A2	B1	C1
11	A2	B1	C2
12	A2	B1	C3
13	A2	B2	C1
14	A2	B2	C2
15	A2	B2	C3
16	A2	B3	C1
17	A2	B3	C2
18	A2	B3	C3
19	A3	B1	C1
20	A3	B1	C2
21	A3	B1	C3
22	A3	B2	C1
23	A3	B2	C2
24	A3	B2	C3
25	A3	B3	C1
26	A3	B3	C2
27	A3	B3	C3

3.3 HARDNESS EVALUATION

Hardness is the property of a material that enables it to resist plastic deformation, usually by penetration. In quantitative hardness techniques a small indenter is forced into the material surface under calculated load indenter diameter. The diameter of the resulting indentation is measured and the hardness is calculated using the specific formula. Softer the material bigger and deeper the indentation and lower the hardness number. But this hardness values are only relative. There are many methods to find the hardness of a material, one of them is the Brinell hardness test. In this method ball indenter of 5mm diameter is pressed against the smooth surface of the material whose hardness is to be determined. A standard normal load of 15.625 kg is applied on the surface as shown in Figure 3.11, the diameter of the indentation formed on the surface is evaluated using the microscope. Therefore, by using appropriate formula, brinell hardness number is determined and is expressed in BHN. As shown in Figure 3.12 at least five readings are

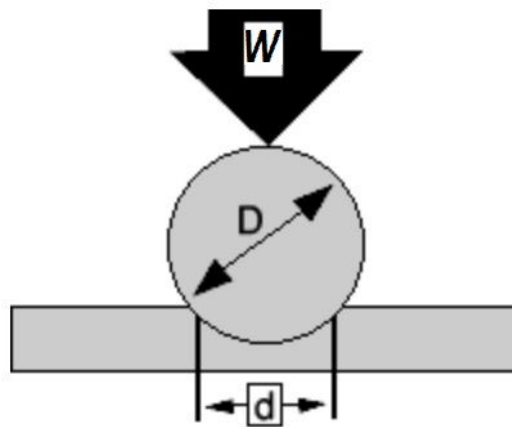


Figure 3.11 Representation of Indentation

taken perpendicular to the longitudinal axis. The final BHN value for each specimen is arrived at considering the statistical variation. Hardness is calculated for all the cast FG alloys under different processing conditions.

$$BHN = \frac{2W}{\pi * D^2 \left[1 - \sqrt{1 - \left(\frac{d}{D} \right)^2} \right]} \quad (3.1)$$

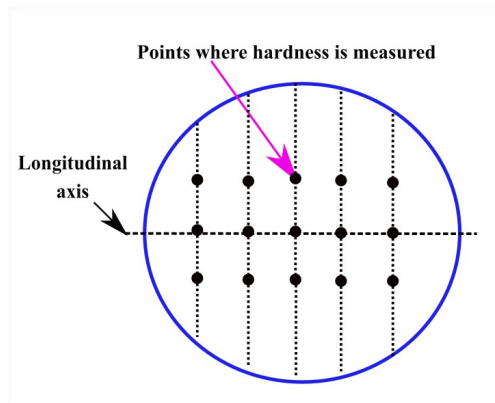


Figure 3.12 Points of measurements in Hardness test

Where W is the load applied in kilograms.

D is the diameter of the indenter in mm.

d is the diameter of the indentation in mm.

The hardness value is determined at the top and bottom portion of the cast.

3.4 MICROSTRUCTURAL CHARACTERIZATION

In the case of FGM's or MMC's, before carrying out any tests for mechanical and tribological properties it becomes necessary to perform microstructural characterization to provide an insight into

- Distribution of primary Si along the length of the specimen and also to find the volume fraction.
- Phase structure and solidification structure.
- Presence and distribution of porosity.

The metallographic specimen of the cast cylindrical FGM or MMC is cut across the cross section at top and bottom portion as shown in Figure 3.13. The sectioned surface obtained by cutting the casting on a milling machine was prepared for metallographic studies by initially grinding and then polishing with a series of abrasive papers starting from mesh size 1000, 600, 220, 4/4,1/4. Final polishing was performed on a series of disc polishers using fine SiC powder in water and then with 15 micron diamond paste until the surface was scratch free (ASTM-3-95E 1995). The samples so obtained were etched with keller's reagent ($2.5\%HNO_3 + 1.5\%HCL + 1\%HF + 95\%H_2O$) for developing the

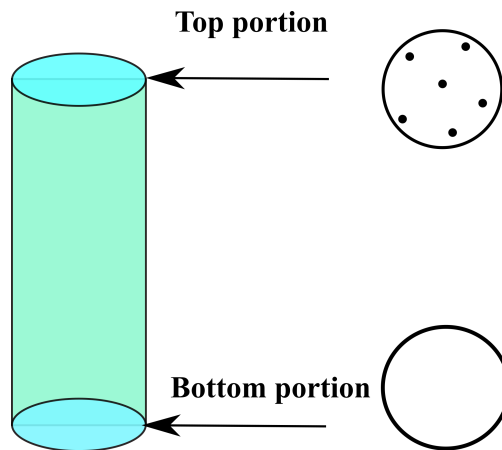


Figure 3.13 Metallographic specimen

microstructure (Pace 2011). Scanning electron microscope(Model:VEGA3 TESCAN) shown in Figure 3.14 is used to capture and analyze the image. The image captured is analyzed for phase/volume fraction analysis (ASTM-E562 1995), (ASTM-E1245 1995), Si and graphite distribution.



Figure 3.14 Scanning electron microscope

3.5 MECHANICAL PROPERTIES

3.5.1 Tensile test

The properties of FGM vary from one end to other end hence it is necessary to calculate the ultimate tensile strength, yield strength, elongation etc .the same can be investigated using tensonmeter. This test helps us to gain an in depth knowledge of strength of materials. In this test the behavior of the material against certain forces can also be determined and also suitable materials for various applications which require certain requirement in material property can also be predicted using tensile test. In the present study, tensile samples are prepared in accordance with ASTM E-8 as shown in Figure 3.15. The tensile specimens prepared at top and bottom portion of FGM are shown in Figure 3.16 Therefore, in order to validate the gradation, tensile tests were performed on electronic

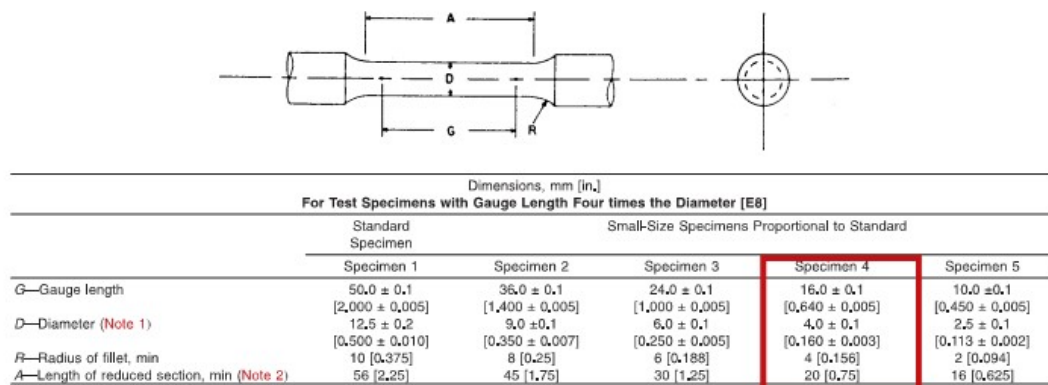


Figure 3.15 Round tension test specimen (ASTM E8 standards)

tensometer (Model:PC 2000) with 2-Tonne capacity shown in Figure 3.17. Figure 3.18 shows the tensometer specimen holder.

3.5.2 Diametrical compression test

In a functionally graded alloy or composite due to gradation of a phase and / or the reinforcement properties vary from one end of the component to the other end. The extent of the variation depends on the gradation of the material. The variation in mechanical properties may be sometimes desirable. Therefore in addition to microstructural characterization it is desirable that the change in mechanical property of interest due to gradation is also evaluated. In the present study diametral compression test is considered



Figure 3.16 Pictorial image of Tensile specimen

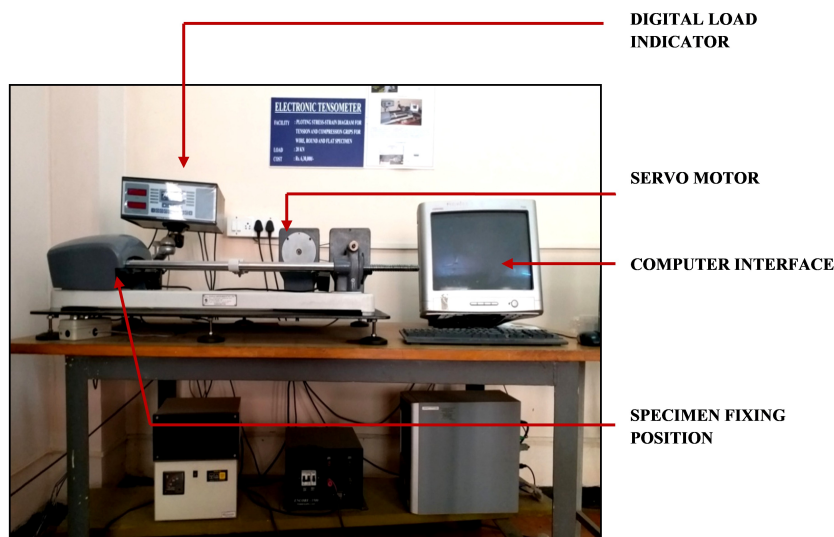


Figure 3.17 Electronic tensometer

to observe the behavior of the different regions.

A significant difference exists between bending test and diametral compression test while measuring the tensile strength. In bending test, the material is subjected only to uniaxial stress but, in the case of diametral compression test the specimen is associated with a transverse compressive stress. This is considerably larger than the tensile stress developed. Hence the results obtained from the two different methods are significantly different. Also the maximum stresses developed during loading are not limited to the surface of the material in diametral compression test as compared to bending test. Hence



Figure 3.18 Tensometer specimen holder

the failure occurring in material is not due to surface defects alone. This is important for FGM system as the properties vary based on phase/composition and depend both on surface as well as interior of the sample.

Mathematical equations were developed to describe stress-strain for elastic discs and spheres under diametrical compression under point loading conditions as shown in Figure 3.19 The Hertz solution predicts that the maximum principal stress occurs at the

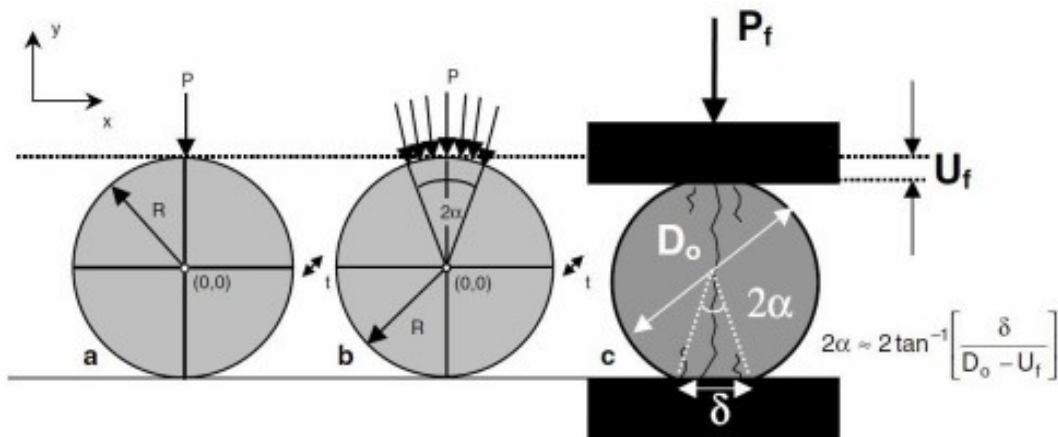


Figure 3.19 Schematic representation of different loading conditions (a) Hertz point (b) Hondros, and (c) Uni-axial diametrical compression (Procopio et al. 2003)

centre of the disc, and is tensile in nature along the x-direction (Hertz 1895). Assuming that the maximum principal stress is responsible for the failure of the specimen, the

tensile strength obtained is given by Equation 3.2

$$\sigma_t = \frac{2P}{\pi * D_c * t} \quad (3.2)$$

Where, σ_t = Tensile strength in N/mm²,

P = Load applied in N,

D_c = Diameter of the specimen in mm.

t = thickness of the specimen in mm.

Diametral compression test was carried out using TENSOMETER using ASTM Standards. At the point of application of load, thickness of specimens were flattened to a width equal to 0.2D. A electronic tensometer as shown in Figure 3.17 is used to conduct the diametral compression test. At the point of application of load, thickness of specimens were flattened to a width equal to 0.2D (4.0 mm on either side of vertical diameter) in order to distribute the load and to obtain an accurate tensile strength (Shaw et al. 1975). The deformation of the test specimen was noted down by an extensometer for every 5 kN increase of compressive load. It is observed that the width of the flattened portion increased with the increase of load and thus the compressive stress in the transverse direction normal to flattened portion was assumed to act over a rectangular portion of width b and thickness t. The thickness of the flattened portion was assumed to be constant. The compressive stress in the transverse direction was considered as load at failure (maximum load) divided by the projected area of the flattened portion as shown in Equation 3.2. The width of flat portion (b) is determined using Equation 3.3. where r is radius of test specimen and δr is measured radial deformation.

$$b = 2 * \sqrt{r^2 - (r - 0.5\delta r)^2} \quad (3.3)$$

3.6 WEAR

The concept of wear incorporates the presence of small particles between the contacting surfaces. It is possible that the abrading particles first penetrate the metal and then cause tearing of the surface introducing surface stress cracks, which lead to the ultimate break down of the surfaces. The complexity of wear is emphasized by a consideration of

the number of factors required for its description (Blau 1981). The main factors that influence wear and friction are as follows.

1. Variables Connected with Metallurgy.

- Hardness, Toughness, Constitution and Structure

2. Variables Connected with Service.

- Contacting Materials, Normal Pressure, Sliding Speed and Temperature

3. Other Factors

- Lubrication and Corrosion

Sliding and Adhesive wear refer to a type of wear generated by the sliding of one solid surface along another surface. Erosion, cavitation, rolling contact, abrasion, oxidative wear, fretting, and corrosion are traditionally excluded from the class of "sliding" wear problems even though some sliding (slip) may occur in some of these types of wear. Apparently, sliding wear is a category of wear that is "left over" when all other types of wear are identified under separate headings (Totten 2017).

3.6.1 Wear quantification

The material lost during dry sliding wear conditions can be measured and quantified by the following direct and indirect methods.

- **Mass Loss Measures of Wear:**

Measured as the difference between weight of specimen before and after wear of the material. The problem with this approach includes the need to clean the specimen carefully to avoid having extraneous matter on the surface which will contribute to any weight difference.

- **Linear Measures of Wear:**

Measures the amount of wear as dimensional change using pin-on-disc sliding wear methodology according to ASTM G99 standards.

- **Area Measures of Wear:**

Measures the amount of wear over a localized area on two surfaces like wear in

worn areas on gear teeth, bearing retainers and on sliding pads with contoured surfaces.

- **Volume Measures of Wear:**

Measures the wear amount in volume units (mm^3), which enables a comparison of wear among materials having different densities.

Wear can be expressed in the following forms:

- Linear wear rate (K_L) = [(Thickness of the layer removed) / (sliding distance)]
= (mm/mm) (Dimensionless)
- Volumetric wear rate (K_V) = [(Volume of layer removed / sliding distance)]
= ($\text{mm}^3 / \text{mm-mm}^2$) (Dimensionless)
- Wear coefficient (K) = [(volume of the material removed * flow stress) / (Normal load x sliding distance)]
= [$(\text{mm}^3\text{-N}) / (\text{mm}^2 \text{-N-mm})$] (Dimensionless)
- Specific wear rate (SWR) = [(Volume of layer removed) / (Normal load x sliding distance)]
= ($\text{mm}^3/\text{N-mm}$)

3.6.2 Pin on disc wear testing machine

The wear tests were performed on a Pin-on-Disc type wear testing machine (Model TR-20LE, Ducom make) shown in Figure 3.20 The tests were conducted as per ASTM standards (ASTMG-99 1995). The normal load was applied on the pin by dead weight through a pulley string arrangement. The system had a maximum load capacity of 200N. The rpm and the sliding speed of the disc were 0-2000rpm and 0-10m/s respectively. The disc is made of En-32 steel (0.14%C, 0.18%Si, 0.52%Mn, 0.015%S, 0.019%P, 0.13%Ni, 0.05%Cr, 0.06%Mo, balance Fe), having dimensions of 160mm diameter and 8mm thickness with a hardness value of HRC65 (Figure 3.21) The measurement in reduction of height of the specimen due to wear and coefficient of friction were measured continuously by electronic sensors.

The LVDT used is capable of measuring a maximum displacement of +2 mm and the



Figure 3.20 Photograph of tribometer



Figure 3.21 Pin on disc

measuring range of wear is +2000 micron with an accuracy of $+1\mu\text{m}$. A load cell is used to measure frictional force. It has a maximum load capacity of 200 N and measures the frictional load at an accuracy of $+0.1\text{N}$. The data acquired was processed in the controller and transmitted to the PC using Winducom 2006 software.

Wear was measured as reduction in specimen (pin) length in microns. Frictional force and coefficient of friction data were measured as a function of time. The tests were conducted under dry conditions and at room temperature according to ASTM G99-95a standards. The wear test was carried out at a temperature of 25°C and relative humidity

of 45-50%. Pins of 10 mm diameter and 42 mm length were machined as shown in Figure 3.22 and run against a hardened and ground ($R_a = 0.1\mu\text{m}$) EN 32 steel disc of hardness HRC 58-62 and of track dia 70mm. The mating surfaces of the pin and the

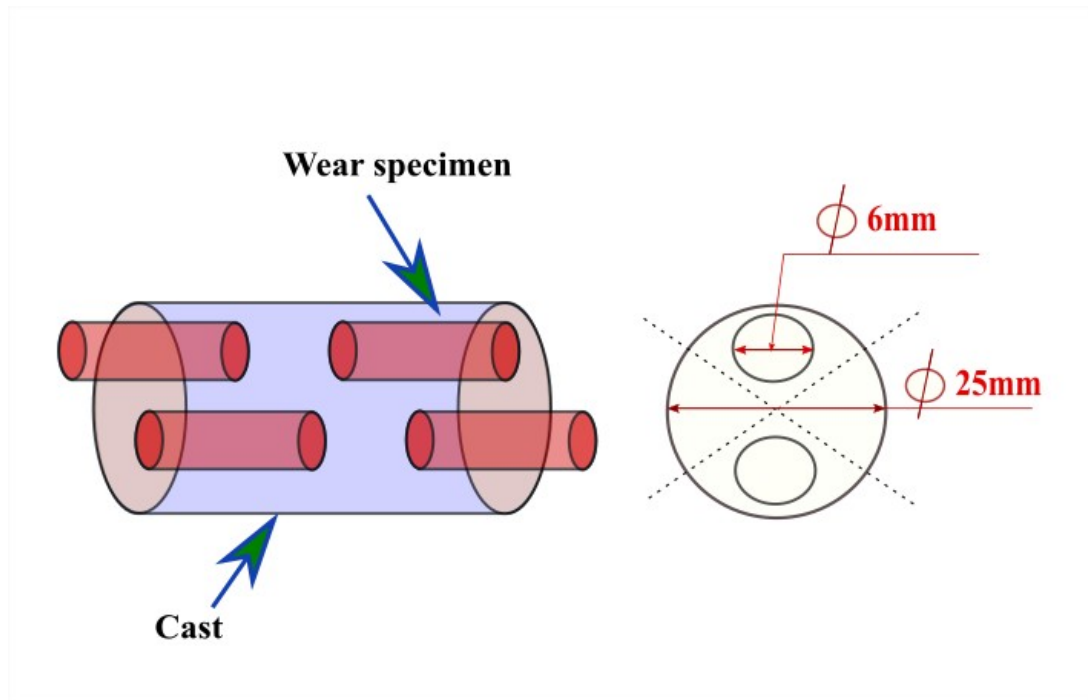


Figure 3.22 Wear specimen

disc were polished using 600 mesh emery paper before the start of the wear test. The polished pins were cleaned and degreased using ultrasonic cleaner, first with water and soap, followed by ethanol and finally with acetone. Each test specimen was run under varying loads (10,20, 30N) and a constant sliding speed (1.5 m/sec) for a constant sliding distance (1800 m). The frictional force generated on the specimen was monitored by using a frictional force sensor and was measured in Newton. Specific wear rate and coefficient of friction was analyzed for the optimized sample. The wear debris and worn surface of test specimens were analyzed by Scanning Electron Microscope (SEM) to understand the wear mechanism.

CHAPTER 4

Al-18wt%Si FGM SYNTHESIZED WITHOUT LATERAL VIBRATIONS

4.1 INTRODUCTION

This chapter deals with investigation of chill material, chill volume and pouring temperature to fabricate Al-Si based FGM. Taguchi technique has been employed to arrive at optimized results. From the literature review and as author's knowledge no methodical research has been reported to obtain the best possible optimized conditions to synthesize the FGM through directional solidification. An attempt has been made in this chapter to optimize the process parameters namely chill material, chill volume and pouring temperature to fabricate FGM through directional solidification using Al-18wt%Si alloy without lateral vibrations.

4.2 CASTING OF FGM

In the current study, three parameters namely chill material, chill volume and pouring temperature were identified. Each parameter was investigated at three levels to study the influence of process parameters on hardness at top and bottom portion. The identified process parameters and their levels are presented in Table 4.1 The measured values of

Table 4.1 Control factors and level

Factors	Code	Levels		
		1	2	3
Chill Material	A	Copper	Mild steel	Cast iron
Chill Volume (cm ³)	B	8.5*8.5*3	8.5*8.5*5	8.5*8.5*8
Pouring Temperature (K)	C	700	750	800

hardness are summarized and presented in Table 4.2

Table 4.2 Response table for hardness (Without Vibrations)

Experimental run				Top portion		Bottom portion	
	A	B	C	Hardness	S/N ratio	Hardness	S/N ratio
1	1	1	1	50.24	34.02	48.21	-33.66
2	1	1	2	50.33	34.04	48.14	-33.65
3	1	1	3	50.34	34.04	48.12	-33.65
4	1	2	1	50.97	34.15	47.99	-33.62
5	1	2	2	51.10	34.17	47.95	-33.62
6	1	2	3	51.12	34.17	47.95	-33.62
7	1	3	1	53.29	34.53	47.26	-33.49
8	1	3	2	54.23	34.68	47.12	-33.46
9	1	3	3	55.26	34.85	47.00	-33.44
10	2	1	1	50.14	34.00	48.22	-33.66
11	2	1	2	50.17	34.01	48.21	-33.66
12	2	1	3	50.21	34.02	48.21	-33.66
13	2	2	1	50.42	34.05	48.09	-33.64
14	2	2	2	50.71	34.10	48.09	-33.64
15	2	2	3	50.81	34.12	48.01	-33.63
16	2	3	1	52.21	34.36	47.51	-33.54
17	2	3	2	52.40	34.39	47.45	-33.52
18	2	3	3	52.51	34.40	47.35	-33.51
19	3	1	1	50.02	33.98	48.24	-33.67
20	3	1	2	50.03	33.98	48.23	-33.67
21	3	1	3	50.09	34.00	48.22	-33.66
22	3	2	1	50.37	34.04	48.12	-33.65
23	3	2	2	50.39	34.05	48.11	-33.64
24	3	2	3	50.40	34.05	48.10	-33.64
25	3	3	1	51.45	34.23	47.81	-33.59
26	3	3	2	51.89	34.30	47.81	-33.59
27	3	3	3	52.10	34.34	47.75	-33.58

4.3 EVALUATION OF PROPERTIES OF FGM FABRICATED WITH OPTIMAL PARAMETERS

In the present study, the objective is to have lower hardness at the bottom portion and higher hardness at the top portion. Hence a "smaller the better" quality characteristic is used for the bottom portion and "larger the better" quality characteristic for top portion is selected. The S/N ratios associated with the objective of each trial of the orthogonal array is given by :

$$\text{Larger the best characteristic } \frac{S}{N} = -10 \log \frac{1}{n} (\sum \frac{1}{y^2}) \quad (4.1)$$

$$\text{Smaller is the best characteristic } \frac{S}{N} = -10 \log \frac{1}{n} (\sum y^2) \quad (4.2)$$

The corresponding S/N ratios for each trial in L₂₇ orthogonal array were determined by Equations 4.2 and 4.1 for hardness at the bottom and top portion respectively which gives the combination of process parameters and their levels in L₂₇ orthogonal array. A total of 27 experiments without lateral vibrations were conducted in accordance with parameter level of each factor and observed hardness values were noted and evaluated for corresponding S/N ratio. From the obtained S/N ratios analysis of means were evaluated to determine the optimal level of control factors. The results for hardness response obtained for the FGM's synthesized without vibrations are presented in Tables 4.4 and 4.5. The level of parameters with highest value of S/N ratio at the top portion and lowest

Table 4.4 Analysis of means based on S/N ratio for top portion (Without vibration)

Larger the better quality characteristic			
Level	Chill material	Chill volume	Pouring temperature
1	34.29	34.01	34.15
2	34.16	34.10	34.19
3	34.11	34.45	34.22
Delta	0.19	0.44	0.07
Rank	2	1	3

value of S/N ratio at the bottom portion is the best combination level indicating better

Table 4.5 Analysis of means based on S/N ratio for bottom portion (Without vibration)

Smaller the better quality characteristic			
Level	Chill material	Chill volume	Pouring temperature
1	-33.58	-33.66	-33.61
2	-33.61	-33.63	-33.61
3	-33.63	-33.52	-33.60
Delta	0.05	0.14	0.02
Rank	2	1	3

gradation in hardness from bottom to top of the cast. The optimal process parameters are found to be Copper chill(A1), Chill volume(B3) and pouring temperature (C3). The results of analysis of means based on S/N ratios are also presented in Figures 4.1 and 4.2 for hardness at top and bottom portion respectively. The main effects plots are generated through statistical software(MINITAB: Version 15) for exploring the influence of control factors on hardness at top and bottom To evaluate the influence of control factors quantitatively, based on the obtained values of S/N ratio, analysis of variance(ANOVA) has been performed (Phadke 1989). ANOVA is accomplished by distinguishing the total variability of S/N ratio, which is a measured values of sum of squared deviations from the total mean of S/N ratio in contributions by each of the control factors and the error. The summary of ANOVA results for hardness at top and bottom portion are presented in Table 4.6 and 4.7 respectively. It is seen from the Table 4.6 and 4.7 that chill volume has major contribution of (73.1%) at the top portion and (78.7%) at the bottom portion which has played a significant role in attaining gradation in hardness values across the cast specimen.

Validation experiments at the optimal levels of control factors were performed with error prediction within the 95% confidence limit, which indicates the adequacy of the additivity of hardness models. The best combination of control factors for obtaining the gradation in hardness values for the FGM's synthesized without lateral vibrations are presented in Table 4.8.

Volumetric heat capacity(VHC) which defines the rate of solidification which comprises

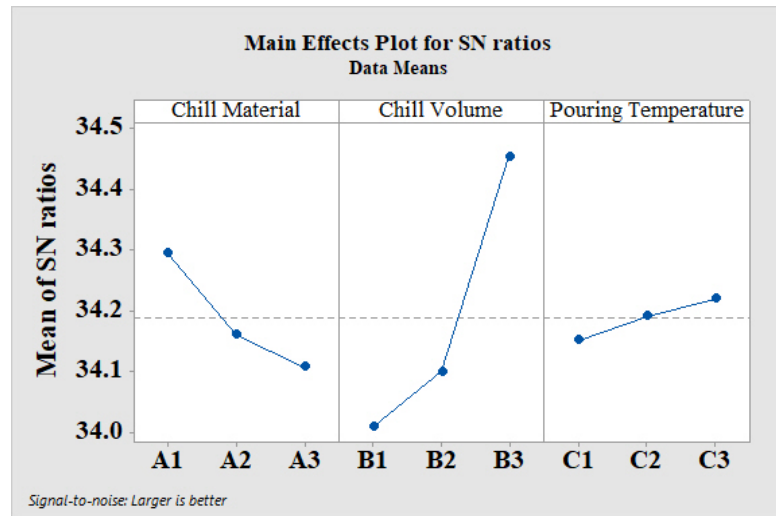


Figure 4.1 Main effects plot for hardness based on S/N ratio for top portion

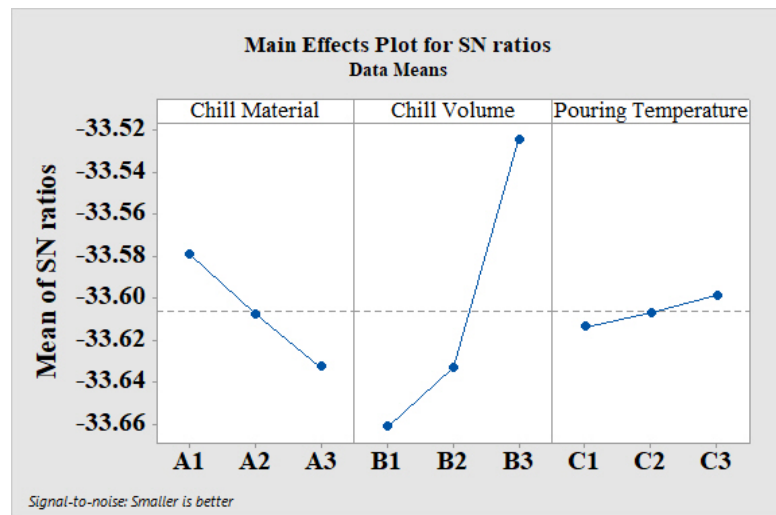


Figure 4.2 Main effects plot for hardness based on S/N ratio for bottom portion

of volume, specific heat and density of the chill material. Therefore, from the Figures 4.3 and 4.4 it is seen that higher the VHC and pouring temperature better is the gradation in hardness values obtained along the length of the cast.

Directionally solidified FGM obtained with optimal process parameters are evaluated for microstructure, strength and tribological characteristics and discussed in the following sections.

Table 4.6 ANOVA for hardness based on S/N ratio for top portion

Source	DF	Sum of squares	Mean square	Contribution (%)
Chill Material	2	6.08	3.04	12.6
Chill Volume	2	35.20	17.60	73.1
Pouring Temperature	2	0.78	0.39	1.6
Error	20	6.11	0.31	12.7
Total	26			100.00

Table 4.7 ANOVA for hardness based on S/N ratio for bottom portion

Source	DF	Sum of squares	Mean square	Contribution(%)
Chill Material	2	0.39	0.20	10.9
Chill Volume	2	2.82	1.41	78.7
Pouring Temperature	2	0.03	0.02	0.9
Error	20	0.34	0.02	9.6
Total	26			100.00

4.3.1 Hardness

In FGM's it is expected that properties in the structure vary from one end to other end due to the segregation of harder particulates towards one side of the structure. Figure 4.5 shows the hardness values of the FGM and ascast plotted across the length from the top surface of the cast specimen. Due to the directional solidification, Primary Si increases progressively and are pushed towards the top surface, this is due to the density differences between the Al matrix and Si particulates. As the primary Si is the strengthening phase in Al-Si alloy, thereby the hardness is mainly influenced by the primary Si content (Watanabe et al. 2007).

To evaluate gradation in the structure, hardness values at top and bottom portion of the cast are obtained at different radial distances from the outer periphery and average result of 5 values at the same position are considered. It is observed that a maximum of (55.26 \pm 1 BHN) at the top surface and a minimum of (47.00 \pm 1 BHN) at the bottom surface revealing a variation in hardness values along the length of the cast. This variation is due

Table 4.8 Optimal control factor setting and optimal values for hardness at top and bottom portion

Response	Optimal process parameter			Optimal value (BHN)
	Chill Material	Chill Volume (cm ³)	Pouring Temperature (°C)	
Hardness (Top)	Copper	8.5*8.5*8	800	55.26
Hardness (Bottom)	Copper	8.5*8.5*8	800	47.00

to increased volume fraction of harder Si particles at the top portion of the cast which has led to gradation within the structure (Chirita et al. 2009b). As the volume fraction of reinforcement particles are increased a significant improvement in mechanical and tribological properties can be seen.

4.3.2 Effect of chill on solidification

Cooling curve are popularly used to recognize temperature - time history during solidification. Solidification behavior which helps in predicting the structural properties of the cast is greatly influenced by the chill material, chill size, pouring temperature.

Figure 4.6 shows that the solidification at the chill/metal interface begins at lower temperature in contrast to the top region. The temperature variation between the top and bottom portion contains the versatility ($\Delta T = T_{top} - T_{bottom}$) versus time which is shown in Figure 4.7. As expected, the melt near the chill was subjected to rapid solidification. The fluctuations between top and bottom portion were more vigorous immediately after pouring the melt, thereby releasing the latent heat. It was observed that difference in temperatures kept dropping significantly from 180⁰C to 20⁰C till 350 sec. After 350 sec, the temperature at the top portion had achieved a nearly constant trend with the temperature at the bottom portion. By completing the solidification, ΔT has declined leading to equilibrium temperature (Rikhtegar and Shabestari 2014). Therefore, it was observed that a steep temperature gradient was established by the chill which acts as the driving factor in the directional solidification of the casting (Manjunath et al. 2018).

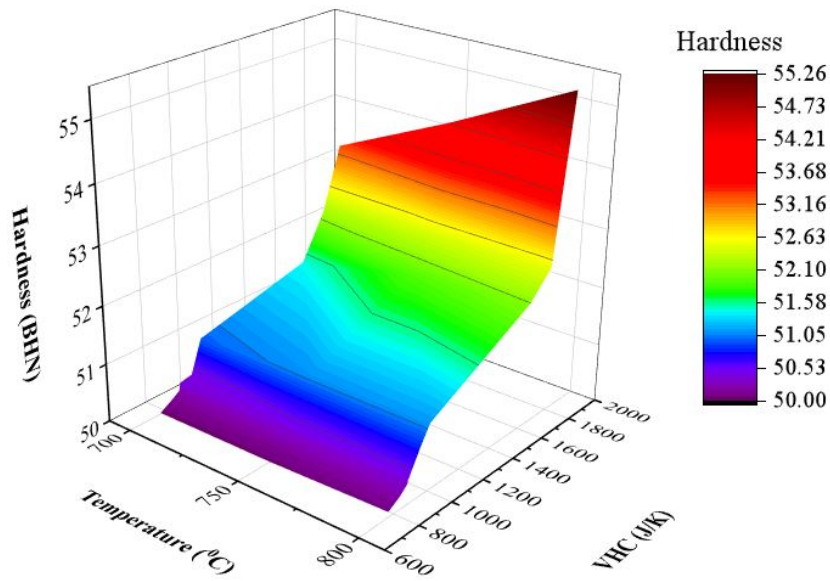


Figure 4.3 Volumetric heat capacity on hardness: Top portion

4.3.3 Microstructure

(Figure 4.8a and 4.8b), presents the microstructures obtained at top and bottom region of the cast. It can be seen from the (Figures 4.8c and 4.8d), that there is a graded distribution of Si particles from bottom to top region of the cast. The segregation of Si particles at top region of the cast is due to placement of chill at the bottom which promotes directional solidification. When the melt is poured in to the mold, Si being lighter than Al, precipitates through the melt. As the viscosity of the melt gradually increases due to rapid freezing at the chill/metal interface, it was found that there is an enrichment of primary Si in the top region of the cast sample which has led to gradation in the properties. Therefore, it is observed that trend in hardness values correlates with the microstructure which dictates the mechanical properties of the material. The size of Si particles is analyzed by a Image-J (Version: IJ 1.46r). (Figure 4.8e), presents the histogram for particle size distribution of the cast for top and bottom region.

As a result, it suggests that the number of Si particles is more in top region in contrast to the bottom region. This is due to the fact that in hypereutectic Al-Si based FGM, the Si growth front rejects the aluminum atoms into the liquid alloy and the primary Si particles formed are segregated as a graded layer in the cast. It is seen that in the

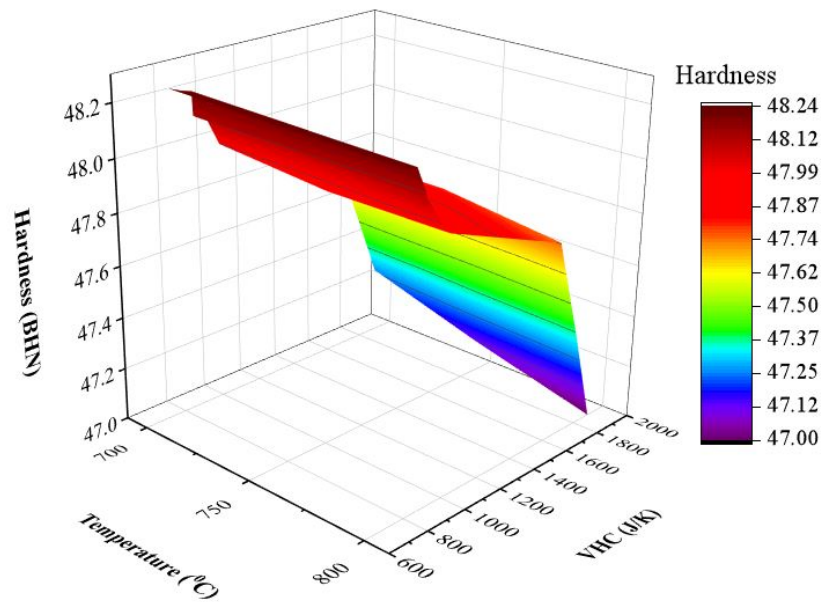


Figure 4.4 Volumetric heat capacity on hardness: Bottom portion

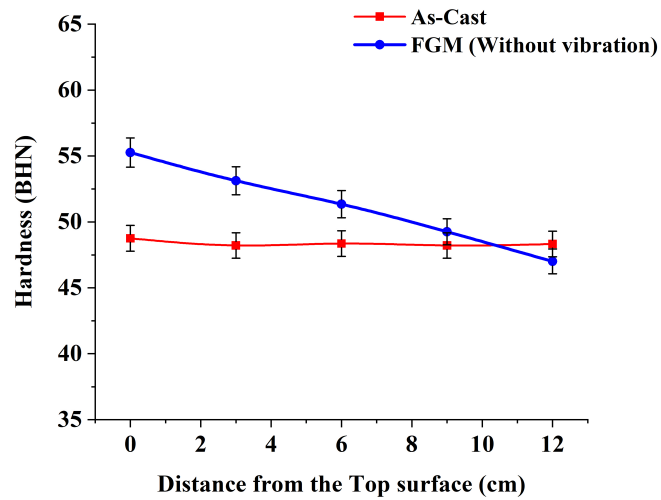


Figure 4.5 Hardness across the section

bottom region, the particle size diameter is in the range from 0 to $60\mu\text{m}$. However, in the top portion it can be seen that the particle size diameter is from 20 to $120\mu\text{m}$ which clearly signifies that the majority of the Si particles are segregated in the top region. This clearly shows that top portion has highly dense particle reinforcements. Whereas, bottom portions shows that these surfaces possess less Si particulates. These variation in particle reinforcements has led to significant changes in gradation and properties along the cast.

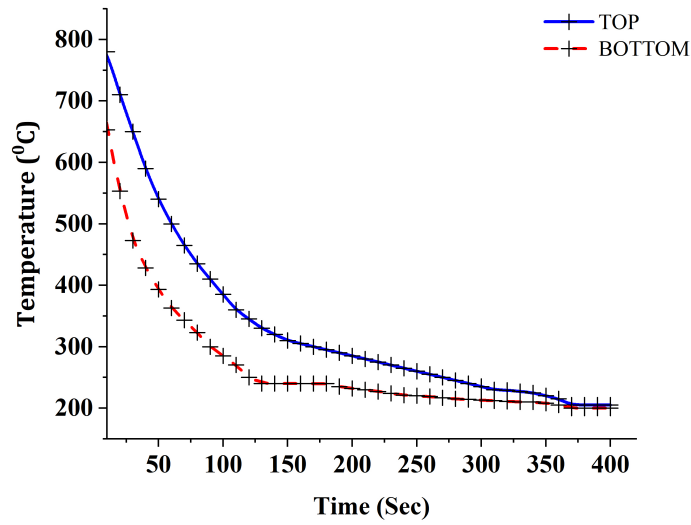


Figure 4.6 Cooling Curves of FGM

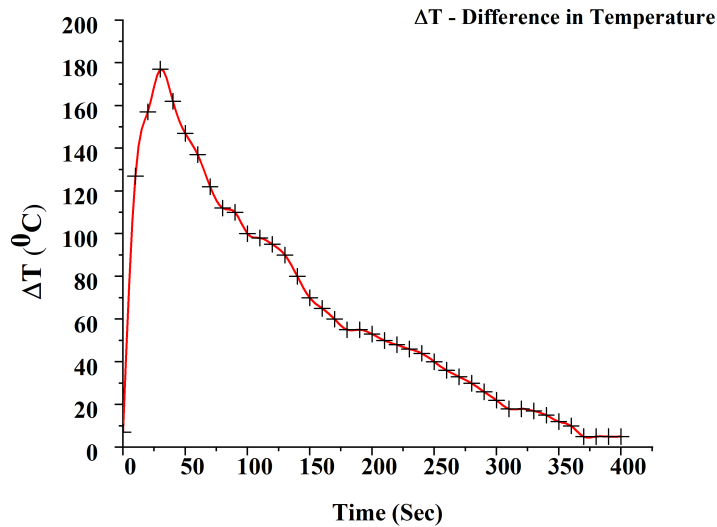


Figure 4.7 Temperature Difference between top and bottom portion vs time

To study soundness of the cast sample and its effect on mechanical properties, porosity of the cast sample was assessed. Figure 4.9 shows the porosity in percentage along the length of the cast sample. It is observed that amplitude of porosity level is less at the end closer to the chill compared to the top portion, this can be attributed to the presence of external chill at the bottom which promotes DS. Due to this porosity difference it can be postulated that it influences the strength along the length of the FGM.

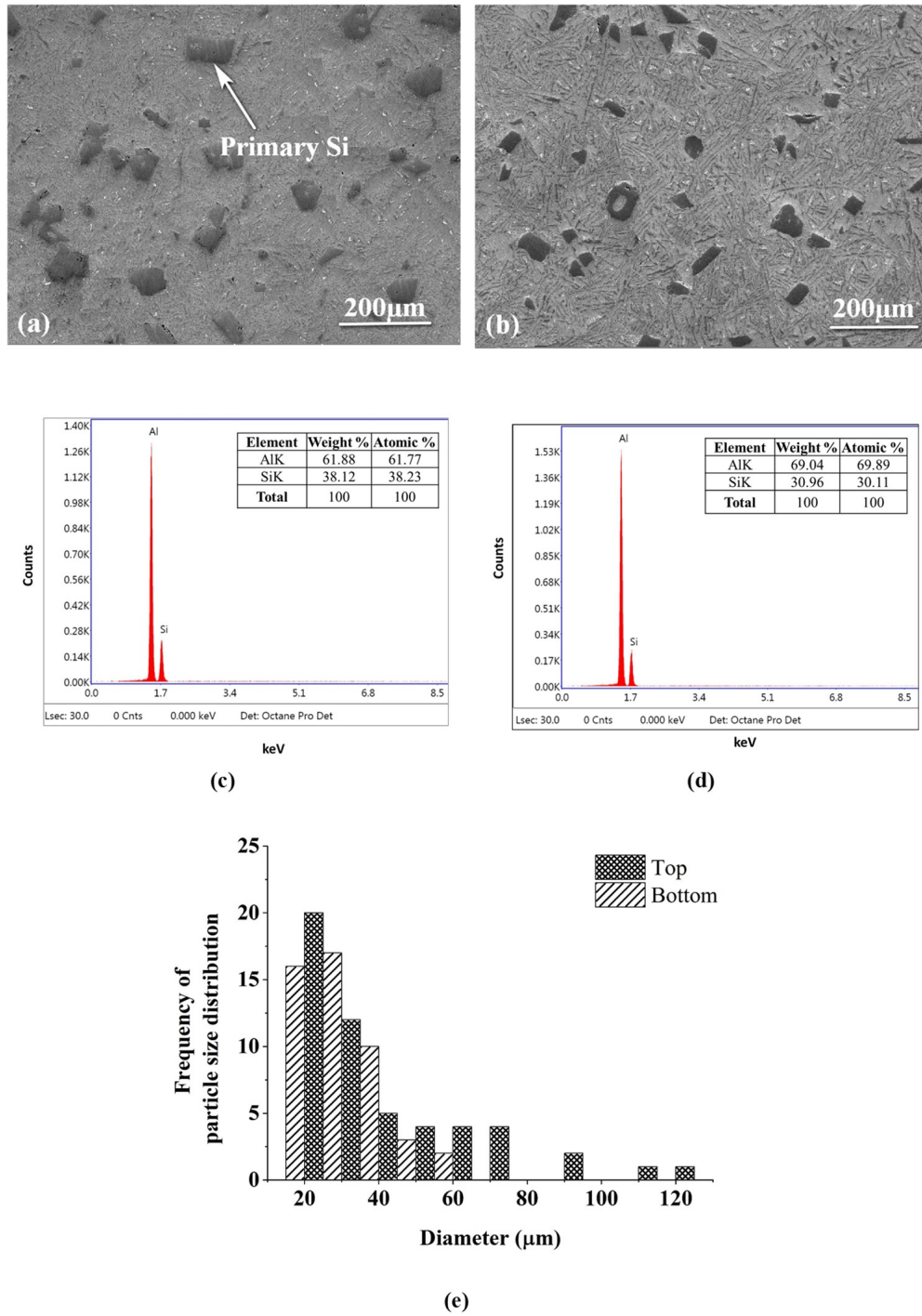


Figure 4.8 Microstructural analysis of FGM (a) Representative SEM image of top portion (b) Representative SEM image of bottom portion (c) EDS for top portion (d) EDS for bottom portion (e) Histogram for frequency of particle size distribution

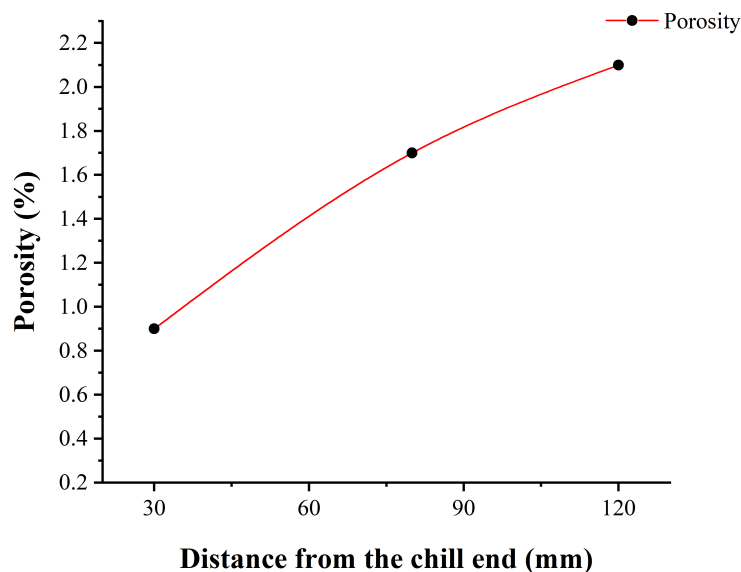


Figure 4.9 Porosity check of Al-18wt% Si FGM fabricated without lateral vibrations

4.3.4 Strength

From microstructural study, it was revealed that top portion is rich in reinforced particulates compared to the bottom portion which is a particle depleted. This variation is due to the presence of the chill at the bottom and due to this primary Si is precipitated towards the top portion leading to larger number of primary Si particles in the top portion. Therefore, it is understood that segregation of particulates from one end to the other end of the cast has led to gradation in the structure which is also evident from the hardness values. The obtained strength values shown in Figure 4.10 reveal that there is enhancement of tensile strength at the bottom region of the cast compared to the top region. This clearly signifies that there is a gradation in strength from bottom to top portion of the FGM (Ramesh Babu et al. 2018). The morphology of the fractured surfaces of FGM taken at a strain of 0.6 are shown in Figure 4.11. The fractography at top region of the cast as shown in Figure 4.11a, reveals quasi-cleavage mode. As a result, the cast specimen at the top region fails due to brittle nature which can be attributed due to precipitation of Si at the top. However, at the bottom region, since the volume fraction of Si particles is less, which results in crack initiation and coalescence of voids leading to dimple morphology. Therefore, the failure due to this characteristic appearance is always ductile in nature

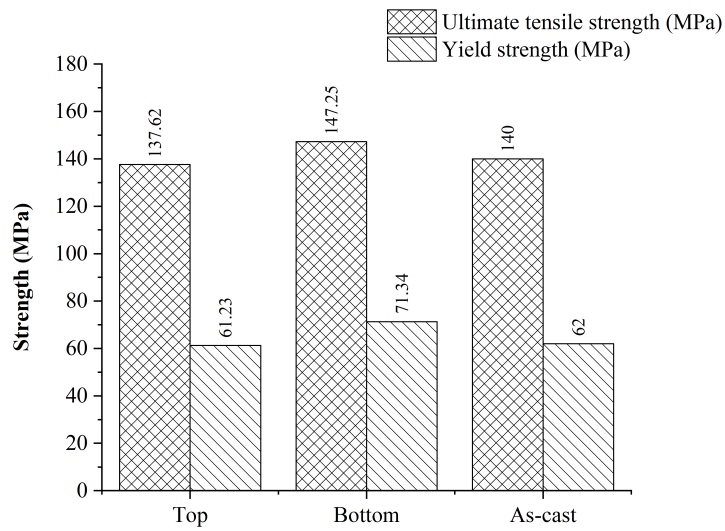


Figure 4.10 Strength of FGM (Without vibrations) and as-cast

(Radhika et al. 2018) as shown in Figure 4.11b

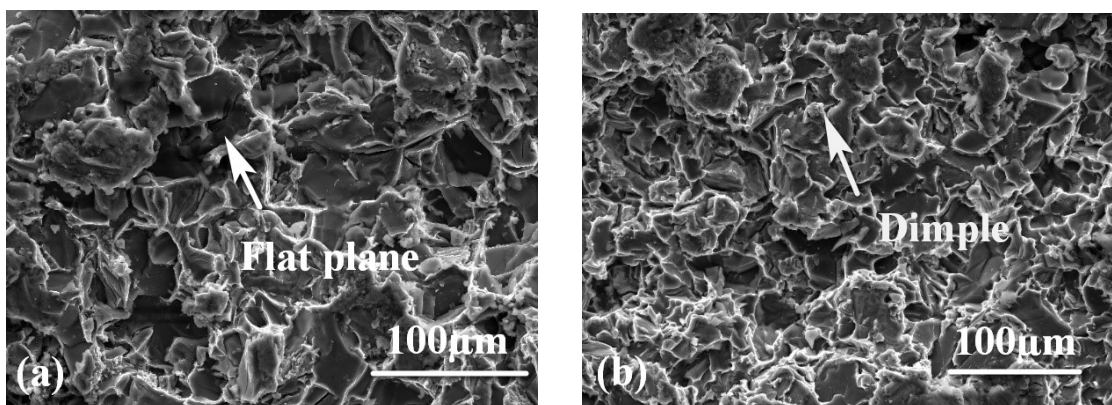


Figure 4.11 Fractography of tensile specimens (Without vibrations): (a) Top portion (b) Bottom portion

4.3.5 Wear analysis

It was expected that the different hardness values at the bottom and top portion of the cast would also show the different wear characteristics. This was confirmed with weight loss, coefficient of friction, specific wear rate and worn surface analysis considered at top and bottom portion. It can be noted from the Figure 4.12 that wear loss increases with increase in load which is in accordance with Archard's wear law (Archard 1953), which states that wear loss increases as the load increases. It is seen that wear loss is less

for the FGM at top portion compared to the bottom portion and base alloy (Ul Haq and Anand 2018a).

The higher wear loss of the base alloy and bottom portion of the FGM indicates that removal of more material which is due to the direct contact of sliding surfaces and the worn out silicon particles penetrate the aluminum matrix which has resulted in easy nucleation. Figure 4.13 shows the coefficient of friction(COF) obtained for the FGM at

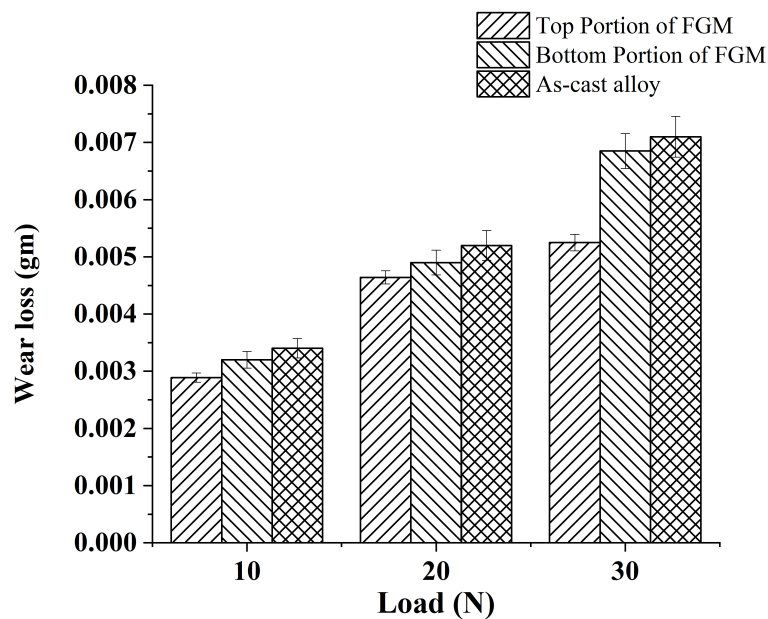


Figure 4.12 Wear loss of FGM (Without vibrations) and as-cast

30N load. It is also seen that top portion exhibited lower COF compared to the bottom and As-cast. This can be attributed to the presence of large number of Si particles Figure 4.14, shows the specific wear rate of the cast at top and bottom portion. As a result, it was found that for the base alloy and bottom portion of the FGM, there is a significant increase in specific wear results . However, it was reported that in the top portion, there is a decrease in specific wear rate. Also, It was found that the difference in specific wear rate between top and bottom portion at 30N load is 14.87%.

4.3.6 Worn out surface analysis

Figure 4.15 shows the SEM images of the worn surfaces for the specimens subjected to a wear load of 30N. Two extreme ends of the specimen processed without lateral vibrations revealed that top region is dominated by delamination wear whereas bottom

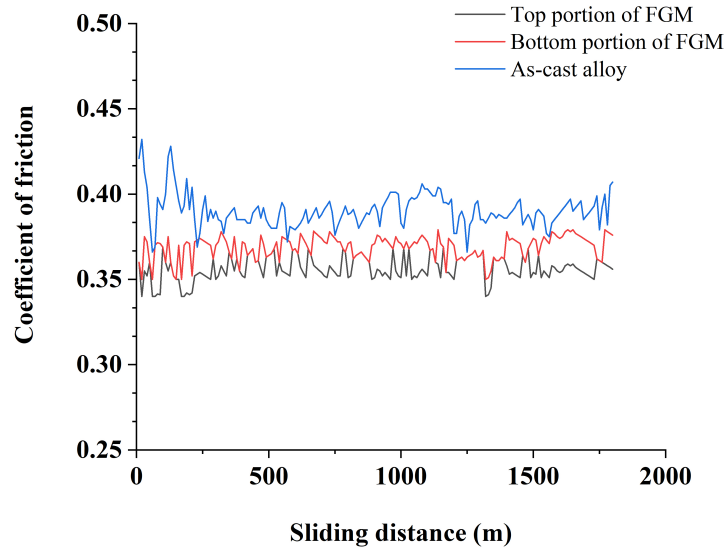


Figure 4.13 Coefficient of friction of FGM (Without vibrations) and as-cast

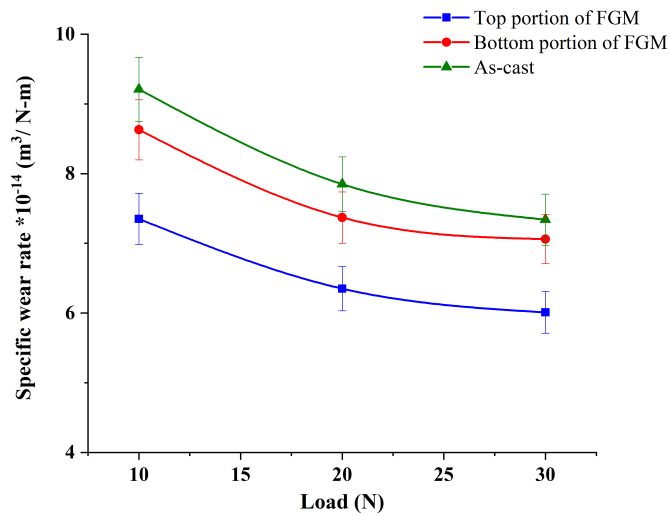


Figure 4.14 Specific wear rate of FGM (Without vibrations) and as-cast

region is dominated by abrasive wear. The wear mechanisms observed could be generally described as: (i) delamination wear (ii) abrasive wear. Worn surfaces at the bottom was characterized by long ploughing lines which run parallel to the sliding direction such features suggest abrasive wear. The scouring seen in the micrographs suggest that it is due to trapping of debris on the hardened steel counter face. The presence of cracks during sliding of the specimens had been associated with the process of delamination on several occasions by other researchers (Kiran Aithal et al. 2012; Reddy et al. 2009).

Delamination is the propagation of cracks preferentially along the sliding direction, which gives rise to the detachment of wear debris which can be seen from the top region. It is seen from the Figure 4.16a that plate shaped particles were found in wear debris.

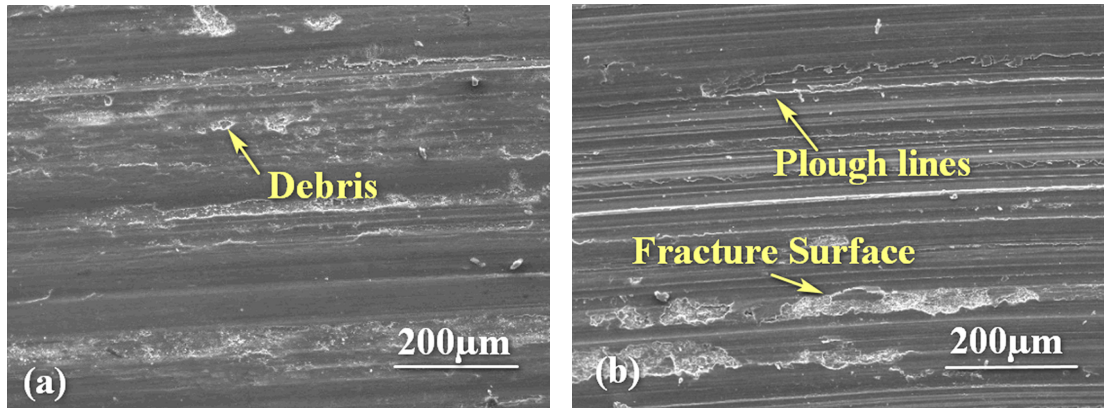
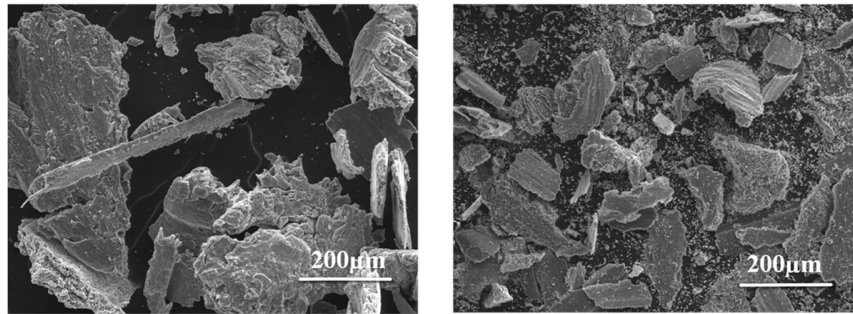


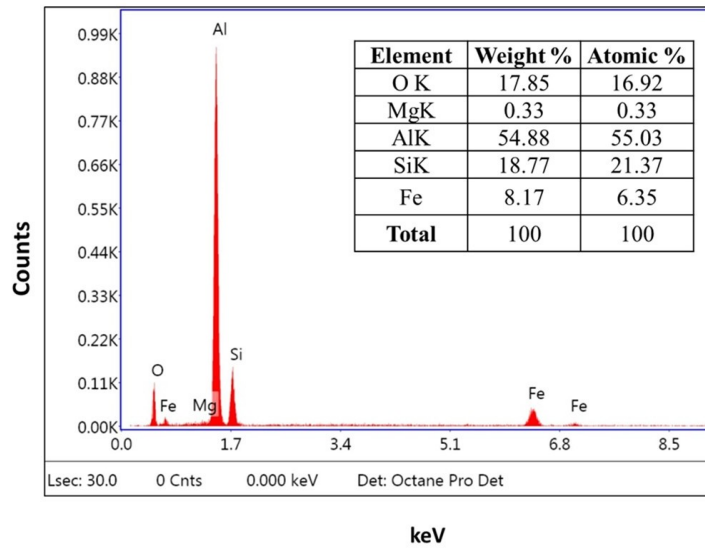
Figure 4.15 SEM images of wear surfaces for the optimized samples (Without vibrations): (a) Top portion (b) Bottom portion

indicating delamination wear mechanism, whereas in Figure 4.16b it was revealed that wear debris were finer, the morphology shows that the bottom portion is dominated by abrasive and delamination wear. Figure 4.16c and 4.16d shows the EDS image of the worn out surface of top portion of the FGM. It is seen from the top portion there is a transfer of (Fe) from counter surface contributing towards improved wear resistance (Abedi and Asl 2019; Iwai et al. 2000; Ul-Haq and Anand 2019). It is also reported that due to the presence of particulates and oxides at the top portion has a contribution in lowering the wear loss and COF. This is due to the fact that oxide layer restrains metal to metal contact giving rise to a delamination wear mechanism (Anand et al. 2017; Ul-Haq and Anand 2018b; Zhang 2013).

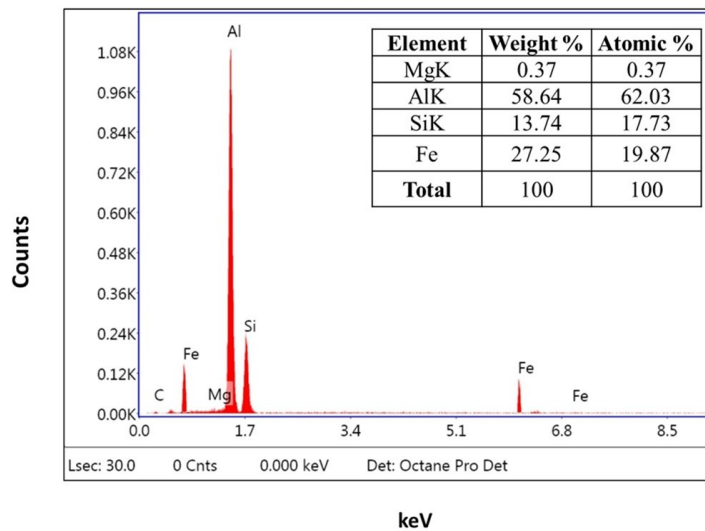


(a)

(b)



(c)



(d)

Figure 4.16 Wear debris analysis of FGM (Without vibrations): (a) Top portion (b) Bottom portion (c) EDS for top portion (d) EDS for bottom portion

4.4 SUMMARY

In this chapter, Al-18wt%Si directionally solidified FGM has been evaluated for mechanical and tribological characteristics. Based on the experimental results following conclusions were drawn.

- Taguchi technique was employed to carry out the optimization of process parameters, revealed gradation in hardness values was better for the chill with higher VHC.
- Obtained hardness values for the sample fabricated with optimal process parameters revealed 55.26 BHN at top portion and 47.00 BHN at bottom portion.
- Microstructure analysis revealed the formation of precipitation of Si particles from bottom to top portion.
- It is observed from strength properties indicating ductile property at bottom portion and brittle nature at the top, which is in accordance with observed hardness and microstructure.
- It is evident that wear loss, specific wear rate, COF decreased at the top due to more number of Si particles.

The next chapter focuses on coupling DS technique with a novel lateral vibration set up for improving gradation in the structure.

CHAPTER 5

Al-18wt%Si FGM SYNTHESIZED WITH LATERAL VIBRATIONS

5.1 INTRODUCTION

This chapter deals with development and characterization of Al-Si based FGM through the novel lateral excitation technique. Optimization of process parameters such as chill material, chill volume and pouring temperature was adopted to finalize the control factors and their levels. This chapter also discusses evaluation of mechanical and tribological properties of Al-18wt%Si FGM synthesized with lateral vibrations.

5.2 CASTING OF FGM

In the current study, FGM is fabricated with experimental technique shown in Figure 3.5. Parametric optimization for the control factors namely chill material, chill volume and pouring temperature were carried out to identify the optimized control factors to attain better gradation in the structure. Each parameter was investigated at three levels to study the influence of process parameters on hardness at top and bottom portion. The identified process parameters and their levels are presented in Table 4.1.

The measured values of hardness are summarized and presented in Table 5.1

5.3 EVALUATION OF PROPERTIES OF FGM FABRICATED WITH OPTIMAL PARAMETERS

In this present study, the objective is to have lower hardness at the bottom portion and higher hardness at the top portion. Hence a "smaller the better" quality characteristic is used for the bottom portion and "larger the better" quality characteristic for top portion is selected. The S/N ratios associated with the objective of each trial of the orthogonal array is calculated by Equations 4.1 and 4.2.

A total of 27 experiments were conducted with lateral vibrations in accordance with parameter level of each factor and observed hardness values were noted and evaluated for

Table 5.1 Response table for hardness (With Vibrations)

Experimental run				Top portion		Bottom portion	
	A	B	C	Hardness	S/N ratio	Hardness	S/N ratio
1	1	1	1	52.63	34.42	49.37	-33.87
2	1	1	2	53.19	34.52	49.34	-33.86
3	1	1	3	53.37	34.55	49.32	-33.86
4	1	2	1	55.72	34.92	48.72	-33.75
5	1	2	2	55.39	34.87	48.72	-33.75
6	1	2	3	55.93	34.95	48.44	-33.70
7	1	3	1	59.63	35.51	47.76	-33.58
8	1	3	2	60.57	35.65	47.62	-33.56
9	1	3	3	61.59	35.79	46.73	-33.39
10	2	1	1	52.56	34.41	49.62	-33.91
11	2	1	2	52.58	34.42	49.45	-33.88
12	2	1	3	52.62	34.42	49.44	-33.88
13	2	2	1	54.46	34.72	48.84	-33.78
14	2	2	2	54.72	34.76	48.82	-33.77
15	2	2	3	54.73	34.76	48.73	-33.76
16	2	3	1	58.54	35.35	48.09	-33.64
17	2	3	2	58.07	35.28	47.96	-33.62
18	2	3	3	58.84	35.39	47.87	-33.60
19	3	1	1	52.24	34.36	49.84	-33.95
20	3	1	2	52.36	34.38	49.76	-33.94
21	3	1	3	52.56	34.41	49.72	-33.93
22	3	2	1	53.53	34.57	48.96	-33.80
23	3	2	2	53.71	34.60	48.87	-33.78
24	3	2	3	54.23	34.68	48.85	-33.78
25	3	3	1	57.06	35.13	48.43	-33.70
26	3	3	2	55.93	34.95	48.39	-33.70
27	3	3	3	57.59	35.21	48.12	-33.65

corresponding S/N ratio. From the obtained S/N ratios analysis of means were evaluated to determine the optimal level of control factors. The results for hardness response obtained for the FGM's synthesized with vibrations are presented in Tables 5.3 and 5.4

Table 5.3 Analysis of means based on S/N ratio for top portion (With vibration)

Larger the better quality characteristic			
Level	Chill material	Chill volume	Pouring temperature
1	35.02	34.43	34.82
2	34.84	34.76	34.82
3	34.70	35.36	34.91
Delta	0.32	0.93	0.09
Rank	2	1	3

Table 5.4 Analysis of means based on S/N ratio for bottom portion (With vibration)

Smaller the better quality characteristic			
Level	Chill material	Chill volume	Pouring temperature
1	-33.70	-33.90	-33.78
2	-33.75	-33.76	-33.76
3	-33.80	-33.60	-33.73
Delta	0.10	0.30	0.05
Rank	2	1	3

The level of parameters with highest value of S/N ratio at the top portion and lowest value of S/N ratio at the bottom portion is the best combination level indicating better gradation in hardness from bottom to top of the cast. This approach helped to determine the influence of each control factor on the gradation of hardness values from bottom to top portion. The optimal process parameters are found to be Copper chill(A1), Chill volume(B3) and pouring temperature (C3). The results of S/N ratios based on analysis of means for hardness at top and bottom portion are also shown in Figures 5.1 and 5.2.

From obtained values of S/N ratio, ANOVA is carried out to study the percentage contribution of each control factor. The summary of ANOVA results for hardness at top

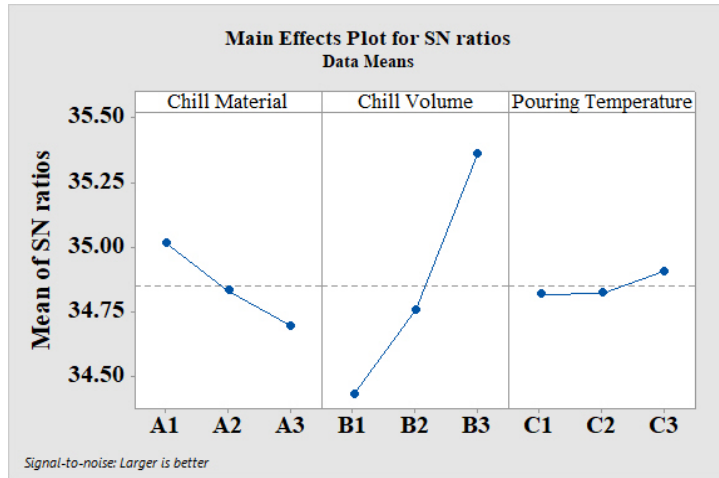


Figure 5.1 Main effects plot for hardness based on S/N ratio for top portion

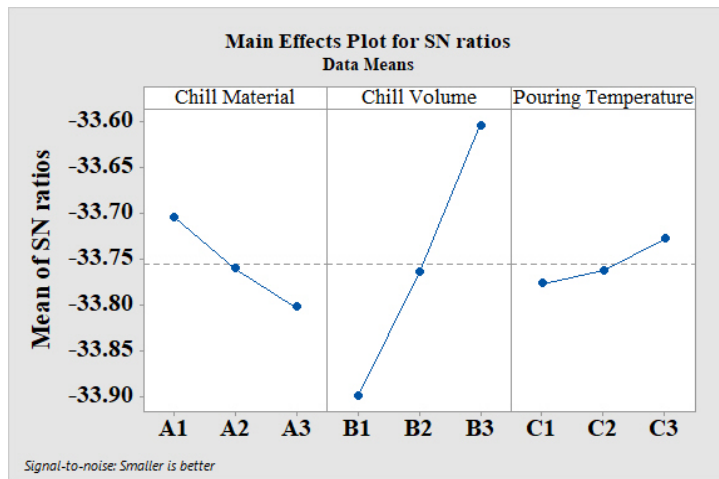


Figure 5.2 Main effects plot for hardness based on S/N ratio for bottom portion

and bottom portion are presented in Table 5.5 and 5.6 respectively. It is seen from the Table 5.5 and 5.6 that chill volume has major contribution of (84.04%) at the top portion and (82.80%) at the bottom portion which has played a significant role in attaining gradation in hardness values across the cast specimen.

At optimal levels of control factors, validation experiments were performed with error prediction within the 95% confidence limit, which indicates the adequacy of the additivity of hardness models. The best combination of optimal process parameters for obtaining the gradation in hardness values along the length of the FGM synthesized with lateral vibrations are presented in Table 5.7. Influence of VHC, pouring temperature on the gradation in hardness values is shown in Figures 5.3 and 5.4, it is seen that higher the

Table 5.5 ANOVA for hardness based on S/N ratio for top portion

Source	DF	Sum of squares	Mean square	Contribution (%)
Chill Material	2	19.82	9.91	10.06
Chill Volume	2	165.67	82.84	84.04
Pouring Temperature	2	1.87	0.93	0.95
Error	20	9.77	0.49	4.96
Total	26			100.00

Table 5.6 ANOVA for hardness based on S/N ratio for bottom portion

Source	DF	Sum of squares	Mean square	Contribution(%)
Chill Material	2	1.35	0.68	9.08
Chill Volume	2	12.34	6.17	82.80
Pouring Temperature	2	0.34	0.17	2.29
Error	20	0.87	0.04	5.83
Total	26			100.00

value of VHC and pouring temperature better is the gradation obtained along the length of the cast.

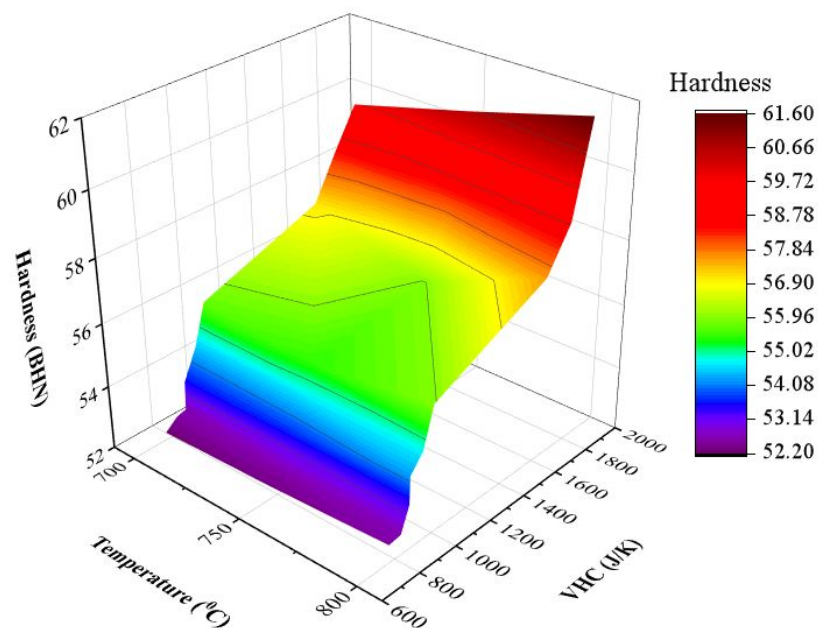


Figure 5.3 Volumetric heat capacity on hardness: Top portion

Table 5.7 Optimal control factor setting and optimal values for hardness at top and bottom portion

Response	Optimal process parameter			Optimal value (BHN)
	Chill Material	Chill Volume (cm ³)	Pouring Temperature (°C)	
Hardness (Top)	Copper	8.5*8.5*8	800	61.60
Hardness (Bottom)	Copper	8.5*8.5*8	800	46.72

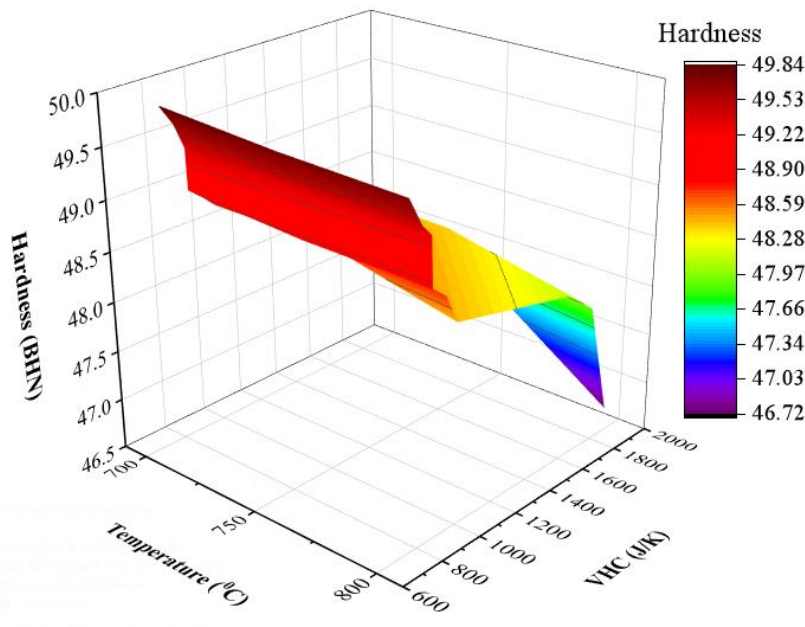


Figure 5.4 Volumetric heat capacity on hardness: Bottom portion

The FGM obtained with optimized control factors are evaluated for microstructure, strength and tribological characteristics and discussed in the following sections.

5.3.1 Hardness

Due to the influence of lateral excitation, it is expected that Si particles precipitate from the bottom to the top portion. As evident from Figure 5.5, there is a substantial increase of hardness value at the top portion compared to the bottom portion of a structure. By providing bottom chill, a steep temperature gradient is expected. This higher difference in temperature causes faster heat transfer at the chill-melt interface. Due to the influence of

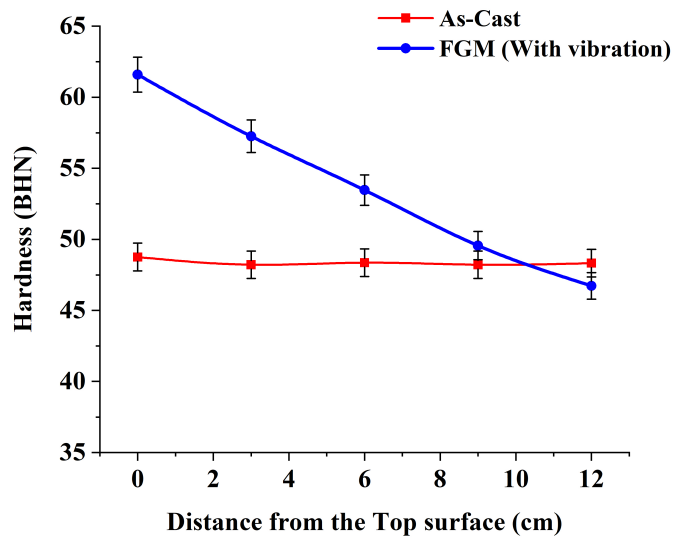


Figure 5.5 Hardness across the section

lateral excitation the heat transfer rate further increases and the enhances the segregation of Si particles at faster rate. Due to the increased solidification rate the precipitated Si are not allowed to settle down towards the bottom portion, thereby enhancing the gradation in hardness across the cast specimen.

It is observed that a maximum of $(61.60 \pm 1 \text{ BHN})$ at the top surface and a minimum of $(46.72 \pm 1 \text{ BHN})$ at the bottom surface revealing a variation in hardness values along the length of the cast. This variation can be attributed to the increased volume fraction of harder Si particles at the top portion of the cast which has led to gradation within the structure (Chirita et al. 2009b). As the volume fraction of harder particles are increased in the top portion, a significant improvement in mechanical and tribological properties can be seen.

5.3.2 Effect of chill on solidification

Figure 5.6 presents cooling curve obtained for directionally solidified FGM fabricated under the influence of lateral excitation. It is seen that solidification begins at lower temperature chill/melt interface compared to the top portion. Also because of lateral excitation the temperature difference is further increased which is shown in Figure 5.7. It is observed that temperatures kept dropping drastically from 180°C to 20°C till

200 sec. After 200 sec the temperature at top portion had achieved an equilibrium temperature. This rapid solidification rate can be attributed to lateral excitation. Due to this temperature variation between the top and bottom portion it is understood that steep gradation in temperature is established by the chill and lateral excitation which has enhanced the directional solidification at faster rate (Rikhtegar and Shabestari 2014).

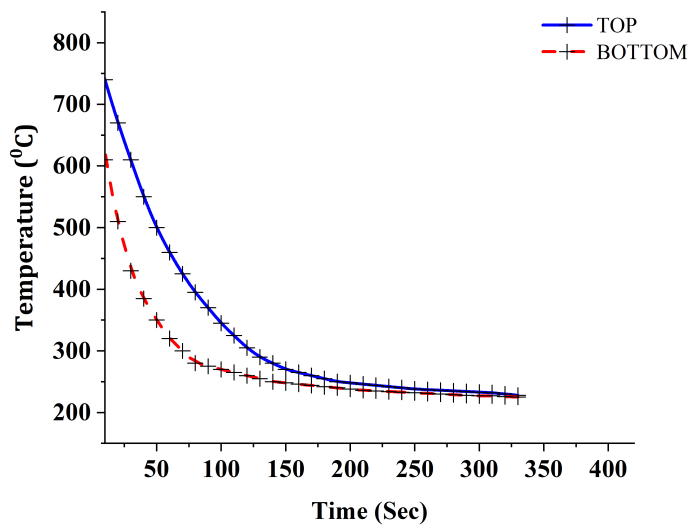


Figure 5.6 Cooling Curves of FGM

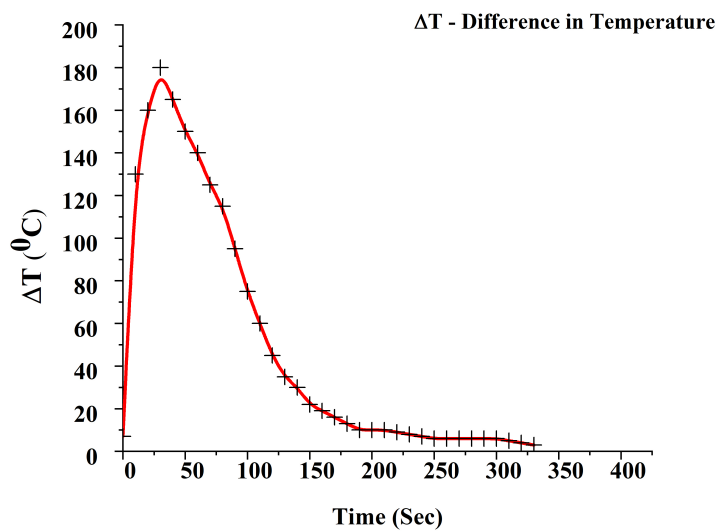


Figure 5.7 Temperature Difference between top and bottom portion vs time

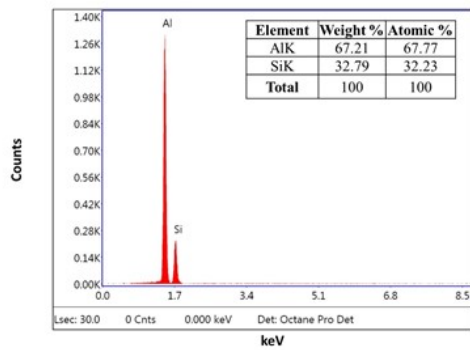
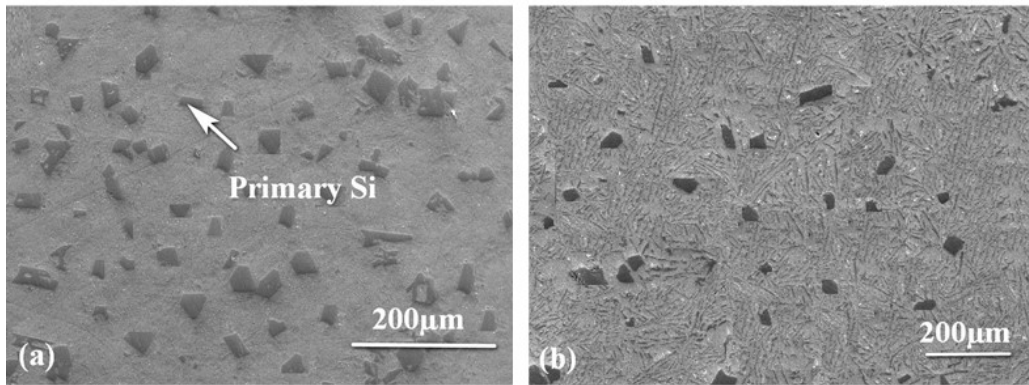
5.3.3 Microstructure

The microstructures of the FGM solidified under optimal process parameter conditions clearly indicate that force generated due to lateral excitation greatly influences the solidification features of the cast. Figure 5.8(a) and 5.8(b) shows microstructures obtained at top and bottom portion of the FGM structure. It is observed that large number of Si particles have segregated towards the top portion whereas the bottom portion is particle depleted. This is because of placement of bottom chill and when lateral excitation is provided to the mold, it has resulted in creating waves in the melt. Due to this non-linear convection, it has helped Si to segregate towards the top portion which can be seen from the Figures 5.8c and 5.8d. Therefore, it is observed that trend in hardness values correlates with the microstructure which dictates the mechanical and tribological properties of the material.

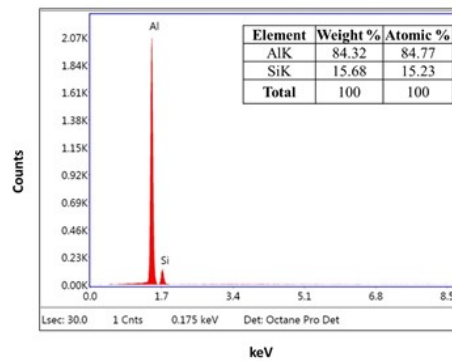
Figure 5.8e, shows histogram for the particle size distribution of the FGM for top and bottom region. As a result, it suggests that the number of Si particles is more in top region in compared to the bottom region. It is observed that in the bottom region, the particle size diameter is in the range from 10 to 55 μm . However, in the top portion it can be seen that the particle size diameter is from 0 to 50 μm . It is also seen that frequency of particle size distribution is more in top portion in contrast to the bottom portion. These variation in particle reinforcements has led to significant changes in gradation and properties along the cast. Figure 5.9 shows porosity percentage across the length of an FGM which can be attributed to the influence of vibrations resulting in improved gradation properties.

5.3.4 Strength

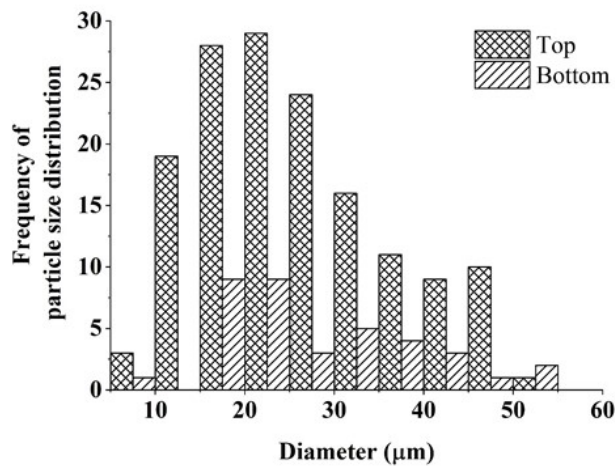
It was revealed through the microstructural study that top portion is rich in reinforced particulates compared to the bottom portion. This variation is due to the presence of the bottom chill and to the influence of lateral excitation. As a result primary Si is precipitated towards the top portion leading to larger number of primary Si particles in the top portion. Therefore, it is understood that segregation of particulates from one end to the other end of the cast has led to gradation in the structure which is also evident



(c)



(d)



(e)

Figure 5.8 Microstructural analysis of FGM (a) Representative SEM image of top portion (b) Representative SEM image of bottom portion (c) EDS for top portion (d) EDS for bottom portion (e) Histogram for frequency of particle size distribution

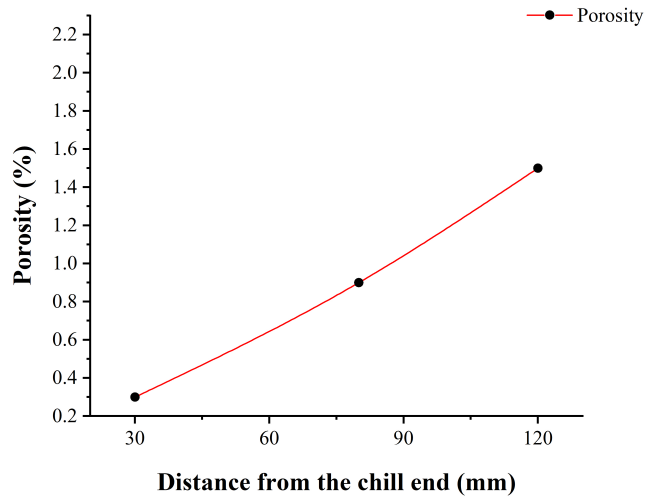


Figure 5.9 Porosity check of Al-18wt% Si FGM fabricated with lateral vibrations

from the hardness values. It was revealed through strength values shown in Figure 5.10 that there is enhancement of tensile strength at the bottom region of the cast compared to the top region. The morphology of the fractured surfaces of FGM taken at a strain

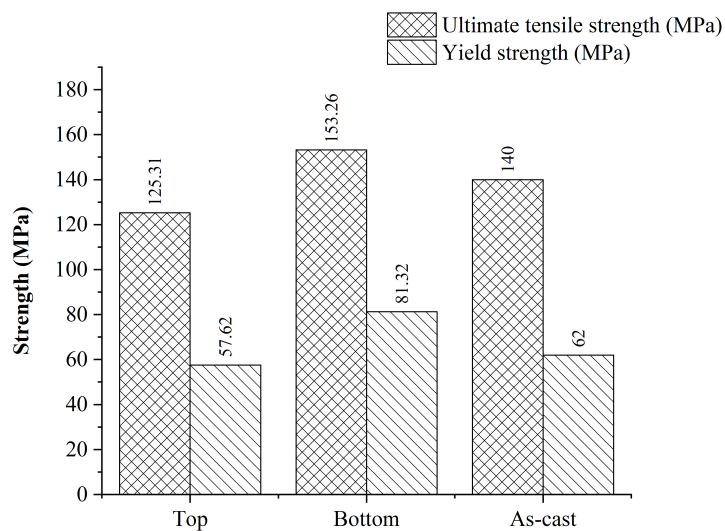


Figure 5.10 Strength of FGM (With vibrations) and as-cast

of 0.6 are shown in Figure 5.11. The fractography at top region of the cast as shown in Figure 5.11a, reveals quasi-cleavage mode. As a result, due to precipitation of Si at the top. The failure is brittle in nature. However since the volume fraction of Si particles at the bottom region is less, it has resulted in crack initiation and coalescence

of voids leading to dimple morphology. Therefore, the failure due to this characteristic appearance is always ductile in nature as shown in Figure 5.11b (Radhika et al. 2018).

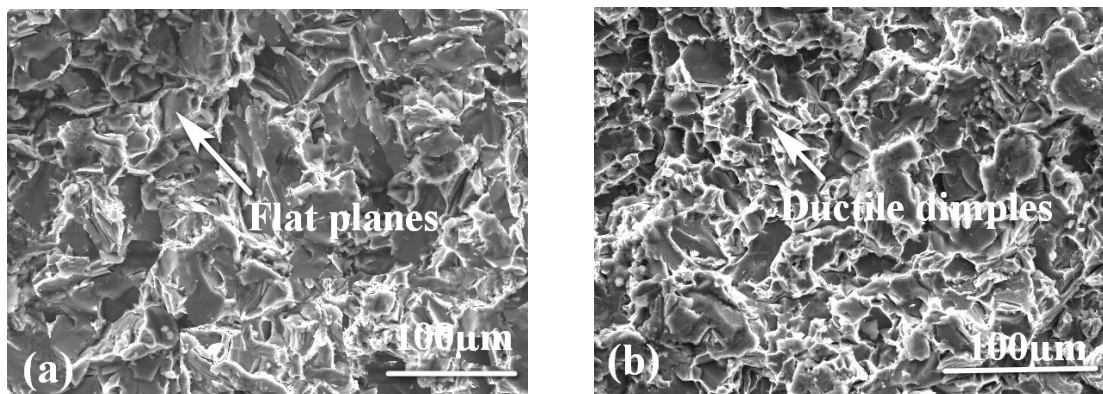


Figure 5.11 Fractography of tensile specimens (with vibrations): (a) Top portion (b) Bottom portion

5.3.5 Wear analysis

Loss of material is one of the prime areas at presently engaging the attention of most of the technologists. One of the outcomes expected out of this investigation is to realize that the highly potential Al-Si alloy, if functionally graded, should be capable of replacing some of the conventional materials in the automotive, aircraft and aerospace industries where the tribological properties of the materials are a major requirement (Dwivedi et al. 2008; Sarkar 1975). With the variation in hardness from top to bottom portion of the cast. It was expected that FGM show the different wear characteristics. This was confirmed with weight loss, coefficient of friction, specific wear rate and worn surface analysis considered at top and bottom portion.

It is observed from the Figure 5.12 that wear loss increases with increase in load which is in accordance with Archard's wear law (Archard 1953), which states that wear loss increases as the load increases. It is noted that wear loss is less at top portion compared to the bottom portion of the FGM and base alloy (Ul Haq and Anand 2018a). The higher wear loss of the FGM indicates removal of more material which is due to the direct contact of sliding surfaces and the worn out silicon particles penetrate the aluminum matrix resulting in easy nucleation. Figure 5.13 shows the coefficient of friction (COF) obtained for the FGM at 30N load. It is found that coefficient of friction increases

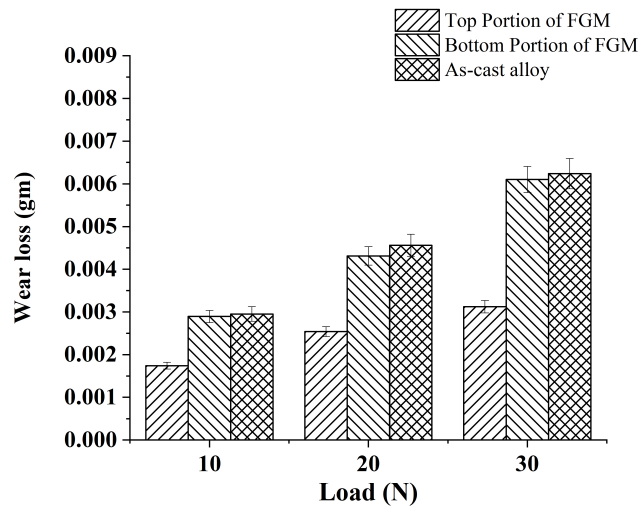


Figure 5.12 Wear loss of FGM (With vibrations) and as-cast

uniformly with increasing load. The COF at the top portion of the casting was lower than that of the bottom portion. It is attributed to the density difference between the Si and Al matrix, wherein Si is having lower density compared to Al which caused Si to push towards the top of the casting. Here more amount of harder Si will lead to reduced COF.

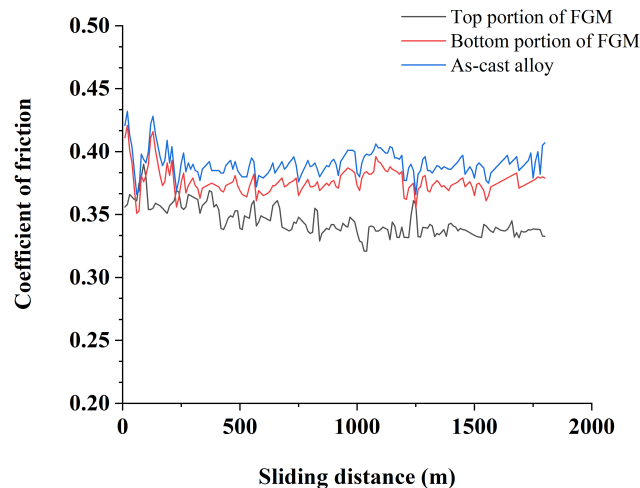


Figure 5.13 Coefficient of friction of FGM (With vibrations) and as-cast

Figure 5.14, shows the specific wear rate of the cast at top and bottom portion. As a result, it was found that for the base alloy and bottom portion of the FGM, there is a significant increase in specific wear results. However, it was reported that in the top

portion, there is a decrease in specific wear rate. Also, It was found that the difference in specific wear rate between top and bottom portion at 30N load is 41.89%, which can be attributed to the distribution of silicon across the top region.

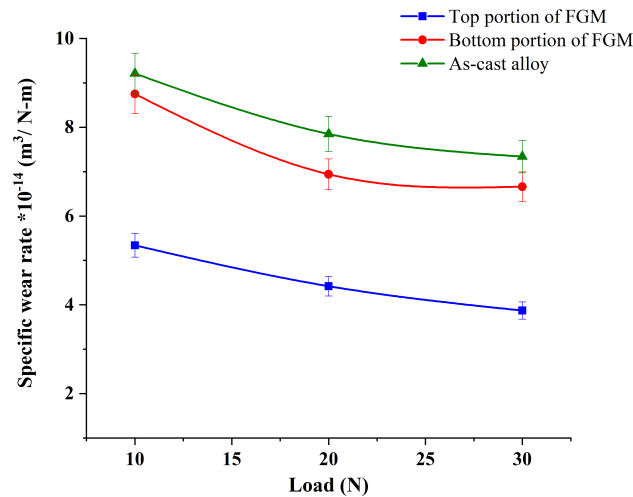


Figure 5.14 Specific wear rate of FGM (With vibrations) and as-cast

5.3.6 Worn out surface analysis

SEM images of the worn surfaces for the specimens subjected to a wear load of 30N are shown in Figure 5.15. FGM castings processed with lateral vibrations revealed that top portion is dominated by delamination wear whereas bottom portion is dominated by abrasive wear. Two wear mechanisms observed could be generally described as: (i) delamination wear (ii) abrasive wear. Worn surfaces at the bottom revealed that long ploughing run parallel to the sliding direction which suggest abrasive wear. The scouring seen in the micrographs suggest that it is due to trapping of debris on the hardened steel counter face which is more in the specimens processed with lateral vibrations. The presence of cracks during sliding of the specimens had been associated with the process of delamination on several occasions by other researchers (Kiran Aithal et al. 2012; Reddy et al. 2009). This type of wear gives rise to the detachment of wear debris which can be seen from the top region. Figure 5.16 (a) shows wear debris of the top portion which shows plate shaped particles indicating delamination wear mechanism, whereas Figure 5.16 (b) shows wear debris of the bottom portion revealing that wear are finer which is due to precipitation of Si from bottom to top portion which is in accordance

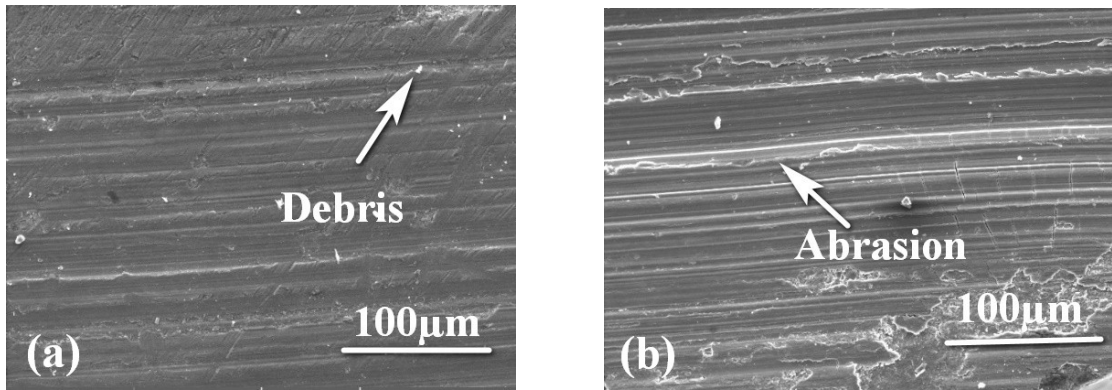
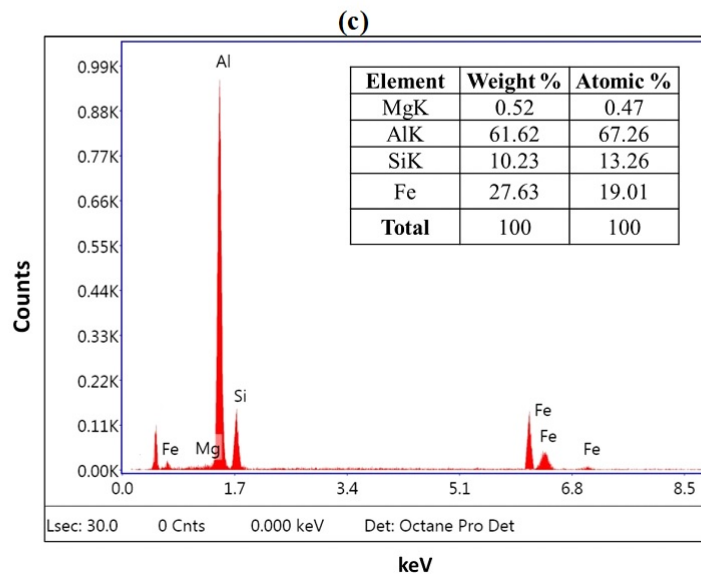
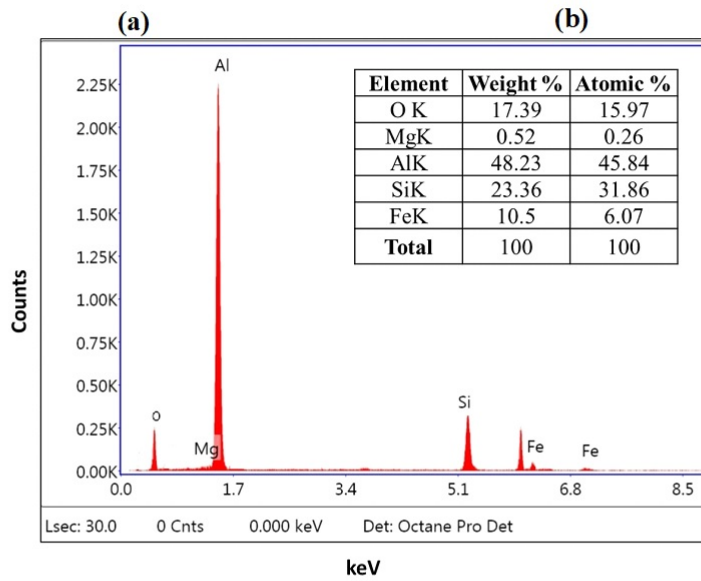
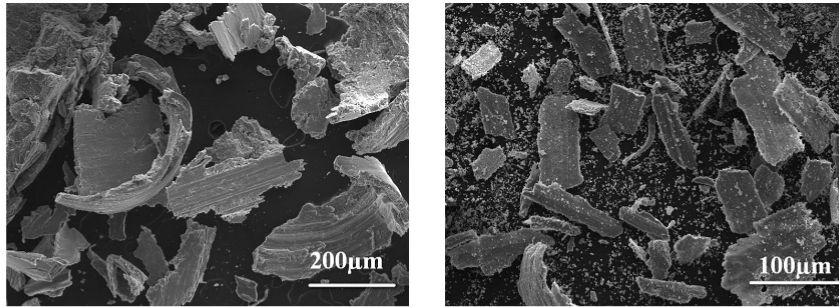


Figure 5.15 SEM images of wear surfaces for the optimized samples (With vibratoins):
(a) Top portion (b) Bottom portion

with microstructure and hardness results. The morphology shown in bottom portion show that it is dominated abrasive and delamination wear.

Figure 5.16 (c) and 5.16 (d) shows the EDS of worn-out surface taken at top and bottom portion. EDS of top portion show that there is a transfer of (Fe) from the counter surface which has contributed towards improved wear resistance (Abedi and Asl 2019; Iwai et al. 2000; Ul Haq and Anand 2019). EDS at the bottom portion show presence of oxides contributing in lowering COF and wear loss which can be attributed to formation of oxide layer giving rise to delamination wear mechanism (Anand et al. 2017; Ul Haq and Anand 2018b; Zhang 2013).



(d)

Figure 5.16 Wear debris analysis of FGM (With vibrations): (a) Top portion (b) Bottom portion (c) EDS for top portion (d) EDS for bottom portion

5.4 SUMMARY

In this chapter, Al-18wt%Si FGM was fabricated through DS technique coupled with lateral vibrations. The obtained cast has been evaluated for mechanical and tribological characteristics. Based on the experimental results following conclusions were drawn.

- Optimization of process parameters was carried out through taguchi technique, obtained ANOVA results revealed that chill volume has a major contribution in enhancing the gradation in hardness values.
- Hardness values obtained for the sample fabricated with optimal process parameters revealed 61.60 BHN at top portion and 46.72 BHN at bottom portion.
- The micro structure of the obtained FGM revealed that top portion is hyper-eutectic in nature due to the presence of large number of primary Si and the bottom portion with eutectic in nature.
- The particle size distribution, tensile strength of the FGM showed a enhanced graded characteristics which correlates the hardness values and microstructure.
- Top portion showed significant decrease in wear loss, specific wear rate, COF indicating that that primary Si has been distributed all over the surface instead of segregating in lumps which can be attributed to the influence of lateral excitation which is also visible through worn-out surface analysis.

The next chapter focuses on addition of 2wt% graphite to the Al-18wt%Si alloy to fabricate FGC. This is accomplished through coupling DS technique with a novel lateral vibration set up. The main purpose of adding graphite is to provide self-lubricating tribological characteristic which will serve as potential property in automotive applications.

CHAPTER 6

Al-18wt%Si REINFORCED WITH 2wt% GRAPHITE FGC SYNTHESIZED WITH LATERAL VIBRATIONS

6.1 INTRODUCTION

This chapter deals with development and characterization of Al-18wt%Si reinforced with 2wt% graphite based FG composite. The FGC's are obtained with the novel directional solidification technique under the influence of lateral vibrations. Optimization of process parameters such as chill material, chill volume and pouring temperature was adopted to finalize the control factors and their levels. This chapter also discusses evaluation of mechanical and tribological properties of FGC synthesized with lateral vibrations to understand the significance of vibrations.

6.2 CASTING OF FGM

A directional solidification technique coupled with lateral vibrations as shown in Figure 3.5 was used to prepare Al-Si- Graphite reinforced FGC. The size of graphite particle was maintained at 5-10 μ m. A group of researchers (Akhlaghi and Zare-Bidaki 2009; Hassan et al. 2007) have found that less dense graphite tend to float in the melt resulting in non-uniform distribution in the composites. This non-uniform distribution increases with increase in reinforcement percentage, thereby leading to reduced interaction and bonding between the matrix and reinforcement. Hence 2wt% graphite is used in the present work.

The main problem associated with the processing of Al-Si-Graphite FGC is the poor wettability of graphite particulates with Al-Si melt. This poor wettable nature results in inadequate interface bonding between Al-Si melt and graphite particulate. Moreover, graphite particles cannot be easily added to the molten aluminum alloy (Krishnan et al. 1981). It was reported that the graphite particles must be preheated to 400⁰C for 1hour

before adding it to the molten alloy (Rajaram et al. 2010). The Al-Si base alloy is heated in a resistance furnace and the temperature is maintained at 800⁰c and the necessary melt treatment was carried out by degassing.

In order to improve the wettability of graphite particle with the melt, Magnesium of (1wt%) was added. The preheated mixture of graphite is reinforced to the molten metal and stirred for 10 minutes. The lateral vibration set up is set in to vibrations with a frequency of 10Hz. The melt comprising of Al-Si alloy matrix and graphite particles is poured in to the mold placed in vibration set up. Parametric optimization for the control factors namely chill material, chill volume and pouring temperature were carried out to identify the optimized control factors to attain better gradation in the structure. Each parameter was investigated at three levels to study the influence of process parameters on hardness at top and bottom portion. The identified process parameters and their levels are presented in Table 4.1. The measured values of hardness are summarized and presented in Table 6.1

6.3 EVALUATION OF PROPERTIES OF FGM FABRICATED WITH OPTIMAL PARAMETERS

FGC's are those materials in which gradation in properties take place from one end of the cast to the other end. In the present work this gradation is obtained by the DS technique coupled with lateral vibrations which has been clearly explained in previous section. Due to precipitation of Si in linear direction, the FGC fabricated have hypereutectic structure at the top region with larger volume of Si particles, whereas bottom region have eutectic structure filled with lesser volume of Si particles. This can be attributed to the presence of chill and influence of lateral vibrations leading to better gradation of properties along the length of the cast.

In this present study, the objective is to have lower hardness at the bottom portion and higher hardness at the top portion. Hence a "smaller the better" quality characteristic is used for the bottom portion and "larger the better" quality characteristic for top portion is selected. The S/N ratios associated with the objective of each trial of the orthogonal array is calculated by Equations 4.1 and 4.2. A total of 27 experiments were carried out

Table 6.1 Response table for hardness (With Vibrations)

Experimental run				Top portion		Bottom portion	
	A	B	C	Hardness	S/N ratio	Hardness	S/N ratio
1	1	1	1	54.86	34.79	49.53	-33.90
2	1	1	2	55.42	34.87	49.51	-33.89
3	1	1	3	55.63	34.91	49.49	-33.89
4	1	2	1	57.62	35.21	49.20	-33.84
5	1	2	2	57.97	35.26	49.17	-33.83
6	1	2	3	58.18	35.30	49.16	-33.83
7	1	3	1	61.88	35.83	48.34	-33.69
8	1	3	2	62.81	35.96	48.31	-33.68
9	1	3	3	66.21	36.42	48.21	-33.66
10	2	1	1	54.82	34.78	49.63	-33.91
11	2	1	2	54.82	34.78	49.61	-33.91
12	2	1	3	54.86	34.79	49.61	-33.91
13	2	2	1	56.71	35.07	49.21	-33.84
14	2	2	2	56.97	35.11	49.21	-33.84
15	2	2	3	56.97	35.11	49.21	-33.84
16	2	3	1	60.31	35.61	48.70	-33.75
17	2	3	2	60.78	35.68	48.65	-33.74
18	2	3	3	61.05	35.71	48.38	-33.69
19	3	1	1	54.49	34.73	49.73	-33.93
20	3	1	2	54.62	34.75	49.64	-33.92
21	3	1	3	54.82	34.78	49.64	-33.92
22	3	2	1	55.76	34.93	49.49	-33.89
23	3	2	2	55.95	34.96	49.49	-33.89
24	3	2	3	56.49	35.04	49.41	-33.88
25	3	3	1	58.19	35.30	49.11	-33.82
26	3	3	2	59.32	35.46	49.09	-33.82
27	3	3	3	59.84	35.54	48.85	-33.78

with lateral vibrations in accordance with parameter level of each factor and observed hardness values were noted and corresponding S/N ratio were evaluated. From the obtained S/N ratios analysis of means were evaluated to determine the optimal level of control factors. The results for hardness response obtained for the FGC synthesized with vibrations are presented in Tables 6.3 and 6.4 The level of parameters with highest

Table 6.3 Analysis of means based on S/N ratio for top portion (With vibration)

Larger the better quality characteristic			
Level	Chill material	Chill volume	Pouring temperature
1	35.39	34.80	35.14
2	35.18	35.11	35.20
3	35.05	35.72	35.29
Delta	0.34	0.93	0.15
Rank	2	1	3

Table 6.4 Analysis of means based on S/N ratio for bottom portion (With vibration)

Smaller the better quality characteristic			
Level	Chill material	Chill volume	Pouring temperature
1	-33.80	-33.91	-33.84
2	-33.83	-33.85	-33.84
3	-33.87	-33.74	-33.82
Delta	0.07	0.17	0.02
Rank	2	1	3

value of S/N ratio at the top portion and lowest value of S/N ratio at the bottom portion is the best combination level indicating better gradation in hardness from bottom to top of the cast. This approach helped to determine the influence of each control factor on the gradation of hardness values from bottom to top portion. The optimal process parameters are found to be Copper chill(A1), Chill volume(B3) and pouring temperature (C3). The results of S/N ratios based on analysis of means for hardness at top and bottom portion are also shown in Figures 6.1 and 6.2. From obtained values of S/N ratio, ANOVA is

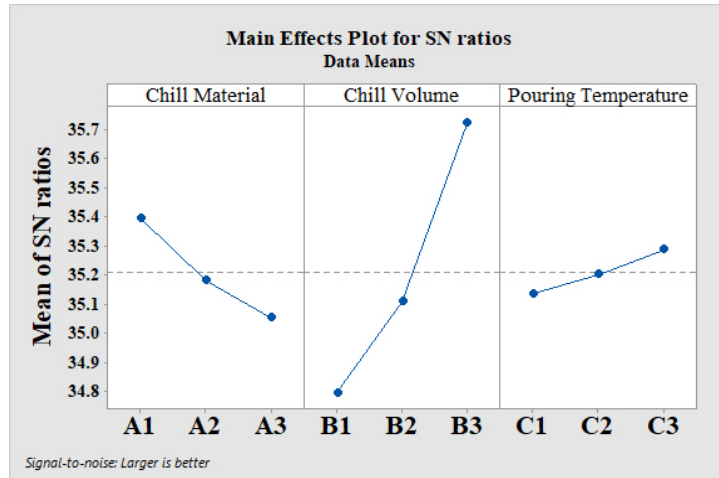


Figure 6.1 Main effects plot for hardness based on S/N ratio for top portion

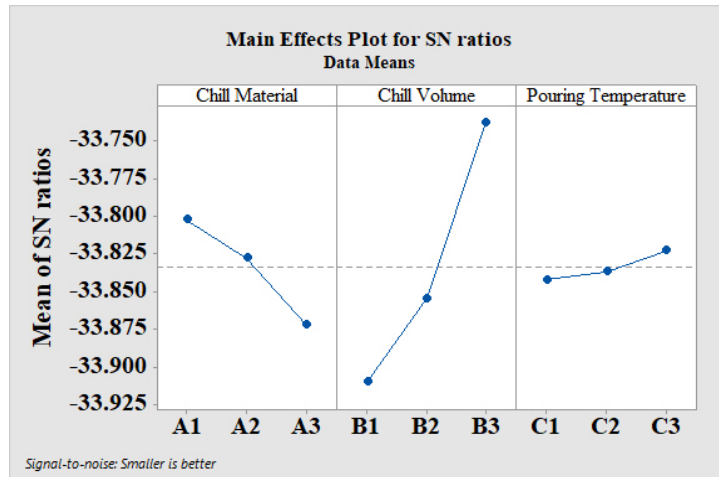


Figure 6.2 Main effects plot for hardness based on S/N ratio for bottom portion

carried out to study the percentage contribution of each control factor. The summary of ANOVA results for hardness at top and bottom portion are presented in Table 6.5 and 6.6 respectively. It is seen from the Table 6.5 and 6.6 that chill volume has major contribution of (78.30%) at the top portion and (79.72%) at the bottom portion which has played a significant role in attaining gradation in hardness values across the cast specimen. At optimal levels of control factors, validation experiments were performed with error prediction within the 95% confidence limit, which indicates the adequacy of the additivity of hardness models. The best combination of optimal process parameters for obtaining the gradation in hardness values along the length of the FGM synthesized with lateral vibrations are presented in Table 6.7. Influence of VHC, pouring temperature

Table 6.5 ANOVA for hardness based on S/N ratio for top portion

Source	DF	Sum of squares	Mean square	Contribution (%)
Chill Material	2	25.29	12.65	10.91
Chill Volume	2	181.58	90.79	78.30
Pouring Temperature	2	4.96	2.48	2.14
Error	20	20.08	1.00	8.66
Total	26			100.00

Table 6.6 ANOVA for hardness based on S/N ratio for bottom portion

Source	DF	Sum of squares	Mean square	Contribution(%)
Chill Material	2	0.71	0.36	12.84
Chill Volume	2	4.43	2.22	79.72
Pouring Temperature	2	0.06	0.03	1.04
Error	20	0.36	0.02	6.39
Total	26			100.00

on the gradation in hardness values is shown in Figures 6.3 and 6.4, it is seen that higher the value of VHC and pouring temperature better is the gradation obtained along the length of the cast. The FGM obtained with optimized control factors are evaluated for microstructure, strength and tribological characteristics and discussed in the following sections.

6.3.1 Hardness

In FGC's, it is expected that properties in the structure vary from one end to other end due to the segregation of harder particulates towards one side of the structure. Figure 6.5 shows the hardness values of the FGC and as-cast plotted along the length of the cast. It is seen that due to the influence of lateral vibrations, particulate reinforcements increases progressively and are pushed towards the top. This is due to the difference in densities between the matrix and particulates. As the primary Si is the strengthening phase in Al-Si alloy, thereby the hardness is mainly influenced by the primary Si content (Watanabe et al. 2007). Thus it is understood that hardness of FGC depends upon the presence of

Table 6.7 Optimal control factor setting and optimal values for hardness at top and bottom portion

Response	Optimal process parameter			Optimal value (BHN)
	Chill Material	Chill Volume (cm ³)	Pouring Temperature (°C)	
Hardness (Top)	Copper	8.5*8.5*8	800	66.25
Hardness (Bottom)	Copper	8.5*8.5*8	800	48.21

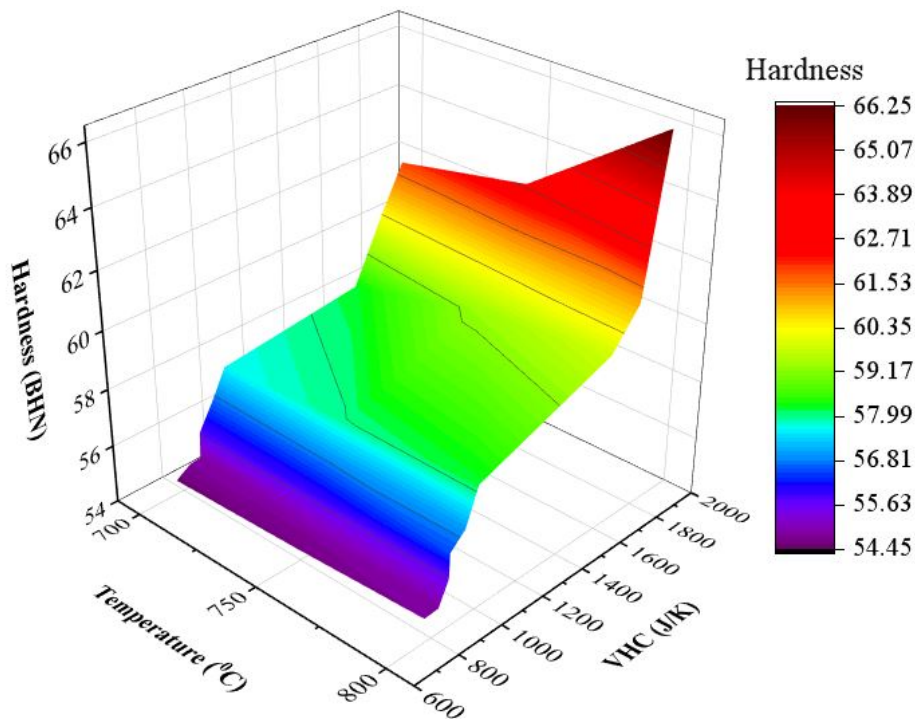


Figure 6.3 Volumetric heat capacity on hardness: Top portion

reinforcements (Askari et al. 2012; Wang et al. 2009).

To evaluate gradation in the structure, hardness values at top and bottom portion of the cast are obtained at different radial distances from the outer periphery and average result of 5 values at the same position are considered. It is observed that a maximum of $(66 \pm 1 \text{ BHN})$ at the top surface and a minimum of $(48 \pm 1 \text{ BHN})$ at the bottom surface revealing a variation in hardness values along the length of the cast. This variation is due to increased volume fraction of harder reinforcement particles at the top portion of

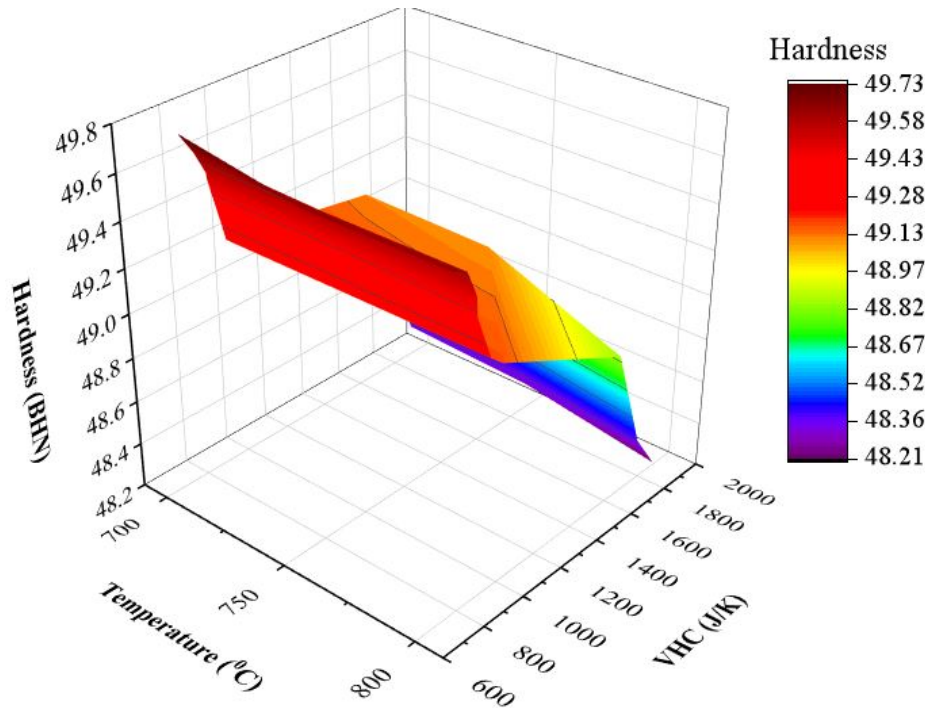


Figure 6.4 Volumetric heat capacity on hardness: Bottom portion

the cast which has led to gradation within the structure Chirita et al. (2009b). As the volume fraction of reinforcement particles are increased a significant improvement in mechanical and tribological properties can be seen.

6.3.2 Effect of chill on solidification

Cooling curves are popularly used to recognize temperature - time history during solidification. Solidification behavior is greatly influenced by the chill material, chill size, pouring temperature which helps in predicting the structural properties of the cast. Figure 6.6 shows that the solidification at the chill/metal interface begins at lower temperature in contrast to the top region. The temperature variation between the top and bottom portion contains the versatility ($\Delta T = T_{top} - T_{bottom}$) versus time which is shown in Figure 6.7.

As expected, the melt near the chill was subjected to rapid solidification. Therefore, it was found that fluctuations between top and bottom portion were more vigorous, immediately after pouring the melt thereby releasing the latent heat. It was observed that difference in temperatures kept dropping significantly from 180⁰C to 20⁰C till 150 sec.

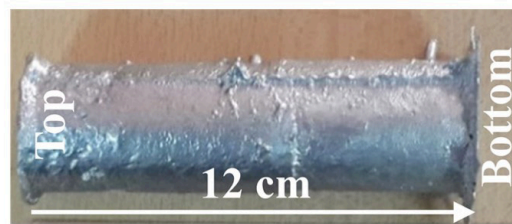
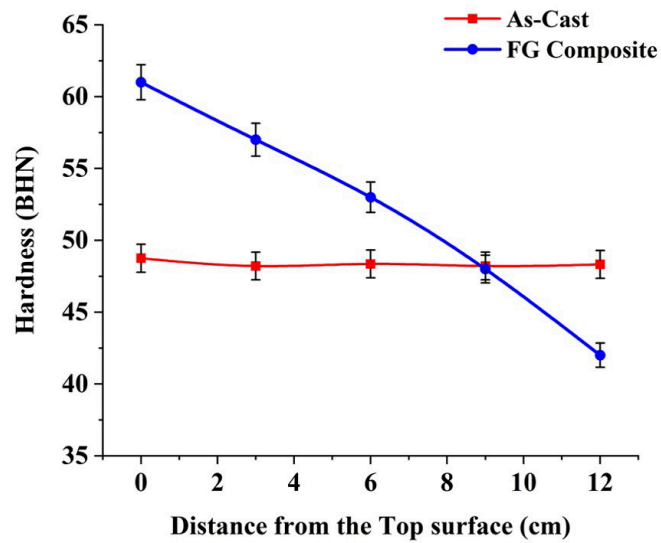


Figure 6.5 Hardness across the section

After 150 sec, the temperature at the top portion had achieved a nearly constant trend with the temperature at the bottom portion. By completing the solidification, ΔT has declined leading to equilibrium temperature (Rikhtegar and Shabestari 2014). Therefore, it is evident that a steep temperature gradient was established by the chill which acts as the driving factor in the directional solidification of the casting (Manjunath et al. 2018).

6.3.3 Microstructure

Figure 6.8a and 6.8b, presents the microstructures obtained at top and bottom region of the cast. It can be seen from the (Figure 6.8c and 6.8d), that there is a graded distribution of Si particles from bottom to top region of the cast. The segregation of Si particles at top region of the cast is due to placement of copper chill at the bottom which promotes directional solidification. When the melt is poured in to the mold, Si being lighter than Al, precipitates through the melt. As the viscosity of the melt gradually increases due to rapid freezing at the chill/metal interface, it was found that there is an enrichment of

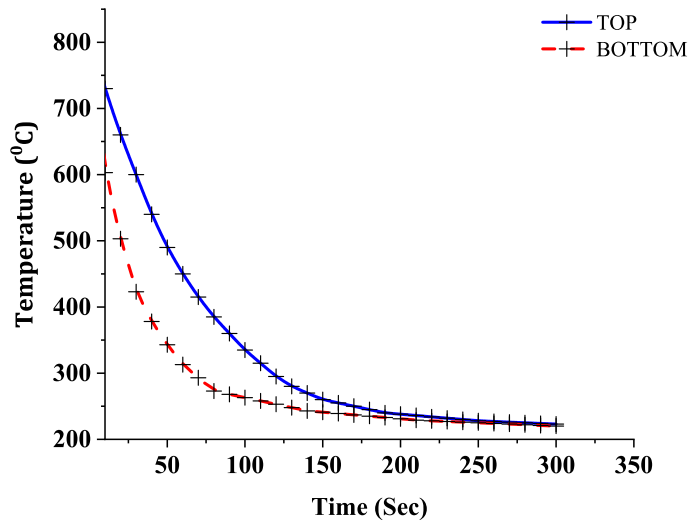


Figure 6.6 Cooling Curves of FGM

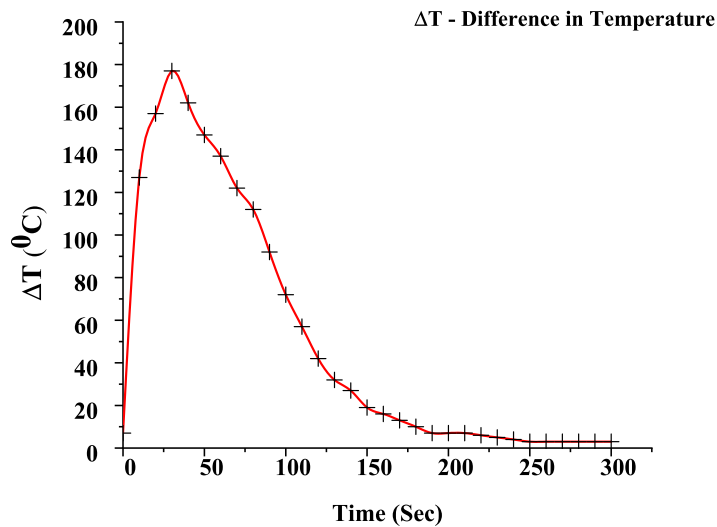
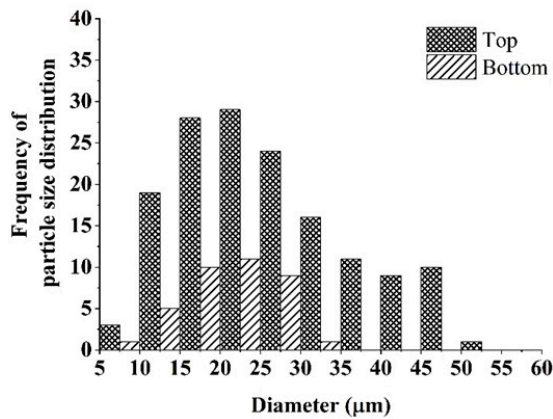
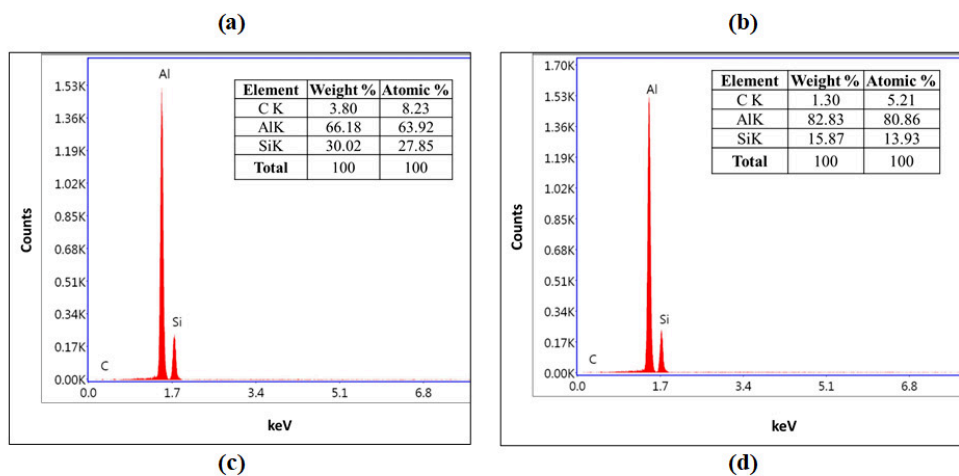
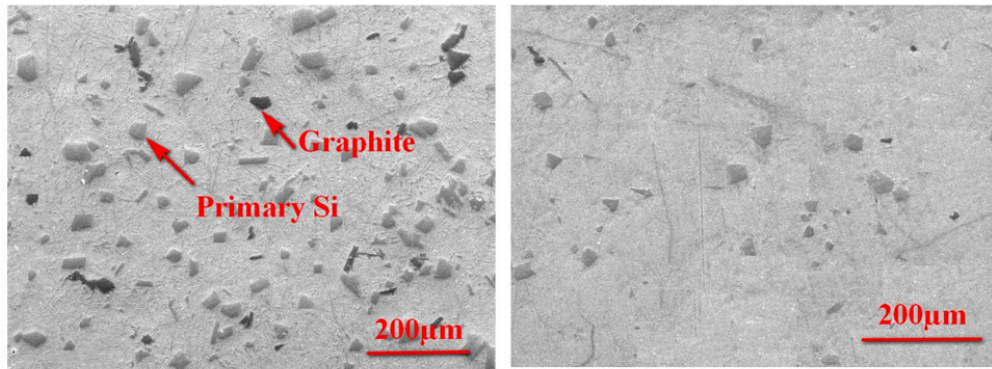


Figure 6.7 Temperature Difference between top and bottom portion vs time

primary Si in the top region of the cast sample which has led to better gradation in the properties. The distribution of Si can be attributed to the lateral excitation which causes waves in the melt with non-linear convection which has helped in separation of primary Si particles (Zhongtao et al. 2008). Therefore, it is observed that trend in hardness values correlates with the microstructure which dictates the mechanical properties of the material.



(e)

Figure 6.8 Microstructural analysis of FGM (a) Representative SEM image of top portion (b) Representative SEM image of bottom portion (c) EDS for top portion (d) EDS for bottom portion (e) Histogram for frequency of particle size distribution

Figure 6.8e, presents the histogram for particle size distribution of the cast for top and bottom region. As a result, it suggests that the number of Si particles is more in top region in contrast to the bottom region. This is due to the fact that in hypereutectic Al-Si FGC, the Si growth front rejects the aluminum atoms into the liquid alloy and the primary Si particles formed are segregated as a graded layer in the cast. It is seen that in the bottom region, the particle size diameter is in the range from 0 to $35\mu\text{m}$. However, in the top portion it can be seen that the particle size diameter is from 5 to $55\mu\text{m}$ which clearly signifies that the majority of the Si particles are segregated in the top region and are spread all over the surface in contrast to the bottom region of the cast. This can be attributed to the influence of vibrations which has assisted primary Si to segregate. This clearly shows that top portion has highly dense particle reinforcements. Whereas bottom portion shows that these surfaces are particle depleted. These variation in particle reinforcements has led to significant changes in gradation and properties along the cast. Figure 6.9 shows porosity percentage across the length of an FGM which can be attributed to the influence of vibrations resulting in improved gradation properties.

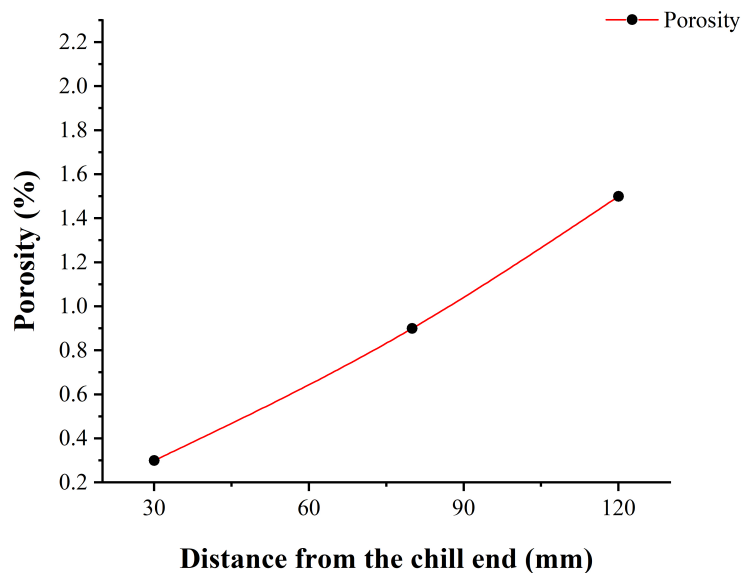


Figure 6.9 Porosity check of Al-18wt% Si reinforced with 2wt% graphite FGC fabricated with lateral vibrations

6.3.4 Strength

From the microstructural study it was revealed that top portion is rich in reinforced particulates compared to the bottom portion which is a particle depleted. This variation is due to the presence of the chill at the bottom and therefore by inducing lateral vibrations, silicon is precipitated towards the top portion. Therefore, it is understood that segregation of particulates from one end to the other end of the cast has led to gradation in the structure which is also evident from the hardness values. From the Figure 6.10, it is revealed that there is enhancement of tensile strength at the bottom region of the cast compared to the top region. It is also seen that vibrations had a positive influence on microstructure and therefore on mechanical properties either increasing or decreasing it (Chirita et al. 2009b). This clearly signifies that there is a gradation in strength from bottom to top portion of the FG composite (Ramesh Babu et al. 2018) The fractography

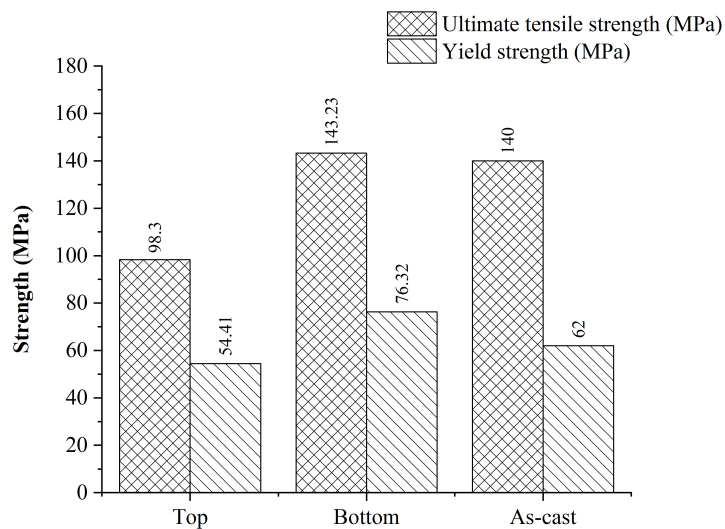


Figure 6.10 Strength of FGC (With vibrations) and as-cast

at top region of the cast as shown in Figure 6.11a, reveals quasi-cleavage mode. As a result, the cast specimen at the top region fails due to brittle nature which can be attributed to the reinforcement particle and also due to high precipitation of Si at the top. However, at the bottom region, since the volume fraction of Si particles is less, which results in crack initiation and coalescence of voids leading to dimple morphology. Therefore, the failure due to this characteristic appearance is always ductile in nature

(Radhika et al. 2018) as shown in Figure 6.11b.

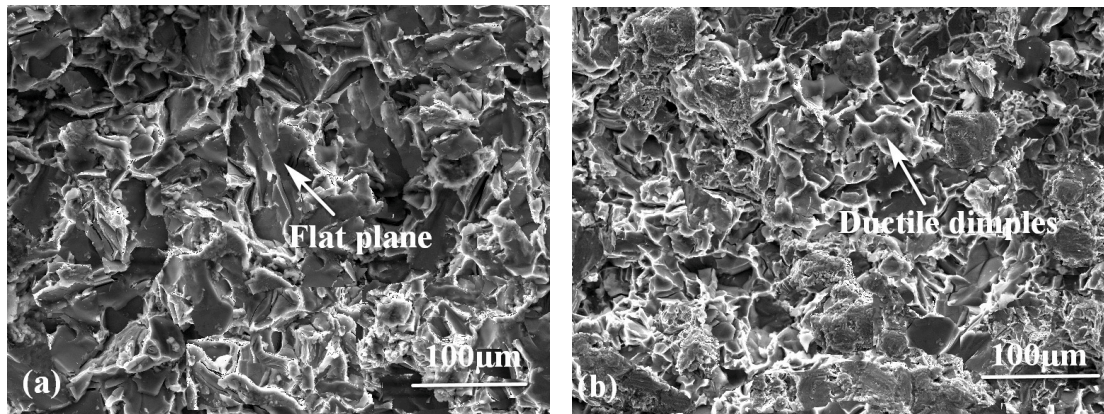


Figure 6.11 Fractography of tensile specimens: (a) Top portion (b) Bottom portion

6.3.5 Diametrical compression

In FGM's the properties vary across the length of the castings. Therefore, it becomes very difficult to establish the mechanical properties such as tensile strength of the specimen by conventional method. This section gives an insight in to the diametral compression test from bottom to top of the casting conducted on Al-Si-Graphite reinforced FG composite. Figure 6.12 shows samples at top and bottom portion of FGC subjected to diametrical compression test. The top portion which is hypereutectic in nature, fracture was observed from the centre of disc approximately at an angle of 45° to the diametral plane as shown in Figure 6.12(a). The crack formation shows to an extent brittle tendency of the material and the crack at an angle to diametral plane is indicative of failure on the shear plane.

It is clear that the fracture along the diametral plane was not formed at bottom part of the casting due to its ductile nature and the material was compressed as shown in Figure 6.12(b). From the Figure 6.13 it can be seen that the gradation in the properties has taken place from bottom to top region of the cast which correlates the results obtained from microstructure and hardness.

6.3.6 Wear analysis

It was expected that the different hardness values at the bottom and top portion of the cast would also show the different wear characteristics. This was confirmed with wear loss, coefficient of friction, specific wear rate and worn surface analysis considered at

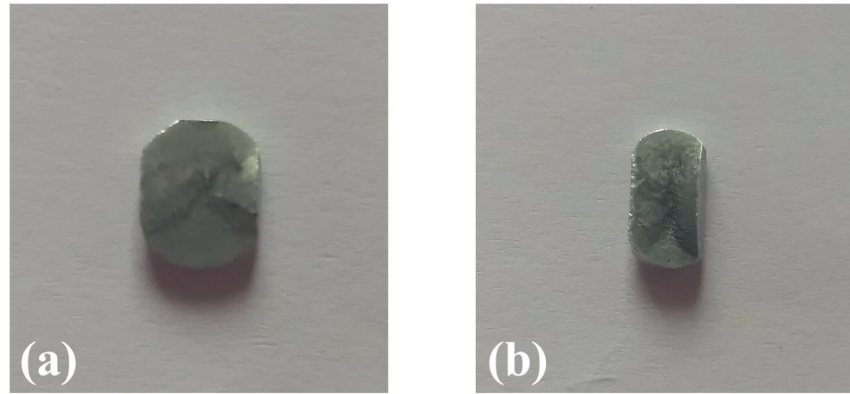


Figure 6.12 Diametrical compression (a) Top portion (b) Bottom portion

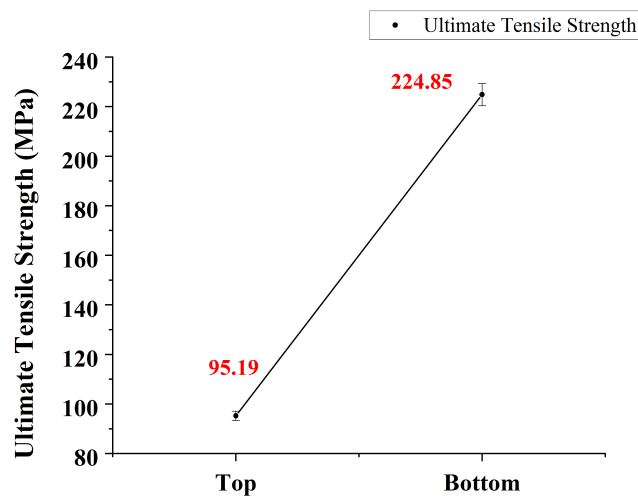


Figure 6.13 Ultimate strength of sample subjected to DC test

top and bottom portion. It can be noted from the Figure 6.14 that wear loss increases with increase in load which is in accordance with Archard's wear law (Archard 1953). It is seen that wear loss is less for the reinforced alloy compared to the base alloy (Ul Haq and Anand 2018a).

The higher wear loss of the base alloy and bottom portion of the FGC indicates that removal of more material which is due to the direct contact of sliding surfaces and the worn out silicon particles penetrate the aluminum matrix which has resulted in easy nucleation. Moreover, due to more number of reinforcement particles at the top portion of FGC, it can be observed that wear loss is less, indicating the beneficial effects of graphite particulates. Therefore, addition of graphite particulates has resulted in lesser

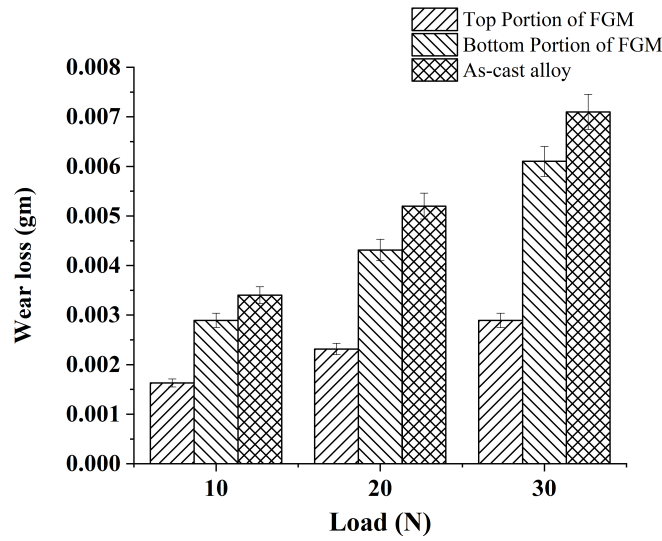


Figure 6.14 Variation of wear loss with load

wear loss (Rajaram et al. 2010).

It can be noted from the Figure 6.15 that lower value of coefficient of friction at the top portion of the FGC can be credited to the worn-out graphite particulates, which acts as the lubricating system between the sliding parts. Moreover, due to the presence of graphite-rich tribofilm underneath the surfaces, it has enabled to minimize the degree of shear stress transferred between the contact parts, which has resulted in less plastic flow in the subsurface region. Figure 6.16, shows the specific wear rate of the cast at top and

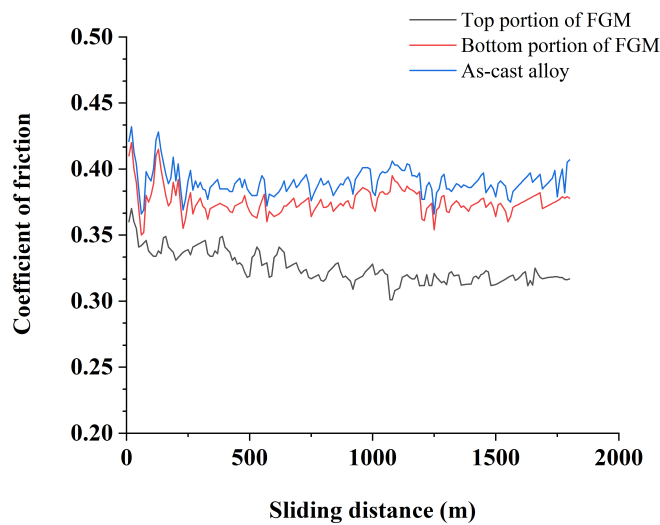


Figure 6.15 Coefficient of friction of FGC and as-cast

bottom portion. As a result, it was found that for the base alloy and bottom portion of the FGC, there is a significant increase in specific wear rate. However, it was reported that in the top portion, there is a decrease in specific wear rate. Also, It was found that the difference in specific wear rate between top and bottom portion at 30N load is 46.57%, which can be attributed to the presence of reinforcement particle across the top region. This clearly shows that obtained wear results matches with microstructure and hardness.

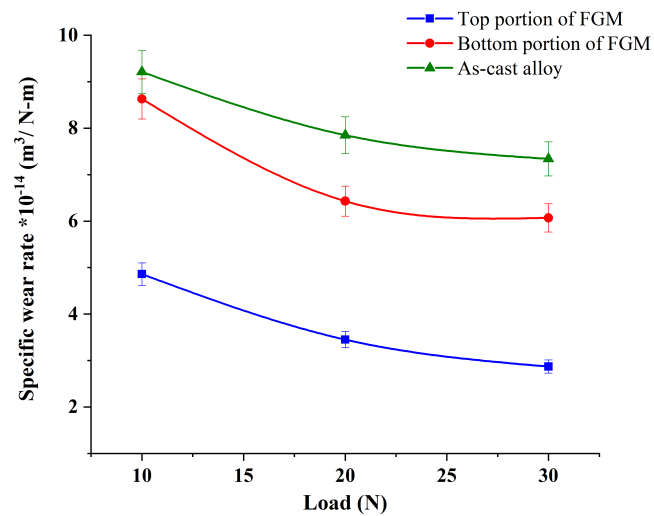


Figure 6.16 Specific wear rate of FGC and as-cast

6.3.7 Worn out surface analysis

Figure 6.17 shows the SEM images of the worn surfaces for the specimens subjected to a wear load of 30N. Two extreme ends of the cast processed with lateral vibrations revealed that top region is dominated by delamination wear whereas bottom region is dominated by delamination and abrasive wear. The wear mechanisms observed could be generally classified as: (i) delamination wear (ii) abrasive wear. The presence of cracks during sliding of the specimens had been associated with the process of delamination on several occasions by other researchers (Kiran Aithal et al. 2012; Reddy et al. 2009). Delamination gives rise to the detachment of wear debris which can be seen from the Figure 6.17a. The worn surface at the bottom was characterized by long ploughing lines which run parallel to the sliding direction resulting in plastic flow of the material. These features suggest abrasive wear as seen from the Figure 6.17b.

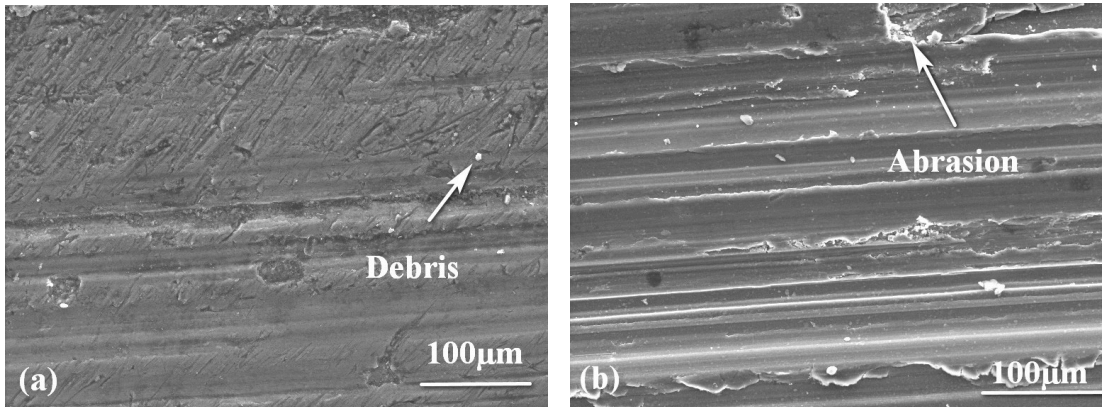
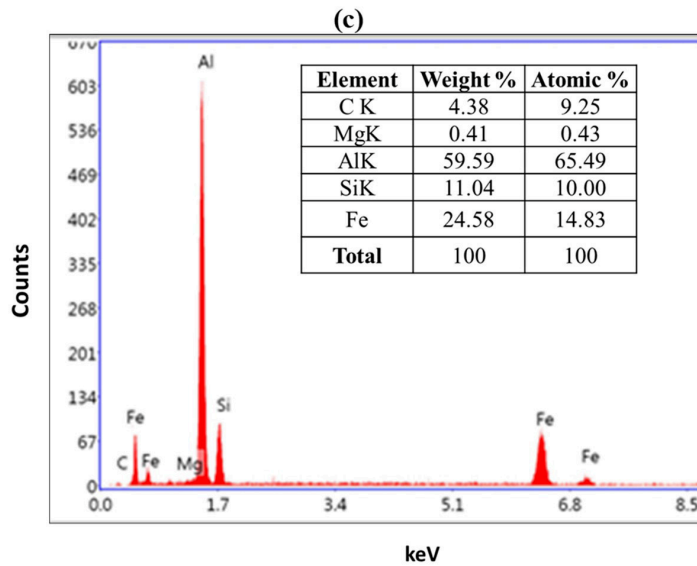
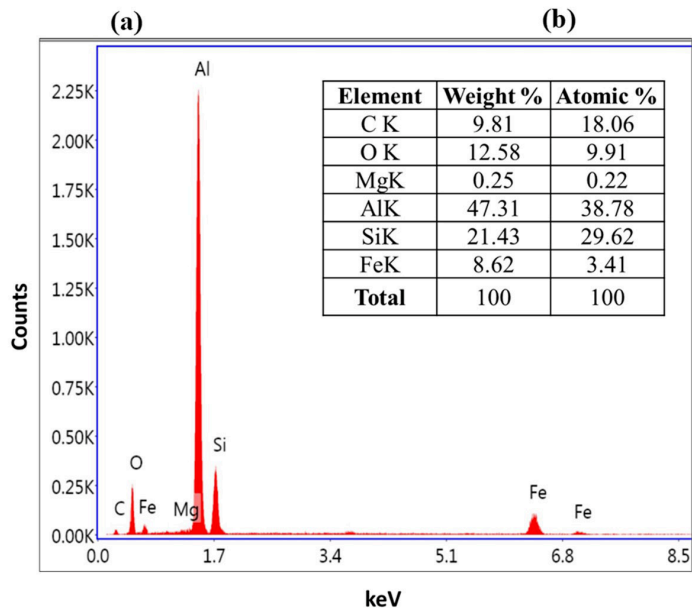
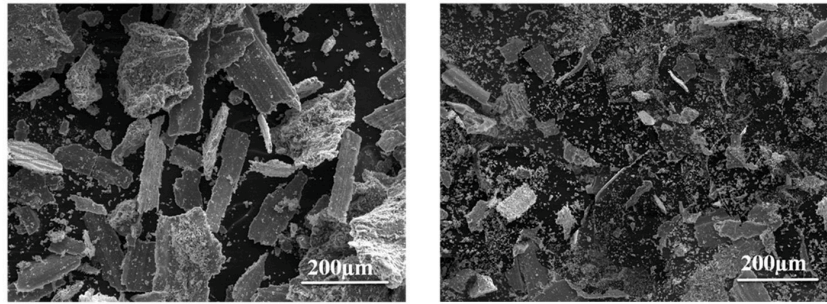


Figure 6.17 SEM images of wear surfaces for the optimized samples: (a) Top portion
(b) Bottom portion

It is seen from the (Figure 6.18(a)) that plate shaped particles were found in wear debris indicating delamination wear mechanism, whereas in (Figure 6.18(b)) it was revealed that wear debris were finer, the morphology shows that the bottom portion is dominated by abrasive and delamination wear. (Figure 6.18(c) and 6.18 (d)) shows the EDS image of the worn out surface of top portion of the FGC. It is observed from the top portion there is a transfer of (Fe) from counter surface contributing towards improved wear resistance (Abedi and Asl 2019; Iwai et al. 2000; Ul Haq and Anand 2019). It is also reported that due to the presence of particulates and oxides at the top portion has a contribution in lowering the wear loss and COF. This is due to the fact that oxide layer restrains metal to metal contact giving rise to a delamination wear mechanism (Anand et al. 2017; Ul Haq and Anand 2018b; Zhang 2013). The wear mechanisms and morphologies observed in FGC suggests the dominant role of graphite in wear behavior of FGC.



(d)

Figure 6.18 Wear debris analysis of FGC : (a) Top portion (b) Bottom portion (c) EDS for top portion (d) EDS for bottom portion

6.4 SUMMARY

In this chapter, 2wt% graphite was added to Al-18wt%Si alloy to develop a FGC so that better gradation in the tribological characteristics can be obtained. To achieve this, DS technique coupled with lateral vibrations was utilized. The obtained cast has been evaluated for mechanical and tribological characteristics. Based on the experimental results following conclusions were drawn.

- Taguchi optimization in the present investigation revealed chill with higher VHC and when the melt poured at 800⁰C showed better gradation in the hardness values across the length of the casting.
- Hardness values obtained with optimal conditions, showed that hardness increased as the frequency of reinforcement particle percentage increased and vice-versa.
- Presence of bottom chill and influence of lateral excitation revealing steep temperature gradient between top and bottom portion, thereby enhancing DS.
- Histogram of particle distribution from microstructure analysis showed improved segregation of reinforcements at the top portion, Whereas bottom portion showed that it is particle depleted. These variation can be attributed to the influence of lateral vibrations.
- Strength properties obtained showed higher stresses were developed at the bottom portion compared to the top portion. This can be attributed to the presence of lateral excitation.
- From diametrical compression it was seen that as the top portion was hyper-eutectic in nature, fracture was observed from the centre of disc approximately at an angle of 45⁰ the diametrical plane. Whereas from the bottom portion, it is clear that the fracture along the diametral plane was not formed due to its ductile nature and the material was compressed which correlates the results obtained from microstructure and hardness.
- Segregation of reinforcement particulates at the top portion has a contribution in lowering wear loss, specific wear rate, COF indicating beneficial effects of

graphite particulates which acts as self-lubricating system between the sliding parts. This dominant role of graphite particulates of a developed FGC enables it as the potential candidate to be used in the solid valve lifters for automotive application.

CHAPTER 7

CONCLUSIONS

The present investigation deals with development of novel directional solidification technique coupled with lateral vibration to fabricate FGM's. Two Al based FGM's were fabricated, one with Al-18wt%Si (without and with lateral excitation) and the other with Al-18wt%Si reinforced with 2wt% graphite (with lateral excitation). Taguchi technique was employed to optimize the process parameters. Castings obtained with optimal process parameters were investigated for hardness, effect of chill during directional solidification, microstructure, strength, wear loss, specific wear rate, coefficient of friction, worn out surface and wear debris analysis. Based on the optimization and experimental investigation, the following conclusions have been derived.

1. A novel experimental technique was developed to synthesize Al/Si FGM through directional solidification coupled with lateral vibrations.
2. Al-Si based FGM were fabricated using Al-18wt%Si and Al-18wt%Si reinforced with 2wt% graphite. Taguchi optimization and ANOVA results of FGM castings fabricated revealed that chill volume had a major contribution of all the process parameters followed by chill material and pouring temperature.
3. With higher VHC of a chill and higher pouring temperature of the melt, it was seen that there was a significant improvement in hardness gradation across the length of a cast. Due to the influence of lateral vibrations and bottom chill during solidification revealed steep temperature gradient between top and bottom portion before attaining an equilibrium temperature. Thereby enhancing directional solidification at a faster rate.
4. From microstructure analysis of an FGM, it was observed that top portion is rich in reinforcement particulate. Whereas, bottom portion is particle depleted. The

amount of primary Si (hard phase) that has segregated in varying volume fraction from bottom to top portion of the specimen influences hardness. Also it was observed that due to lateral vibrations, precipitation of reinforcement particulates was further increased enhancing gradation in hardness and strength.

5. Due to higher segregation primary Si, wear resistance of an FGM observed at the top portion is more compared to the bottom portion. It is also observed the FGM fabricated from Al-18wt%Si reinforced with 2wt% graphite and with the influence of lateral vibrations, top portion exhibited greater wear resistance compared to the bottom portion. This is due to presence of graphite particulates at the top which acts as a self-lubricating system between the sliding parts. The comparison of top and bottom surfaces of the FGM clearly shows that the wear loss and COF is more at the bottom. The top surface subjected to wear has significant reduction in wear loss and COF. This can be attributed to the simple reason of increase in Si % and reinforcement compared to bottom surface. Wear mechanisms observed in the SEM images revealed that there is a shift from delamination at lower concentrations in the top portion to abrasion at higher concentrations in the bottom part.

CHAPTER 8

SCOPE FOR FUTURE WORK

Although the development of Al-Si based FGM through directional solidification coupled with lateral vibration technique has been studied in detail. Still, there is a scope for further investigation.

- Studies can be made, to evaluate the properties of FGM's fabricated with different alloys for any specific application.
- Studies can be made by supplying coolant around the chill during directional solidification. Thereby, efficiency of heat extraction rate of a chill can be enhanced.
- Different chill materials with varying VHC can be used to study the influence of chill during directional solidification.
- Further studies can be made on age-hardening, heat treatment, corrosion, fatigue, high temperature wear resistance for any specific application.
- Mathematical models can be developed to study the influence of lateral excitation during directional solidification.

References

- Abedi, T. and Asl, S. K. (2019). “Synthesis of a novel functionally graded coatings of Ni-Cr/Al₂O₃ nanocomposite coating by pulse electrodeposition”. *Mater. Res. Express*, 6(5), 56403.
- Abu-Dheir, N., Khraisheh, M., Saito, K., and Male, A. (2005). “Silicon morphology modification in the eutectic Al–Si alloy using mechanical mold vibration”. *Mater. Sci. Eng. A*, 393(1-2), 109–117.
- Aithal, S. K. (2013). *Development and characterization of Functionally Graded Al-Si Alloy System and Al-Si/Al-SiCp Composites using centrifuge casting*. Ph.d thesis, National institute of Technology karnataka, surathkal.
- Akhlaghi, F. and Zare-Bidaki, A. (2009). “Influence of graphite content on the dry sliding and oil impregnated sliding wear behavior of Al 2024–graphite composites produced by in situ powder metallurgy method”. *Wear*, 266(1-2), 37–45.
- Amorós, J., Cantavella, V., Jarque, J., and Felú, C. (2008). “Green strength testing of pressed compacts: An analysis of the different methods”. *J. Eur. Ceram. Soc.*, 28(4), 701–710.
- Anand, A., Irfan Ul Haq, M., Vohra, K., Raina, A., and Wani, M. (2017). “Role of Green Tribology in Sustainability of Mechanical Systems: A State of the Art Survey”. *Mater. Today Proc.*, 4(2), 3659–3665.
- Archard, J. F. (1953). “Contact and Rubbing of Flat Surfaces”. *J. Appl. Phys.*, 981.
- Askari, E., Mehrali, M., Metselaar, I., Kadri, N. A., and Rahman, M. (2012). “Fabrication and mechanical properties of Al₂O₃/SiC/ZrO₂ functionally graded material by electrophoretic deposition”. *J. Mech. Behav. Biomed. Mater.*, 12, 144–150.
- Banthia, S., Sengupta, S., Das, S., and Das, K. (2019). “Synthesis and characterization

of novel Cu, Cu-SiC functionally graded coating by pulse reverse electrodeposition”. *Appl. Surf. Sci.*, 467-468, 567–579.

Baradeswaran, A. and Elaya Perumal, A. (2013). “Influence of B₄C on the tribological and mechanical properties of Al 7075–B₄C composites”. *Compos. Part B Eng.*, 54, 146–152.

Baradeswaran, A. and Perumal, A. E. (2014). “Wear and mechanical characteristics of Al 7075/graphite composites”. *Compos. Part B Eng.*, 56, 472–476.

Barekar, N., Tzamtzis, S., Dhindaw, B. K., Patel, J., Hari Babu, N., and Fan, Z. (2009). “Processing of aluminum-graphite particulate metal matrix composites by advanced shear technology”. *J. Mater. Eng. Perform.*, 18(9), 1230–1240.

Basavakumar, K., Mukunda, P., and Chakraborty, M. (2008). “Influence of grain refinement and modification on microstructure and mechanical properties of Al–7Si and Al–7Si–2.5Cu cast alloys”. *Mater. Charact.*, 59(3), 283–289.

Basavakumar, K., Mukunda, P., and Chakraborty, M. (2009). “Dry sliding wear behaviour of Al–12Si and Al–12Si–3Cu cast alloys”. *Mater. Des.*, 30(4), 1258–1267.

Bast, J., Hübler, J., and Dommaschk, C. (2004). “Influence of vibration during solidification of molten metals on structure and casting properties”. *Adv. Eng. Mater.*, 6(7), 550–554+469.

Beal, V. E., Erasenthiran, P., Hopkinson, N., Dickens, P., and Ahrens, C. H. (2006). “The effect of scanning strategy on laser fusion of functionally graded H13/Cu materials”. *Int. J. Adv. Manuf. Technol.*, 30(9-10), 844–852.

Bever, M. and Duwez, P. (1972). “Gradients in composite materials”. *Mater. Sci. Eng.*, 10, 1–8.

Bialo, D., Zhou, J., and Duszczyk, J. (2000). “The tribological characteristics of the Al-20Si-3Cu-1Mg alloy reinforced with Al₂O₃ particles in relation to the hardness of a mating steel”. *J. Mater. Sci.*, 35(21), 5497–5501.

- Birman, V. and Byrd, L. W. (2007). “Modeling and Analysis of Functionally Graded Materials and Structures”. *Appl. Mech. Rev.*, 60(5), 195.
- Blau, P. J. (1981). “Interpretations of the friction and wear break-in behavior of metals in sliding contact”. *Wear*, 71(1), 29–43.
- Bonollo, F., Molinas, B., Tangerini, I., and Zambon, A. (2014). “Diametral compression testing of metal matrix composites”. *Mater. Sci. Technol.*, 10(6), 558–564.
- Bouacha, K., Yallese, M. A., Khamel, S., and Belhadi, S. (2014). “Analysis and optimization of hard turning operation using cubic boron nitride tool”. *Int. J. Refract. Met. Hard Mater.*, 45, 160–178.
- Campbell, J. (2011). *Complete Casting Handbook*. Butterworth-Heinemann, first edition.
- Chaturvedi, V., Sharma, A., and Pandel, U. (2017). “Effect of mechanical vibrations on grain refinement of AZ91 Mg alloy”. *Mater. Res. Express*, 4(4), 046501.
- Chen, G., Tong, M., and Zhu, Z. (1999). “Study on the macrosegregation of aluminium in centrifugal-cast ZA27 alloy”. *Mater. Sci. Eng. A*, 265(1-2), 306–309.
- Chirita, G., Stefanescu, I., Barbosa, J., Puga, H., Soares, D., and Silva, F. S. (2009a). “On assessment of processing variables in vertical centrifugal casting technique”. *Int. J. Cast Met. Res.*, 22(5), 382–389.
- Chirita, G., Stefanescu, I., Soares, D., and Silva, F. (2009b). “Influence of vibration on the solidification behaviour and tensile properties of an Al–18wt%Si alloy”. *Mater. Des.*, 30(5), 1575–1580.
- Chirita, G., Stefanescu, I., Soares, D., and Silva, F. S. (2008). “Effect of Gravity / Vibration / Centrifugal Process on Mechanical Properties of an Al-Si Alloy”. *Mater. Sci. Forum*, 588, 395–399.
- Clarke, J. and Sarkar, A. (1979). “Wear characteristics of as-cast binary aluminium-silicon alloys”. *Wear*, 54(1), 7–16.
- Clauss, F. J. (1972). *Solid Lubricants and Self-Lubricating Solids*. Elsevier, 1 edition.

Deaquino-Lara, R., Soltani, N., Bahrami, A., Gutiérrez-Castañeda, E., García-Sánchez, E., and Hernandez-Rodríguez, M. (2015). “Tribological characterization of Al7075–graphite composites fabricated by mechanical alloying and hot extrusion”. *Mater. Des.*, 67, 224–231.

Dommaschk, C. (2003). *Contribution to the subpool influence of solidified metal melting due to vibration*. Ph.D. thesis, University of Freiberg, Germany.

Dorri Moghadam, A., Omrani, E., Menezes, P. L., and Rohatgi, P. K. (2015). “Mechanical and tribological properties of self-lubricating metal matrix nanocomposites reinforced by carbon nanotubes (CNTs) and graphene – A review”. *Compos. Part B Eng.*, 77, 402–420.

Douglas, C. M. (2012). *Design and Analysis of Experiments*. Wiley Series in Probability and Statistics. John Wiley & Sons, Inc., Hoboken, NJ, USA.

Dwivedi, D. K., Sharma, A., and Rajan, T. V. (2008). “Machining of LM13 and LM28 cast aluminium alloys: Part I”. *J. Mater. Process. Technol.*, 196(1-3), 197–204.

Eskin, G. I. (1998). *Ultrasonic Treatment of Light Alloy Melts*. Taylor & Francis.

Fahad, M. K. (1996). “Stresses and failure in the diametral compression test”. *J. Mater. Sci.*, 31(14), 3723–3729.

Fisher, T. P. (1973). “Effects of vibrational energy on the solidification of aluminum alloys”. *Br. Foundrym.*, 66, 71–84.

Fu, Y., Batchelor, A. W., Xing, H., and Gu, Y. (1997). “Wear behaviour of laser-treated plasma-sprayed ZrO₂ coatings”. *Wear*, 210, 157–164.

Gaber, A., Gaffar, M. A., Mostafa, M. S., and Zeid, E. F. A. (2007). “Precipitation kinetics of Al – 1 . 12 Mg 2 Si – 0 . 35 Si and Al – 1 . 07 Mg 2 Si – 0 . 33 Cu alloys”. *J. Alloys Compd.*, 429, 167–175.

Gibbons, G. J. and Hansell, R. G. (2007). “Thermal-sprayed coatings on aluminium for mould tool protection and upgrade”. *J. Mater. Process. Technol.*, 4, 184–191.

Gomes, J., Ribeiro, A., Vieira, A., Miranda, A., and Rocha, L. (2005). “Wear Mecha-

nisms in Functionally Graded Aluminium Matrix Composites: Effect of the Presence of an Aqueous Solution”. *Mater. Sci. Forum*, 492-493, 33–38.

Gruzleski, J. E., Closset, B. M., and Society, A. F. (1990). *The Treatment of Liquid Aluminum-silicon Alloys*. American Foundrymen’s Society, Incorporated.

GUO, H.-m., ZHANG, A.-s., YANG, X.-j., and YAN, M.-m. (2014). “Grain refinement of Al-5%Cu aluminum alloy under mechanical vibration using meltable vibrating probe”. *Trans. Nonferrous Met. Soc. China*, 24(8), 2489–2496.

Gupta, M., Mohamed, F., Lavernia, E., and Srivatsan, T. S. (1993). “Microstructural evolution and mechanical properties of SiC/Al₂O₃ particulate-reinforced spray-deposited metal-matrix composites”. *J. Mater. Sci.*, 28(8), 2245–2259.

Hassan, A. M., Tashtoush, G. M., and Al-Khalil, J. A. (2007). “Effect of Graphite and/or Silicon Carbide Particles Addition on the Hardness and Surface Roughness of Al-4 wt% Mg Alloy”. *J. Compos. Mater.*, 41(4), 453–465.

Hemanth, J. (2000). “Action of chills on soundness and ultimate tensile strength (UTS) of aluminum–quartz particulate composite”. *J. Alloys Compd.*, 296, 193–200.

Hemanth, J. (2002). “Effect of chilling on soundness and ultimate tensile strength (UTS) of aluminium alloy –corundum particulate composite”. *Mater. Des.*, 22(5), 375–382.

Hemanth, J. (2006). “Development, mechanical properties, and fracture toughness of chilled Pb/Sb/Sn/As alloy-Al₂SiO₅ (kaolinite) metal matrix composites”. *J. Compos. Mater.*, 40(6), 547–561.

Hemanth, J. (2014). “Heat Transfer Analysis during External Chilling of Composite Material Castings through Experimental and Finite Element (FE) Modelling”. *Model. Numer. Simul. Mater. Sci.*, 04(01), 1–7.

Hernandez, F. C. R. and Sokolowski, J. H. (2006). “Comparison among chemical and electromagnetic stirring and vibration melt treatments for Al–Si hypereutectic alloys”. *J. Alloys Compd.*, 426(1-2), 205–212.

Hiremath, A., AmarMurthy, A., Pranavathmaja, S., Jajodia, R., and Sreenath, R. (2018).

“Effect of end chills, reinforcement content and carburization on the hardness of LM25 - borosilicate glass particulate composite”. *J. Mech. Eng. Sci.*, 12(4), 4203 – 4215.

Hiremath, A. and Hemanth, J. (2017). “Experimental Evaluation of the Chill Casting Method for the Fabrication of LM-25 Aluminum Alloy-Borosilicate Glass (p) Composites”. *Key Eng. Mater.*, 748, 69–73.

Hondros (1959). “Evaluation of Tensile Young’s Modulus and Poisson’s Ratio of a Bi-modular Rock from the Displacement Measurements in a Brazilian Test”. *Aust. J. Appl. Sci.*, 10, 243–167.

Hooper, J. (1971). “The failure of glass cylinders in diametral compression”. *J. Mech. Phys. Solids*, 19(4), 179–188.

Hua, L., Song, Y. L., Liu, J. N., Liu, J., Han, Y., and Shen, Y. H. (2017). “Forming and Application of Auto Body Panels Made of Tailor Welded Blanks and Ultra-High Strength Steel Sheets”. In “Adv. High Strength Steel Press Hardening”, WORLD SCIENTIFIC, 337–345.

Huang, H., Lodhia, A., and Berry, J. (1990). “Modelling the effectiveness of chills during solidification”. In “AFS Trans.”, 547–552.

Ibrahim, I. A., Mohamed, F. A., and Lavernia, E. J. (1991). “Particulate reinforced metal matrix composites - a review”.

Ivanov, A. A. and Krushenka, G. G. (1993). “Preparation of Al–Si alloying composition by means of vibration”. *Liteinoe Proizv.*, 3, 7–8.

Iwai, Y., Honda, T., Miyajima, T., Iwasaki, Y., Surappa, M., and Xu, J. (2000). “Dry sliding wear behavior of Al₂O₃ fiber reinforced aluminum composites”. *Compos. Sci. Technol.*, 60(9), 1781–1789.

Jain, P. L. (2003). *Principles of Foundry Technology*. McGraw-Hill Education.

Jian, X., Meek, T., and Han, Q. (2006a). “Refinement of eutectic silicon phase of aluminum A356 alloy using high-intensity ultrasonic vibration”. *Scr. Mater.*, 54(5), 893–896.

- Jian, X., Meek, T. T., and Han, Q. (2006b). "Refinement of eutectic silicon phase of aluminum A356 alloy using high-intensity ultrasonic vibration". *Scr. Mater.*, 54(5), 893–896.
- Jian, X., Xu, H., Meek, T., and Han, Q. (2005). "Effect of power ultrasound on solidification of aluminum A356 alloy". *Mater. Lett.*, 59(2-3), 190–193.
- Jinfeng, L., Longtao, J., Gaohui, W., Shoufu, T., and Guoqin, C. (2009). "Effect of Graphite Particle Reinforcement on Dry Sliding Wear of SiC/Gr/Al Composites". *Rare Met. Mater. Eng.*, 38(11), 1894–1898.
- Kalpakjian, S. and Schmid, S. R. (2003). *Manufacturing Processes for Engineering Materials*. Prentice Hall.
- Kato, K., Kurimoto, M., Shumiya, H., Adachi, H., Sakuma, S., and Okubo, H. (2006). "Application of functionally graded material for solid insulator in gaseous insulation system". *IEEE Trans. Dielectr. Electr. Insul.*, 13(2), 362–372.
- Kawasaki, A. and Watanabe, R. (1997). "Concept and P/M fabrication of functionally gradient materials". *Ceram. Int.*, 23(1), 73–83.
- Khanna, N. and Davim, J. (2015). "Design-of-experiments application in machining titanium alloys for aerospace structural components". *Measurement*, 61, 280–290.
- Khor, K. A. and Gu, Y. W. (2000). "Effects of residual stress on the performance of plasma sprayed functionally graded ZrO₂/NiCoCrAlY coatings". *Mater. Sci. Eng. A*, 277(1-2), 64–76.
- Kieback, B., Neubrand, A., and Riedel, H. (2003). "Processing techniques for functionally graded materials". *Mater. Sci. Eng. A*, 362(1-2), 81–105.
- Kiran, A. S., Desai, V., Narendranath, and Mukunda, P. G. (2011). "Evolution of microstructure and hardness of AL-SI functionally graded material cast through centrifuge technique using hypereutectic and eutectic Al-SI". *Int. J. Mech. Mater. Eng.*, 6(2), 275–279.
- Kiran Aithal, S., Desai, V., Narendranath, N., and Mukunda, P. G. (2012). "Microstruc-

ture , Hardness and Wear Characterisation of Al-Si FGMs”. *Indian Foundry J.*, 58(5), 39–48.

Kocatepe, K. (2007). “Effect of low frequency vibration on porosity of LM25 and LM6 alloys”. *Mater. Des.*, 28(6), 1767–1775.

Kocatepe, K. and Burdett, C. F. (2000). “Effect of low frequency vibration on macro and micro structures of LM6 alloys”. *J. Mater. Sci.*, 35(13), 3327–3335.

Koizumi, M. and Niino, M. (1995). *Overview of FGM research in Japan*, volume 20. Cambridge University Press.

Koyee, R. D., Eisseler, R., and Schmauder, S. (2014). “Application of Taguchi coupled Fuzzy Multi Attribute Decision Making (FMADM) for optimizing surface quality in turning austenitic and duplex stainless steels”. *Measurement*, 58, 375–386.

Krishnaiah, K., Shahabudeen (2013). *Applied Design of Experiments and Taguchi Methods*. PHI: India.

Krishnan, B. P., Raman, N., Narayanaswamy, K., and Rohatgi, P. K. (1980). “Performance of an Al-Si-graphite particle composite piston in a diesel engine”. *Wear*, 60(1), 205–215.

Krishnan, B. P., Surappa, M. K., and Rohatgi, P. K. (1981). “The UPAL process: a direct method of preparing cast aluminium alloy-graphite particle composites”. *J. Mater. Sci.*, 16(5), 1209–1216.

Kuhn, H., Medlin, D., and Committee, A. S. M. I. H. (2000). *Mechanical Testing and Evaluation*. ASM Handbook: Mechanical Testing and Evaluation. ASM International.

Kurita, H., Miyazaki, T., Kawasaki, A., Lu, Y., and Silvain, J.-F. (2015). “Interfacial microstructure of graphite flake reinforced aluminum matrix composites fabricated via hot pressing”. *Compos. Part A Appl. Sci. Manuf.*, 73, 125–131.

Kurz, W. and Fisher, D. J. (1986). *Fundamentals of solidification*. v. 1. Trans Tech Publications.

- Lannutti, J. J. (1994). "Functionally Graded Materials : Properties , Potential and Design Guidelines". *Compos. Eng.*, 4(I), 81–94.
- Leela, B. N. and Rao, K. V. S. (2012). "Microstructure and Microhardness of Chill Cast Al-B 4 C Composites". *Int. J. Mech. Eng. Robot. Res.*, 1(3), 450–456.
- Lin, C.-Y., Bathias, C., McShane, H. B., and Rawlings, R. D. (1999). "Production of silicon carbide Al 2124 alloy functionally graded materials by mechanical powder metallurgy technique". *Powder Metall.*, 42(1), 29–33.
- Liu, B. B., Xie, J. X., and Qu, X. H. (2008). "Fabrication of W-Cu functionally graded materials with high density by particle size adjustment and solid state hot press". *Compos. Sci. Technol.*, 68(6), 1539–1547.
- Mahamood, R. M., Member, E. T. A., Shukla, M., and Pityana, S. (2012). "Functionally Graded Material : An Overview". *World Congr. Eng.*, III, 2–6.
- Manjunath, H., Kiran Aithal, S., Harish Kumar, L., Ramesh Babu, N., and Auradi, V. (2018). "Transient Thermal Investigations During External Chilling Of Al-18%Si Castings Through Experimental And Finite Element Modelling". *Mater. Today Proc.*, 5(2), 7191–7197.
- Mazare, L., Miranda, G., Soares, D. F., and Silva, F. S. (2010). "Influence of solidification rates on a Directional Solidification process for the production of Functionally Graded Materials". *Int. J. Mater. Prod. Technol.*, 39(1-2), 44–58.
- Melgarejo, Z. H., Suárez, O. M., and Sridharan, K. (2006). "Wear resistance of a functionally-graded aluminum matrix composite". *Scr. Mater.*, 55(1), 95–98.
- Mishina, H., Inumaru, Y., and Kaitoku, K. (2008). "Fabrication of ZrO₂/AISI316L functionally graded materials for joint prostheses". *Mater. Sci. Eng. A*, 475(1-2), 141–147.
- Müller, E., Drašar, Č., Schilz, J., and Kaysser, W. (2003). "Functionally graded materials for sensor and energy applications". *Mater. Sci. Eng. A*, 362(1-2), 17–39.

Murray, J. L. and McAlister, A. J. (1984). “The Al-Si (aluminum-silicon) system”. *Bull. Alloy phase diagrams*, 5(1), 74.

Murty, B. S., Kori, S. A., and Chakraborty, M. (2003). “Grain refinement of aluminium and its alloys by heterogeneous nucleation and alloying”. *Int. Mater. Rev.*, 47(1), 3–29.

Nemat-Alla, M. M., Ata, M. H., Bayoumi, M. R., and Khair-Eldeen, W. (2011). “Powder Metallurgical Fabrication and Microstructural Investigations of Aluminum/Steel Functionally Graded Material”. *Mater. Sci. Appl.*, 02(12), 1708–1718.

Okamoto, H., Schlesinger, M., and Mueller, E. (editors) (2016). *Alloy Phase Diagrams*. ASM International.

Omrani, E., Barari, B., Dorri Moghadam, A., Rohatgi, P. K., and Pillai, K. M. (2015). “Mechanical and tribological properties of self-lubricating bio-based carbon-fabric epoxy composites made using liquid composite molding”. *Tribol. Int.*, 92, 222–232.

Omura, N., Murakami, Y., Li, M., Tamura, T., Miwa, K., Furukawa, H., Harada, M., and Yokoi, M. (2009). “Effects of Mechanical Vibration on Macrostructure and Mechanical Properties of AC4C Aluminum Alloy Castings”. *Mater. Trans.*, 50(11), 2578–2583.

Pace (2011). *Metallographic hand book*. Tucson, Arizona: Pace Technologies.

Peng, X., Yan, M., and Shi, W. (2007). “A new approach for the preparation of functionally graded materials via slip casting in a gradient magnetic field”. *Scr. Mater.*, 56(10), 907–909.

Phadke, M. S. (1989). *Quality Engineering Using Robust Design*. Prentice-Hall International editions. Prentice Hall.

Pillai, R., Biju Kumar, K., and Pai, B. (2004). “A simple inexpensive technique for enhancing density and mechanical properties of Al-Si alloys”. *J. Mater. Process. Technol.*, 146(3), 338–348.

Pompe, W., Worch, H., Epple, M., Friess, W., Gelinsky, M., Greil, P., Hempel, U., Scharnweber, D., and Schulte, K. (2003). “Functionally graded materials for biomedical applications”. *Mater. Sci. Eng. A*, 362(1-2), 40–60.

- Prasad, B. K., Dan, T. K., and Rohatgi, P. K. (1993). "Characterization and Microstructural Modifications of a Pressure Die Cast Eutectic Aluminium–Silicon Alloy-Graphite Composite". *Mater. Trans. JIM*, 34(5), 474–480.
- Prasad, B. K., Venkateswarlu, K., Modi, O. P., Jha, A. K., Das, S., Dasgupta, R., and Yegneswaran, A. H. (1998). "The effects of primary silicon particles on the sliding wear behavior of aluminum-silicon alloys". *J. Mater. Sci. Lett.*, 17(16), 1381–1383.
- Prasad, S. V. and Asthana, R. (2004). "Aluminum metal-matrix composites for automotive applications: tribological considerations". *Tribol. Lett.*, 17(3), 445–453.
- Procopio, A. T., Zavaliangos, A., and Cunningham, J. C. (2003). "Analysis of the diametrical compression test and the applicability to plastically deforming materials". *J. Mater. Sci.*, 38(17), 3629–3639.
- Qudong, W., Yongjun, C., Wenzhou, C., Yinhong, W., Chunquan, Z., and Wenjiang, D. (2005). "Centrifugally cast Zn–27Al–xMg–ySi alloys and their in situ (Mg₂Si+Si)/ZA27 composites". *Mater. Sci. Eng. A*, 394(1-2), 425–434.
- Radhakrishna, K. and S. Seshan, M. S. (1981). "Effect of Porosity on Mechanical Properties of Aluminum Alloy Castings". *Trans. Indian Inst. Met.*, 34(2), 169–171.
- Radhika, N. and Raghu, R. (2016). "Development of functionally graded aluminium composites using centrifugal casting and influence of reinforcements on mechanical and wear properties". *Trans. Nonferrous Met. Soc. China (English Ed.)*, 26(4), 905–916.
- Radhika, N., Thirumalini, S., and Shivashankar, A. (2018). "Investigation on Mechanical and Adhesive Wear Behavior of Centrifugally Cast Functionally Graded Copper/SiC Metal Matrix Composite". *Trans. Indian Inst. Met.*, 71(6), 1311–1322.
- Radjai, A. and Miwa, K. (2000). "Effects of the intensity and frequency of electromagnetic vibrations on the microstructural refinement of hypoeutectic Al-Si alloys". *Metall. Mater. Trans. A*, 31(3), 755–762.
- Rajan, T. P., Narayan Prabhu, K., Pillai, R. M., and Pai, B. C. (2007). "Solidification and

casting/mould interfacial heat transfer characteristics of aluminum matrix composites”. *Compos. Sci. Technol.*, 67(1), 70–78.

Rajaram, G., Kumaran, S., and Rao, T. S. (2010). “Sliding Wear Behavior of Al-Si/Graphite Composite”. *Tribol. Trans.*, 54(1), 115–121.

Ramesh Babu, N., Ramesh, M., Kiran Aithal, S., and Kotresh, K. (2018). “Effect of Lateral Vibrations during Directional solidification on Mechanical Properties of Al-18%wt Si Alloys”. *Mater. Today Proc.*, 5(2), 6954–6962.

Rasgado, M. T. A. and Davey, K. (2002). “The effect of vibration on surface finish for semisolid and cast components”. *J. Mater. Process. Technol.*, 125, 543–548.

Rasgado, M. T. A. and Davey, K. (2004). “Vibration and casting surface finish”. *J. Mater. Process. Technol.*, 153, 875–880.

Ray, S. (1993). “Synthesis of cast metal matrix particulate composites”. *J. Mater. Sci.*, 28(20), 5397–5413.

Reddy, A., Bai, B., Murthy, K., and Biswas, S. (1994). “Wear and seizure of binary Al-Si alloys”. *Wear*, 171(1-2), 115–127.

Reddy, S., Mukunda, P., Aithal, K., and Shetty, P. B. (2017). “Strength evaluation of flake and spheroidal graphite cast irons using diametral compression test”. *J. Mater. Res. Technol.*, 6(1), 96–100.

Reddy, T. V. S., Dwivedi, D. K., and Jain, N. K. (2009). “Adhesive wear of stir cast hypereutectic Al-Si-Mg alloy under reciprocating sliding conditions”. *Wear*, 266(1-2), 1–5.

Rikhtegar, F. and Shabestari, S. G. (2014). “Investigation on solidification conditions in functionally Si-gradient Al alloys using simulation and cooling curve analysis methods”. *J. Therm. Anal. Calorim.*, 117(2), 721–729.

Rohatgi, P. (2001). “Cast metal matrix composites: Past, present and future”. In “Trans. Am. Foundry Soc. One Hundred Fifth Annu. Cast. Congr.”, 1–25.

Rohatgi, P., Murali, N., Shetty, H., and Chandrashekhara, R. (1976). “Improved damping

- capacity and machinability of graphite particle-aluminum alloy composites”. *Mater. Sci. Eng.*, 26(1), 115–122.
- Rohatgi, P. K., Ray, S., and Liu, Y. (1992). “Tribological properties of metal matrix-graphite particle composites”. *Int. Mater. Rev.*, 37(1), 129–152.
- Rohatgi, P. K., Tabandeh-Khorshid, M., Omrani, E., Lovell, M. R., and Menezes, P. L. (2013). “Tribology of Metal Matrix Composites”. In “Tribol. Sci. Eng.”, Springer New York, New York, NY, 233–268.
- Ross, P. J. (1996). *Taguchi Techniques for Quality Engineering: Loss Function, Orthogonal Experiments, Parameter and Tolerance Design*. McGraw-Hill.
- Royr, A. and Vasseur, S. (1988). “ASM Hand book—Castings”. *ASM Int. Ohio*, 15, 296.
- Sahu, S. P., Satapathy, A., Patnaik, A., Sreekumar, K., and Ananthapadmanabhan, P. (2010). “Development, characterization and erosion wear response of plasma sprayed fly ash–aluminum coatings”. *Mater. Des.*, 31(3), 1165–1173.
- Sarkar, A. (1975). “Wear of aluminium-silicon alloys”. *Wear*, 31(2), 331–343.
- Seah, K., Hemanth, J., and Sharma, S. (1996). “Wear characteristics of sub-zero chilled cast iron”. *Wear*, 192(1-2), 134–140.
- Seifried, S., Winterer, M., and Hahn, H. (2001). “Nanocrystalline gradient films through chemical vapor synthesis”. *Scr. Mater.*, 44(8-9), 2165–2168.
- Sequeira, P. D., Watanabe, Y., Eryu, H., Yamamoto, T., and Matsuura, K. (2007). “Effects of Platelet Size and Mean Volume Fraction on Platelet Orientation and Volume Fraction Distributions in Functionally Graded Material Fabricated by a Centrifugal Solid-Particle Method”. *J. Eng. Mater. Technol.*, 129(2), 304.
- Shabestari, S. and Moemeni, H. (2004). “Effect of copper and solidification conditions on the microstructure and mechanical properties of Al–Si–Mg alloys”. *J. Mater. Process. Technol.*, 153-154(1-3), 193–198.
- Shanmugasundaram, P. and Subramanian, R. (2013). “Wear Behaviour of Eutectic

Al-Si Alloy-Graphite Composites Fabricated by Combined Modified Two-Stage Stir Casting and Squeeze Casting Methods”. *Adv. Mater. Sci. Eng.*, 2013, 1–8.

Shaw, M. C., Braiden, P. M., and DeSalvo, G. J. (1975). “The Disk Test for Brittle Materials”. *J. Eng. Ind.*, 97(1), 77.

Shen, M. and Bever, M. B. (1972). “Gradients in polymeric materials”. *J. Mater. Sci.*, 7(7), 741–746.

Shi-jie, G., Qi-chi, L., Zhi-hao, Z., and Jian-zhong, C. (2006). “Microstructure character of AZ80 magnesium alloy ingots cast under electromagnetic vibration”. *China Foundry*, 4(1), 22–25.

Shivanath, R., Sengupta, P., and Eyre, T. (1977). “Wear of Aluminium-Silicon Alloys.” *Br. Foundrymen*, 70, 349–356.

Somi Reddy, A., Pramila Bai, B., Murthy, K., and Biswas, S. (1995). “Mechanism of seizure of aluminium-silicon alloys dry sliding against steel”. *Wear*, 181-183, 658–667.

Song, C., Xu, Z., and Li, J. (2007a). “Structure of in situ Al/Si functionally graded materials by electromagnetic separation method”. *Mater. Des.*, 28(3), 1012–1015.

Song, C., Xu, Z., Liu, X., Liang, G., and Li, J. (2005). “In situ multi-layer functionally graded materials by Electromagnetic Separation method”. *Mater. Sci. Eng. A*, 393(1-2), 164–169.

Song, C.-J., Xu, Z.-M., and Li, J.-G. (2006). “Study on electromagnetic force for preparation of in-situ Al/Mg₂Si functionally graded materials by electromagnetic separation method”. *Metall. Mater. Trans. B*, 37(6), 1007–1014.

Song, C.-J., Xu, Z.-M., and Li, J.-G. (2007b). “In-situ Al/Al₃Ni functionally graded materials by electromagnetic separation method”. *Mater. Sci. Eng. A*, 445-446, 148–154.

Srivastava, S., Mohan, S., Srivastava, Y., and Shukla, A. J. (2012). “Study of the wear and friction behavior of immiscible as cast-Al- Sn / Graphite composite Abstract :”. *Int. J. Mod. Eng. Res.*, 2(2), 25–42.

- Starke, E. and Staley, J. (2011). "Application of modern aluminium alloys to aircraft". In "Fundam. Alum. Metall.", Elsevier, 747–783.
- Sui, Y., Li, B., Liu, A., Guo, J., and Fu, H. (2010). "Evolution of microstructure in centrifugal cast Al-Cu alloy". *China Foundry*, 7(1), 43–46.
- Suresh, S. and Mortensen, A. (1998). "Fundamentals of Functionally Graded Materials: Processing and Thermomechanical Behavior of Graded Metals and Metal-Ceramic Composites". *ASM Int. Inst. Mater.*
- Taguchi, G. (1986). *Introduction to quality engineering: designing quality into products and processes*. Asian Productivity Organization.
- Timoshenko, S. (1951). *Theory of elasticity*. Engineering societies monographs. McGraw-Hill.
- Totten, G. E. (2017). *Friction, Lubrication, and Wear Technology*. ASM International.
- Tronche, A. and Fauchais, P. (1987). "Hard coatings (Cr₂O₃, WC-Co) properties on aluminium or steel substrates". *Mater. Sci. Eng.*, 92, 133–144.
- Tronche, A. and Fauchais, P. (1988). "Frictional behaviour against steel of aluminium substrates plasma-sprayed with hard coatings". *Mater. Sci. Eng. A*, 102(1), 1–12.
- Ul-Haq, M. I. and Anand, A. (2018a). "Dry Sliding Friction and Wear Behavior of AA7075-Si₃N₄ Composite". *Silicon*, 10(5), 1819–1829.
- Ul-Haq, M. I. and Anand, A. (2018b). "Dry sliding friction and wear behaviour of hybrid AA7075/Si₃N₄/Gr self lubricating composites". *Mater. Res. Express*, 5(6), 066544.
- Ul-Haq, M. I. and Anand, A. (2019). "Friction and Wear Behavior of AA 7075- Si₃N₄ Composites Under Dry Conditions: Effect of Sliding Speed". *Silicon*, 11(2), 1047–1053.
- Vedula, M., Pangborn, R., and Queeney, R. (1988). "Fibre anisotropic thermal expansion and residual thermal stress in a graphite/aluminium composite". *Composites*, 19(1), 55–60.
- Wang, K., Xue, H.-s., Zou, M.-h., and Liu, C.-m. (2009). "Microstructural characteristics

and properties in centrifugal casting of SiCp/Zl104 composite”. *Trans. Nonferrous Met. Soc. China*, 19(6), 1410–1415.

Wankhede, D. M., Narkhede, B. E., Mahajan, S. K., and Choudhari, C. M. (2019). “Influence of Copper Chills and Pouring Temperature on Mechanical Properties of LM6 Castings”. In “*Adv. Mater. Metall.*”, Springer, 207–216.

Watanabe, Y., Eryu, H., and Matsuura, K. (2001). “Evaluation of three-dimensional orientation of Al₃Ti platelet in Al-based functionally graded materials fabricated by a centrifugal casting technique”. *Acta Mater.*, 49(5), 775–783.

Watanabe, Y., Kim, I. S., and Fukui, Y. (2005). “Microstructures of Functionally Graded Materials Fabricated by Centrifugal Solid-Particle and In-Situ Methods”. *Met. Mater.*, 11(5), 391–399.

Watanabe, Y., Sato, H., Ogawa, T., and Kim, I.-S. (2007). “Density and Hardness Gradients of Functionally Graded Material Ring Fabricated from Al-3 mass%Cu Alloy by a Centrifugal In-Situ Method”. *Mater. Trans.*, 48(11), 2945–2952.

Watanabe, Y., Yamanaka, N., and Fukui, Y. (1998). “Control of composition gradient in a metal-ceramic functionally graded material manufactured by the centrifugal method”. *Compos. Part A Appl. Sci. Manuf.*, 29(5-6), 595–601.

Wright, P. J. F. (1955). “Comments on an indirect tensile test on concrete cylinders”. *Mag. Concr. Res.*, 7(20), 87–96.

Yang, J., Lin, C., Wang, T., and Chu, H. (2004). “The tribological characteristics of A356.2Al alloy/Gr(p) composites”. *Wear*, 257(9-10), 941–952.

Yao, L., Hao, H., Ji, S.-h., Fang, C.-f., and Zhang, X.-g. (2011). “Effects of ultrasonic vibration on solidification structure and properties of Mg-8Li-3Al alloy”. *Trans. Nonferrous Met. Soc. China*, 21(6), 1241–1246.

Zhang, S.-w. (2013). “Green tribology: Fundamentals and future development”. *Friction*, 1(2), 186–194.

Zhang, Z., Li, T., Yue, H., Zhang, J., and Li, J. (2009). “Study on the preparation of

Al–Si functionally graded materials using power ultrasonic field”. *Mater. Des.*, 30(3), 851–856.

Zhongtao, Z., Tingju, L., Hongyun, Y., Jian, Z., and Jie, L. (2008). “Preparation of Al/Si functionally graded materials using ultrasonic separation method”. *China Foundry*, 5(3), 194–198.

Zhou, Z. J., Yum, Y. J., and Ge, C. C. (2009). “The Recent Progress of FGM on Nuclear Materials - Design and Fabrication of W/Cu Functionally Graded Material High Heat Flux Components for Fusion Reactor”. *Mater. Sci. Forum*, 631-632, 353–358.

Zhu, J., Lai, Z., Yin, Z., Jeon, J., and Lee, S. (2001). “Fabrication of ZrO₂–NiCr functionally graded material by powder metallurgy”. *Mater. Chem. Phys.*, 68(1-3), 130–135.

List of Publications based on Ph.D. Research Work

Sl No	Title of the paper	Authors	Name of the Journal/Copyrights/Conference/Symposium, Vol., No., Pages	Month, Year of Publication	Category*
1	Evaluation of Mechanical and Tribological Properties of Directionally Solidified AlSi Based FG Composite	<u>Ramesh Babu N.</u> Ramesh MR, Kiran Aithal S	Silicon, https://doi.org/10.1007/s12633-019-00179-5	May, 2019	1
2	Influence of vibrations during directional solidification on microstructure, hardness and strength of Al-Si-graphite FG composite	<u>Ramesh Babu N.</u> Ramesh MR, Kiran Aithal S	Journal of Mechanical Engineering Research and Developments, 42(3), 84-86 http://doi.org/10.26480/jmerd.03.2019.84.86	May, 2019	1
3	Study of dry sliding wear behavior of Al-Si-C FG alloy developed through directional solidification	<u>Ramesh Babu N.</u> Ramesh MR, Kiran Aithal S, Veeresh Kumar, Manjunath H.N	AIP Conference Proceedings, 2080, 020009 DOI: 10.1063/1.5092892	March, 2019	3
4	Effect of Lateral Vibrations during Directional solidification on Mechanical Properties of Al-18%wt Si Alloys	<u>Ramesh Babu N.</u> Ramesh MR, Kiran Aithal S, Kotgi Kotresh	Materials today: proceedings , 5(2):6954-6962 DOI: 10.1016/j.matpr.2017.11.358	January, 2018	3
5	Effect of external chill coupled with lateral excitation on mechanical properties of LM28 based FG composite	<u>Ramesh Babu N.</u> Ramesh MR, Kiran Aithal S	Journal of Mechanical Engineering and Sciences	Under review	1

6	Characterization of microstructure, tensile strength, wear behavior of Al-18wt%Si directionally solidified FG alloy processed with and without lateral vibrations based on optimized hardness	<u>Ramesh Babu N,</u> Ramesh MR, Kiran Aithal S	Journal of alloys and compounds	Under review	1
---	---	---	---------------------------------	--------------	---

*Category:

1: Journal paper, full paper reviewed

2: Journal paper, Abstract reviews

3: Conference/Symposium paper, full paper reviewed

4: Conference/Symposium paper, abstract reviewed

5: Others (including papers in Workshops, copyrights/patents, NITK Research Bulletins, Short notes etc.)

N. Ramesh Babu 21/05/20

Mr. Ramesh Babu N

Research Scholar

Name & Signature, with Date

Dr. Ramesh MR

Research Guide

Name & Signature, with Date

BIODATA

- Name :** Ramesh Babu N
- Father's Name:** Narayanappa
- Date of Birth:** 01-Jul-1985
- Nationality:** Indian
- Permanent Address:** No 433, Venkateshwara Nilaya, Cheluvaiah Road, Near 7th Cross, Ramamurthy Nagar, Bangalore:560016
- Mobile Number:** +91-7411333604.
- Email-id:** rameshbabu.n085@gmail.com



8. Educational qualifications:

Qualification	College	University/ Board	Year of passing
Ph.D in Mechanical Engineering	National Institute of Technology, Karnataka	National Institute of Technology, Karnataka	Pursuing
M.Tech in Machine Design	BMS College of Engineering	VTU, Belagavi	2010
B.E in Mechanical Engineering	Dr. Ambedkar Institute of Technology	VTU, Belagavi	2008

I hereby declare that the above-mentioned information is true and correct to best of my knowledge

N. Ramesh Babu 21/05/20

(Ramesh Babu N)